Novel Predistortion Techniques for RF Power Amplifiers

Ming Xiao

A thesis submitted to
The University of Birmingham
for the degree of
DOCTOR OF PHILOSOPHY

School of Electronic, Electrical
and Computer Engineering
The University of Birmingham

October, 2009

ABSTRACT

As the mobile phone is an essential accessory for everyone nowadays, predistortion for the RF power amplifiers in mobile phone systems becomes more and more popular. Especially, new predistortions for power amplifiers with both nonlinearities and memory effects interest the researchers. In our thesis, novel predistortion techniques are presented for this purpose. Firstly, we improve the digital injection predistortion in the frequency domain. Secondly, we are the first authors to propose a novel predistortion, which combines digital LUT (Look-up Table) and injection. These techniques are applied to both two-tone tests and 16 QAM (Quadrature Amplitude Modulation) signals. The test power amplifiers vary from class A, inverse class E, to cascaded amplifier systems.

Our experiments have demonstrated that these new predistortion techniques can reduce the upper and lower sideband third order intermodulation products in a two-tone test by 60 dB, or suppress the spectral regrowth by 40 dB and reduce the EVM (Error Vector Magnitude) down to 0.7% rms in 16 QAM signals, disregarding whether the tested power amplifiers or cascade amplifier systems exhibit significant nonlinearities and memory effects.

ACKNOWLEDGEMENTS

The research would not have been possible without my supervisor, Dr Peter Gardner. I would like to take this opportunity to thank him for his encouragement, advice and all the supports including academic and non-academic. The internal assessor, Prof. Hall, provided helpful comments for my PhD reports. Research fellow, Mury Thian, gave suggestions on my papers. Other members of the Communication Engineering research group and the department, who contributed in various helps such as lab equipment set up (Allan Yates) and computer installation (Gareth Webb). Dr Steven Quigley and Dr Sridhar Pammu, gave useful advice and support on FPGA broad.

There are some people who did not contribute to the work itself, but supported me during the work, my parents, my girl friend, Jian Chen, and my friends, Zhen Hua Hu, Qing Liu, Jin Tang, and Kelvin.

Finally I acknowledge my financial support provided by the Engineering and Physical Sciences Research Council.

ABBREVIATIONS

ACPR	**A**djacent **C**hannel **P**ower **R**atio
ADC	**A**nalog-to-**D**igital **C**onverter
AM	**A**mplitude **M**odulation
ANFIS	**A**daptive **N**euro-**F**uzzy **I**nference **S**ystem
ANN	**A**rtificial **N**eural **N**etwork
ARMA	**A**uto-**R**egressive **M**oving **A**verage filter
BP	**B**ack **P**ropagation
BPF	**B**and **P**ass **F**ilter
CDMA	**C**ode **D**ivision **M**ultiple **A**ccess
CMOS	**C**omplementary **M**etal **O**xide **S**emiconductor
DAC	**D**igital-to-**A**nalog **C**onverter
DC	**D**irect **C**urrent
DECT	**D**igital **E**nhanced **C**ordless **T**elecommunications
DSP	**D**igital **S**ignal **P**rocessing/**P**rocessor
DUT	**D**evice **U**nder **T**est
EDET	**E**nvelope **DET**ector
EPD	**E**nvelope **P**re**D**istorter
EVM	**E**rror **V**ector **M**agnitude
FIR	**F**inite **I**mpulse **R**esponse
FIS	**F**uzzy **I**nference **S**ystem
FPGA	**F**ield **P**rogrammable **G**ate **A**rray
GPS	**G**lobal **P**ositioning **S**ystem
GSM	**G**lobal **S**ystem for **M**obile communication
IC	**I**ntegrated **C**ircuit
IF	**I**ntermediate **F**requency
IIR	**I**nfinite **I**mpulse-**R**esponse
IM3	Third -order **I**nter**M**odulation
IM3L	**L**ower Third-order **I**nter**M**odulation product
IM3U	**U**pper Third-order **I**nter**M**odulation product
LTI	**L**inear **T**ime **I**nvariant
LUT	**L**ook-**U**p **T**able
L+I	**L**ook-up table plus **I**njection
PA	**P**ower **A**mplifier
PC	**P**ersonal **C**omputer

PD	**P**re**D**istorter
PLL	**P**hase **L**ock **L**oop
PM	**P**hase **M**odulation
QAM	**Q**uadrature **A**mplitude **M**odulation
QPSK	**Q**uadrature **P**hase-**S**hift **K**eying
RF	**R**adio **F**requency
TWT	**T**raveling **W**ave **T**ube
UMTS	**U**niversal **M**obile **T**elecommunications **S**ystem
VMOD	**V**ector **MOD**ulator
VSA	**V**ector **S**ignal **A**nalyzer
WLAN	**W**ireless **L**ocal **A**rea **N**etwork

CONTENTS

FIGURES

TABLES

CHAPTER 1

INTRODUCTION

Nowadays, the mobile phone is an essential accessory for everyone. Thus, researchers and engineers in communication technology are exploring new devices for wireless transceivers for the demanded market. The power amplifier is the key component in the transmitter. For a power amplifier, high power efficiency is a basic requirement because of the energy issue. At the same time, high linearity is more and more desirable today, to minimize the frequency interference and allow higher transmission capacity in wideband communication systems. The more linear the transmitters, the more user channels can be fitted in to the available spectrum. Particularly with the trend of mobile phone technology moving towards multi-band and multi-mode systems, where different wireless communication standards such as global positioning system (GPS), digital enhanced cordless telecommunications (DECT), global system for mobile communications (GSM), universal mobile telecommunications system (UMTS), Bluetooth and wireless local area network (WLAN) are to be integrated altogether. Power amplifiers with both excellent linearity and high power efficiency are increasingly essential in the transmitters. However, it is well known that high linearity will sacrifice the power efficiency in power amplifiers. The only solution for this problem is linearization. As a result, linearization techniques which allow power amplifiers to have both high power efficiency and high linearity, interest the researchers.

1.1 Power efficiency, linearity and linearization

All power amplifiers have nonlinear properties, which become dominant in their saturation range. On the other hand, the maximum power efficiency generally occurs

in their saturation range. The linearization scheme is to balance these two conditions, which is shown in Fig. 1-1.

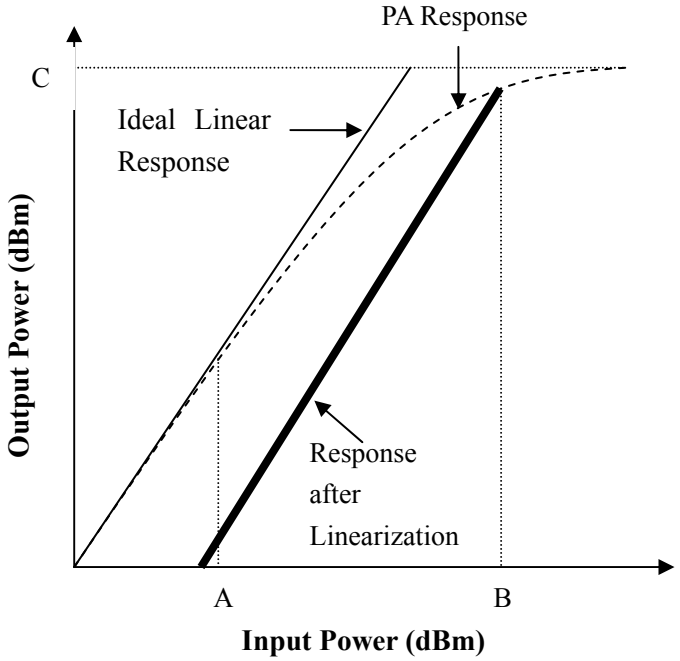

Figure 1-1 Power amplifier linearization scheme

The dashed line represents a general power amplifier (PA) transfer characteristic. It saturates at point C at the output port. Normally, it will be required to work at its maximum output power as high as C, in order to achieve high power efficiency. However, if we want the linearity as priority, it will have to be only working at the maximum input power at A. This will result in a large decrease of power efficiency which is not acceptable in most applications. This situation can be improved by a linearization scheme. The aim for linearization is to make most of the operating range of the power amplifier linear, which is shown as bold line in Fig. 1-1. After this correction, the amplifier can again work at input maximum power at B, which is close to its saturation, but with a linear performance. There are different kinds of linearization techniques which can implement this purpose. They can be categorized into analogue and digital means.

1.2 Analogue linearization

1.2.1 Feedback

The basic structure of feedback circuit is shown in Fig. 1-2.

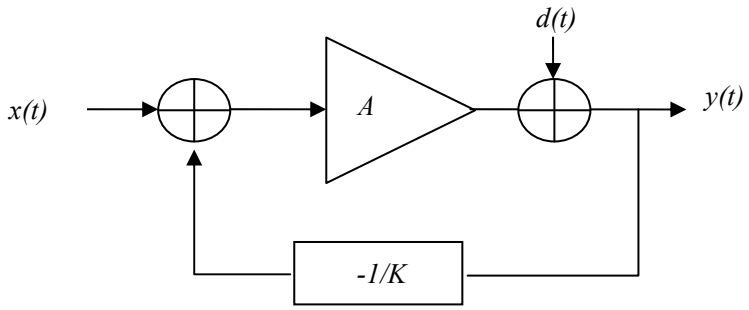

Figure 1-2 General feedback structure

In this structure, the input signal is *x(t)*, the gain of the PA is *A*, the gain of the feedback loop is *-1/K*, and the distortion is *d(t)* which is added after the gain of the PA. The output can be obtained directly as:

$$y(t) = \frac{AK}{K + A} x(t) + \frac{K}{A + K} d(t) \tag{1.1}$$

If we assume that the amplifier gain is much greater than the feedback loop gain, i.e., $A>>K$, (1.1) can be simplified to:

$$y(t) = Kx(t) + \frac{K}{A} d(t) \tag{1.2}$$

From (1.2), we can see that the gain of the signal is lowered from *A* down to *K*, and

the distortion will be significantly reduced by *K/A*.

A typical feedback loop for linearization techniques is Cartesian feedback, further detail can be found in [1].

1.2.2 Feed forward

Fig. 1-3 shows a feed forward linearization scheme [2].

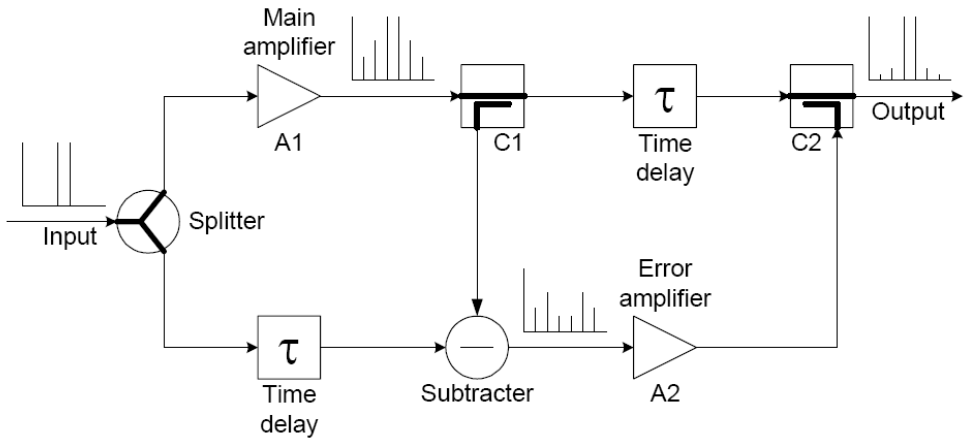

Figure 1-3 Feed forward linearization

In the lower branch of the circuit, a sample of the input is subtracted from a sample of output of the main amplifier, to generate an error signal, or intermodulation products in the spectral domain. This error signal is amplified though an error amplifier, to have the same amplitude as the output error of the main amplifier. A time delay line is inserted between the two couplers in the upper branch, which make the errors from the two branches have 180 degree phase difference. The errors cancel each other in the last coupler, making the output linear again.

1.2.3 Limitation of these techniques

In the feedback predistortion, the output signal goes back to the subtractor through the feedback loop. This will take a certain time. When considering this delay of the feedback loop, the overall equation is:

$$y(t) = Ax(t) - \frac{A}{K} y(t - \Delta t) + d(t) \tag{1.3}$$

where Δt denotes the delay of the feedback loop. It is only when *y(t)* is equal or near to *y(t-*Δt*)*, that (1.3) can equal to (1.1). In RF field, a small time delay can cause a great phase shift. Hence, the difference between *y(t)* and *y(t-*Δt*)* can be significant and fatal in an RF transmitter.

On the other hand, the feed forward technique has a power efficiency problem. The lower branch amplifier consumes a certain power. However, this output does not make a positive contribution, but a subtraction from the output of main amplifier. From the point of view of power, the error amplifier is making extravagant consumption. Practically, this kind of linearization (i.e. Feed forward) has 20% of power efficiency at best. This compares poorly with other linearization schemes such as predistortion, where efficiencies greater than 50% can be achieved.

1.3 Digital predistortion for linearization

Besides analogue linearization, there are different kinds of digital predistortion techniques. The basic idea is shown in Fig. 1-4.

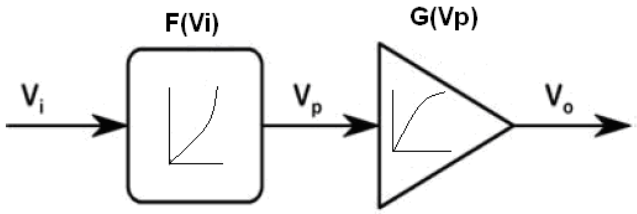

Figure 1-4 Schematic of an amplifier and its predistorter

The function $F(V_i)$ denotes the normalized digital predistortion transfer function, while the function $G(V_i)$ denotes the normalized amplifier transfer function. Mathematically, if $F(V_i)$ is the inverse function of $G(V_i)$, the overall output would become the same as the input, as proved in (1.4).

$$V_0 = G(V_p) = G(F(V_i)) = G(G^{-1}(V_i)) = V_i \tag{1.4}$$

Digital predistortion techniques have several advantages. Firstly, it does not have a loop nor delay issue. Secondly, it is operated before the amplifier, which means the signal processing does not consume large power. Thirdly, all the signal processing can be achieved in a DSP, making it much simpler in physical layout. Because of these advantages, we choose digital predistortion as the principle linearization technique in our research.

As shown in Fig. 1-4, and (1.4), predistortion can compensate nonlinearities in power amplifiers. However, RF power amplifiers also exhibit memory effects due to its components such as filters, matching elements, DC blocks and so on. Mathematically, memory effects will make the output of the amplifier depend not only on the simultaneous input signal, but also on the recent history of inputs. It can be also observed in spectrum asymmetry in a two-tone test. The predistortion function, like $F(V_i)$ in Fig.1-4 , is vulnerable to memory effects, and needs to be further developed.

1.4 Scope of the thesis

This thesis investigates and implements published and novel techniques in digital predistortion linearization. The organization of this thesis is as follows:

Since the ideal digital predistorter is the inverse function of the power amplifier's transfer characteristic, Chapter 2 will firstly review published models which describe the nonlinearities for the power amplifiers, and then their inverse models which perform as predistorters. Meanwhile, we will explore memory effects as well, which decrease the results of these digital linearization techniques. Further, we will introduce another digital predistortion technique named injection. We will analyze its mechanism and compare it with conventional digital predistortion.

After examining published injection techniques, we present our injection technique in Chapter 3 and 4. Chapter 3 will focus on its application in two-tone tests, while Chapter 4 will focus on 16 QAM wideband signals. In these two chapters, we will fully explore this injection technique, including its advantages, technical problems existing in related published work and our solutions. Hence, our novel injection yields further improvements in terms of intermodulation reductions in two-tone test cases and spectral regrowth reductions in wideband signal cases.

This new injection technique is firstly combined with LUT predistortion in Chapter 5. The aim is to make this new predistortion (L+I) inherit the advantages from LUT and injection. The overall performance is better than any single technique, in terms of adjacent channel power ratio (ACPR) and error vector magnitude (EVM) reduction. This has been demonstrated with a cascaded PA system which shows both significant nonlinearities and memory effects.

CHAPTER 2

BACKGROUND

This chapter generally outlines several published models of power amplifiers and predistorters.

2.1 Power amplifier modeling

The objective of linearization is to produce highly linear power amplifiers. Specifically, a perfect predistorter is an inverse model of the power amplifier. As a result, to explore various PA models is the priority of the research. The PA models can be divided into two general categories. One is the memoryless nonlinear model and the other is nonlinear with memory effect model [2].

2.1.1 Memoryless nonlinear power amplifier model

This kind of model only describes the nonlinearities that exist in the PA. In other words, in a two-tone test, the intermodulation products do not depend on the frequencies and tone spacing of the carriers. This kind of model is suitable to describe the PA response for single sine waves and narrow bandwidth signals.

2.1.1.1 AM/AM and AM/PM conversion

AM/AM and AM/PM conversion provide the basis for a well-know memoryless PA model. AM/AM describes the relationship between input power and output power,

while AM/PM describes the relationship between input power and output phase shift [3].

Suppose the input signal is:

$$x(t) = r(t)\cos[\omega_0 t + \psi(t)] \tag{2.1}$$

Where ω_0 is the carrier frequency, and $r(t)$ and $\Psi(t)$ are the modulated envelope and phase, respectively. The output signal written in the form of AM/AM ($A(r)$) and AM/PM ($\Phi(r)$) conversion is:

$$y(t) = A[r(t)]\cos[\omega_0 t + \psi(t) + \Phi[r(t)]] \tag{2.2}$$

These conversions can be observed experimentally by inputting a sinusoidal signal into the PA [4]. Fig. 2-1 and Fig. 2-2 show example plots of AM/AM and AM/PM conversions.

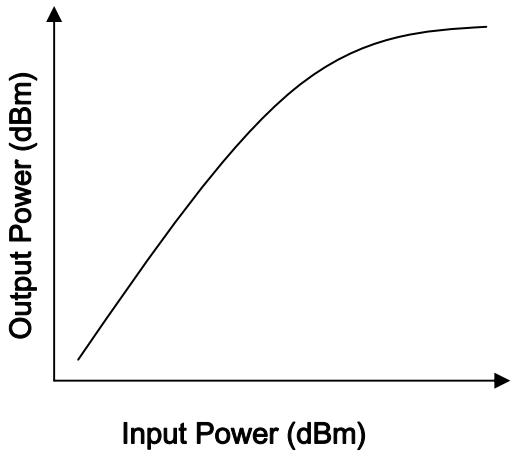

Figure 2-1 AM/AM conversion

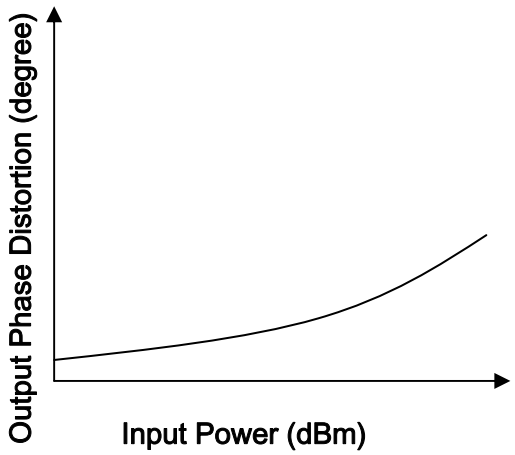

Figure 2-2 AM/PM conversion

2.1.1.2 Memoryless polynomial model

The input-output relation of a memoryless PA can be written in the form of a polynomial:

$$y = a_1 x + a_2 x^2 + a_3 x^3 + a_4 x^4 + a_5 x^5 + \ldots \tag{2.3}$$

where x and y represent the input and output signal, and a are complex coefficients.

This model can calculate the two-tone test simply. If a two-tone signal is:

$$x(t) = V\cos(\omega_1 t) + V\cos(\omega_2 t) \tag{2.4}$$

We substitute (2.4) into (2.3), and get:

$$\begin{aligned} y(t) = {} & a_1 V\left[\cos(\omega_1 t) + \cos(\omega_2 t)\right] + a_2 V^2\left[\cos(\omega_1 t) + \cos(\omega_2 t)\right]^2 \\ & + a_3 V^3\left[\cos(\omega_1 t) + \cos(\omega_2 t)\right]^3 + a_4 V^4\left[\cos(\omega_1 t) + \cos(\omega_2 t)\right]^4 \\ & + a_5 V^5\left[\cos(\omega_1 t) + \cos(\omega_2 t)\right]^5 + \ldots \end{aligned} \tag{2.5}$$

All the resulting harmonic and intermodulation products are listed in Table 2-1.

Order	Terms	a_1V	a_2V^2	a_3V^3	a_4V^4	a_5V^5
Zero	DC		1		9/4	
First	ω_1	1		9/4		25/4
	ω_2	1		9/4		25/4
Second	$2\omega_1$		1/2		2	
	$2\omega_2$		1/2		2	
	$\omega_1\pm\omega_2$		1		3	
Third	$3\omega_1$			1/4		25/16
	$3\omega_2$			1/4		25/16
	$2\omega_1\pm\omega_2$			3/4		25/8
	$2\omega_2\pm\omega_1$			3/4		25/8
Fourth	$4\omega_{12}$				1/8	
	$4\omega_2$				1/8	
	$3\omega_1\pm\omega_2$				1/2	
	$3\omega_2\pm\omega_1$				1/2	
	$2\omega_1\pm\omega$				3/4	
Fifth	$5\omega_1$					1/16
	$5\omega_2$					1/16
	$4\omega_1\pm\omega_2$					5/16
	$4\omega_2\pm\omega_1$					5/16
	$3\omega_1\pm2\omega_2$					5/8
	$3\omega_2\pm2\omega_1$					5/8

Table 2-1 Two-tone intermodulation products up to fifth order

In narrow band systems, the even-order products cause less concern than the odd-order products, since they are out of band and can be filtered out easily. The two-tone test output spectrum close to the carriers is shown in Fig. 2-3.

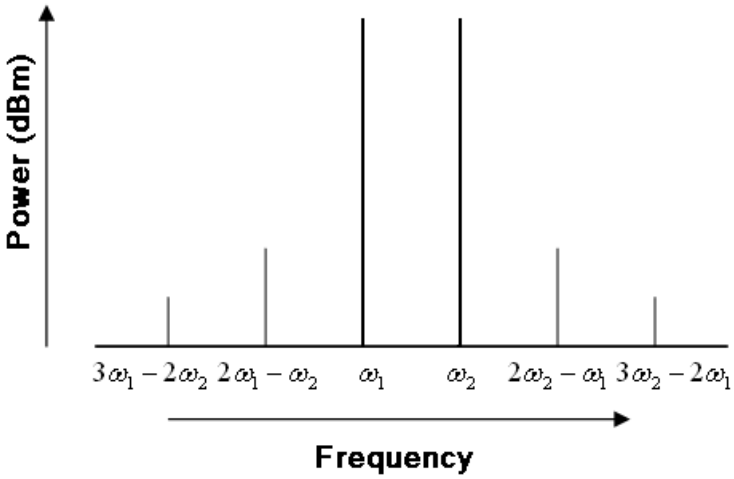

Figure 2-3 Two-tone test output spectrum close to carriers

Similarly, the multi-tone intermodulation distortion analysis by using memoryless polynomial model can be obtained, as shown in [5].

2.1.1.3 Saleh model (frequency-independent)

In 1981, Saleh proposed nonlinear models of TWT amplifiers— the Saleh model [6]. It still applies the AM/AM and AM/PM conversion. However, (2.2) gives two arbitrary functions of amplitude distortion *A(r)* and phase distortion *Φ(r)* , while Saleh model gives more explicit formulas by introducing four parameters, as shown in (2.6).

$$\begin{aligned} A(r) &= \alpha_a r / \left(1 + \beta_a r^2\right) \\ \Phi(r) &= \alpha_\Phi r^2 / \left(1 + \beta_\Phi r^2\right) \end{aligned} \tag{2.6}$$

Furthermore, he also proposed a practical model to implement the principle AM/AM and AM/PM conversions, as shown in Fig. 2-4.

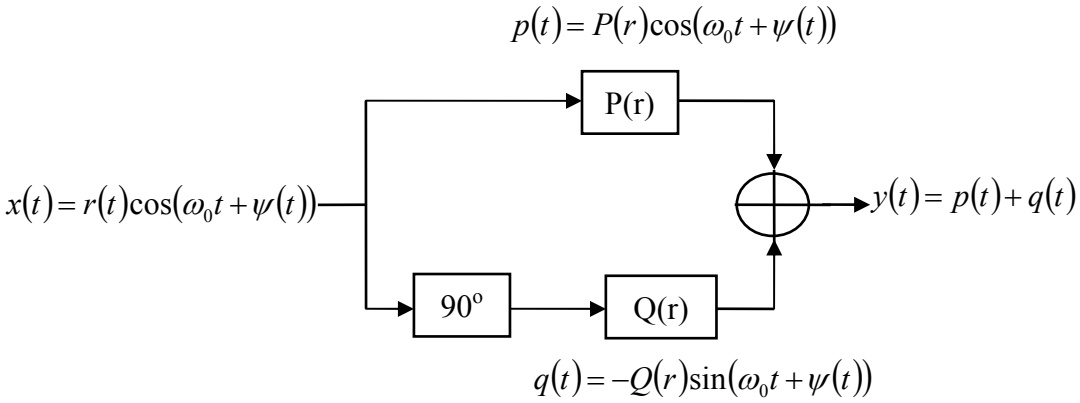

Figure 2-4 Quadrature nonlinear model of PA in [6]

In Fig.2-4:

$$\begin{aligned} P(r) &= A(r)\cos[\Phi(r)] \\ Q(r) &= A(r)\sin[\Phi(r)] \end{aligned} \tag{2.7}$$

Suppose the input is the same as (2.1), this model will give the output of:

$$\begin{aligned} y(t) &= p(t) + q(t) \\ &= P(r)\cos[\omega_0 t + \psi(t)] - Q(r)\sin[\omega_0 t + \psi(t)] \\ &= A(r)\cos[\Phi(r)]\cos[\omega_0 t + \psi(t)] - A(r)\sin[\Phi(r)]\sin[\omega_0 t + \psi(t)] \\ &= A(r)\cos[\omega_0 t + \psi(t) + \Phi(r)] \end{aligned} \tag{2.8}$$

which is the same as (2.2).

2.1.2 Memory effects

Memory effects cause the amplitude and phase of distortion components to vary with the modulation frequency [7] , hence generating asymmetry between intermodulation products.

Take the third order intermodulation products (IM3) for example. In a memoryless PA, according to Table 2-1, the lower and upper sideband IM3 levels are:

$$IM3 = \frac{3}{4} a_3 V^3 \tag{2.9}$$

Equation (2.9) shows that IM3 is not a function of tone spacing and that the upper and lower IM3 should have the same magnitude. But in some cases [8, 9], these IM3s are asymmetric, and their ratio changes as the tone spacing varies, and this is caused by memory effects.

Memory effects can have thermal or electrical origins. Thermal memory effects are caused by electro-thermal couplings, while electrical memory effects [10] are caused by the way the impedances seen by the baseband, fundamental and harmonic signal components vary with the modulation frequency. Both of these memory effects can affect modulation frequencies up to a few megahertz. As a result, PA models considering memory effects are more practical in wideband communication.

2.1.3 Nonlinear with memory effect power amplifier model

Different from the memoryless model, these models describe both of the nonlinearities and memory effects that exist in PAs.

2.1.3.1 Frequency-dependent nonlinear quadrature model

Saleh also proposed a frequency-dependent model in [6], which is shown in Fig.2-5.

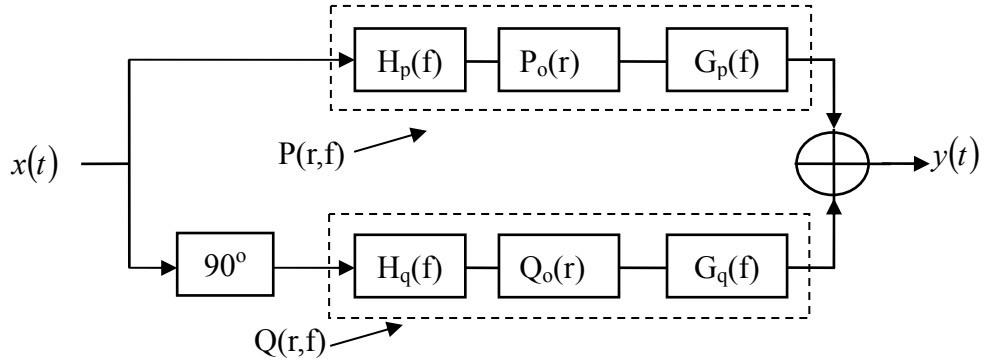

Figure 2-5 Saleh's frequency-dependent model of a TWT amplifier in [6]

Fig.2-5 is an extension of Fig.2-4, which adds linear filters $H_{p/q}$ and $G_{p/q}$ in I and Q branches. For example, the signal passing through the in-phase branch can be divided into three steps: first, the input amplitude is scaled by $H_p(f)$; next, the resulting signal passes through the frequency-independent envelope nonlinearity $P_o(r)$; and finally, the output amplitude is scaled by $G_p(f)$. These three similar steps apply to the quadrature branch as well. The scaling coefficients $H_{p/q}(f)$ and $G_{p/q}(f)$ are sensitive to different frequencies, and make the model frequency-dependent.

Alternatively, Abuelma'Atti expands the in-phase and quadrature nonlinearities in Fig. 2-4, to the first order Bessel functions (2.10) [11]. The new model is shown in Fig. 2-6.

$$\begin{aligned} P(r) &= \sum_{n=1}^{N} \gamma_{nI} J_1\left(\frac{n\pi r}{D}\right) \cdot G_{nI}(f) \\ Q(r) &= \sum_{n=1}^{N} \gamma_{nQ} J_1\left(\frac{n\pi r}{D}\right) \cdot G_{nQ}(f) \end{aligned} \tag{2.10}$$

In (2.10), $\gamma_{nI(Q)}$ is used to provide a minimum mean-square fit to the samples of input and output two-tone tests of amplifiers while $G_{nI(Q)}(f)$ is a filter which is sensitive to frequency. This model is more complicated compared with the Saleh

model. Due to its complexity, the choice of fitting functions is not addressed here.

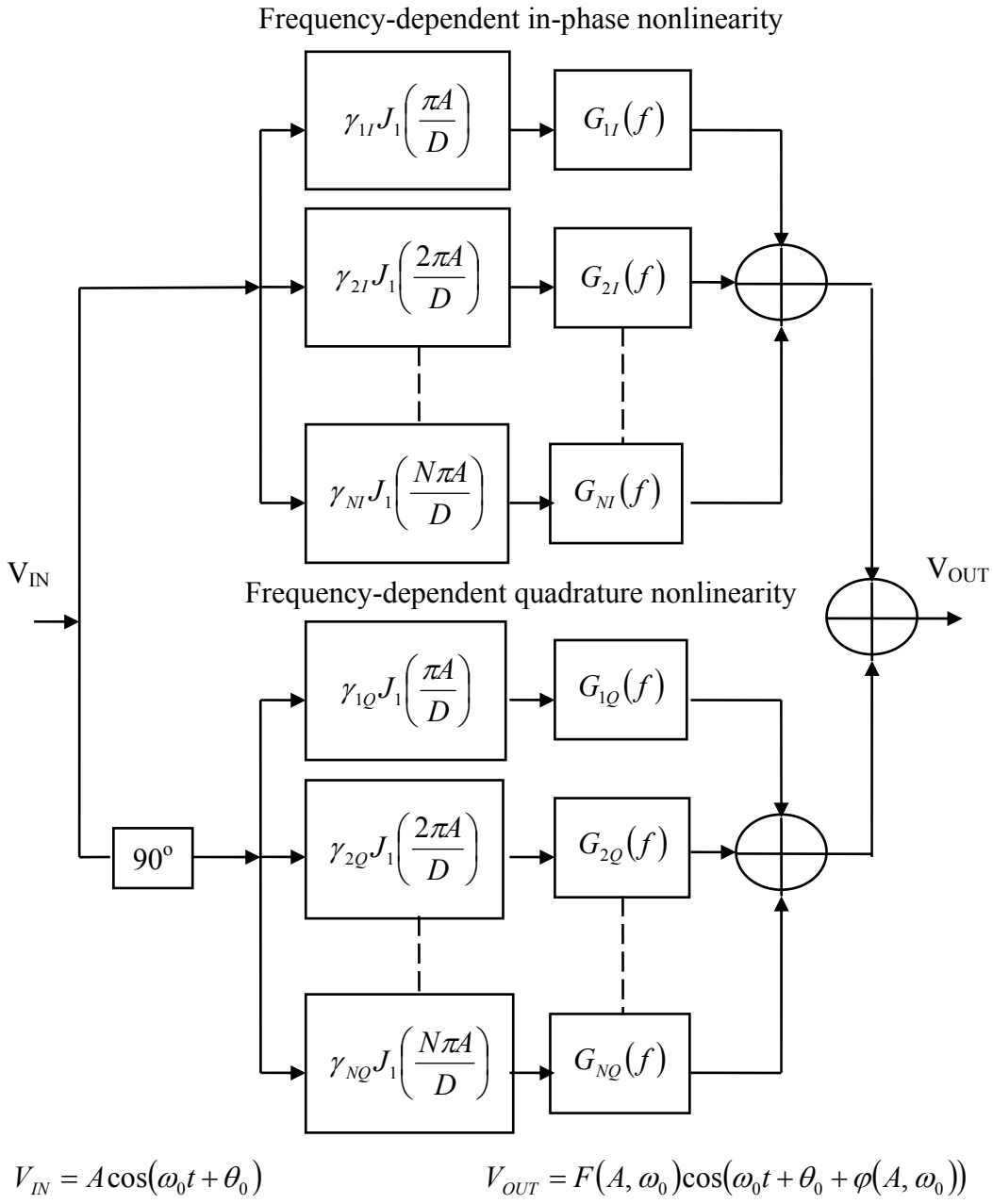

Figure 2-6 Abuelma'Atti's frequency-dependant Quadrature model in [11]

2.1.3.2 Clark's ARMA model

Clark proposed an extension of the memoryless envelope model in [12]. This model applies an auto-regressive moving average (ARMA) filter at the input as shown in Fig.

2-7.

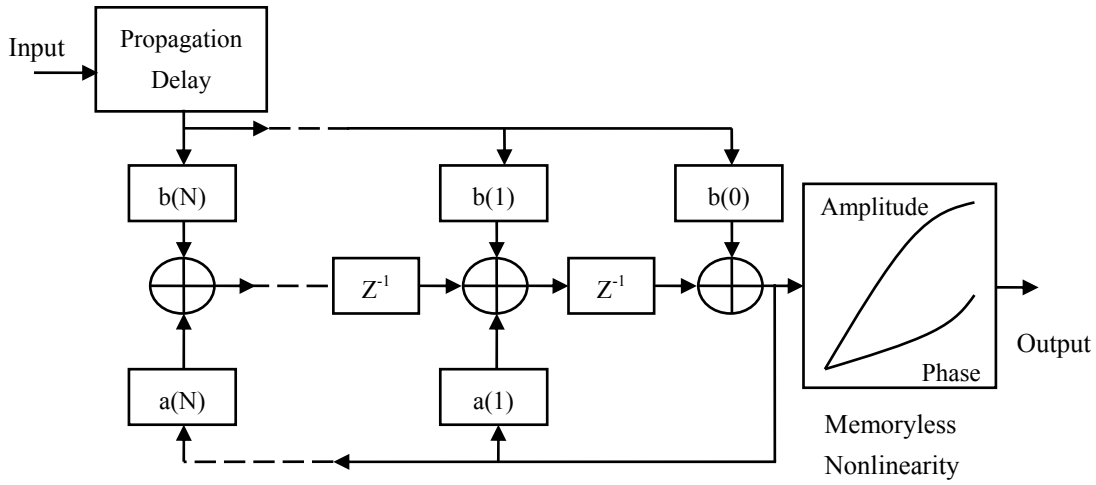

Figure 2-7 Nonlinear ARAM model of PA

The filter is an infinite impulse-response (IIR) filter (2.11), which makes it frequency-dependent.

$$y(k)=\sum_{i=0}^{N} b_i x(k-i)-\sum_{i=1}^{N} a_i y(k-i) \tag{2.11}$$

2.1.3.3 Volterra series

Mathematically, Volterra series is a universal nonlinear model with memory [2, 13], which can be expressed in (2.12):

$$\begin{aligned} D(t)&=\sum_{n=0}^{\infty} D_n(t) \\ D_n(t)&=\int_{-\infty}^{\infty}\cdots\int_{-\infty}^{\infty} h_n(\tau_1,,,\tau_n)x(t-\tau_1)\ldots x(t-\tau_n)d\tau_1\ldots d\tau_n \end{aligned} \tag{2.12}$$

The functions $h_n(\tau_1,,,\tau_n)$ are nth-order Volterra kernels.

Practically, there is a serious drawback of the Volterra model, in that it needs a large number of coefficients to represent Volterra kernels. Therefore, it is derived into two special cases: memory polynomial model [13-17] and Wiener model [16].

Paper [18] proposed a Wiener system. It consists of several subsystems connected in parallel, as shown in Fig. 2-8.

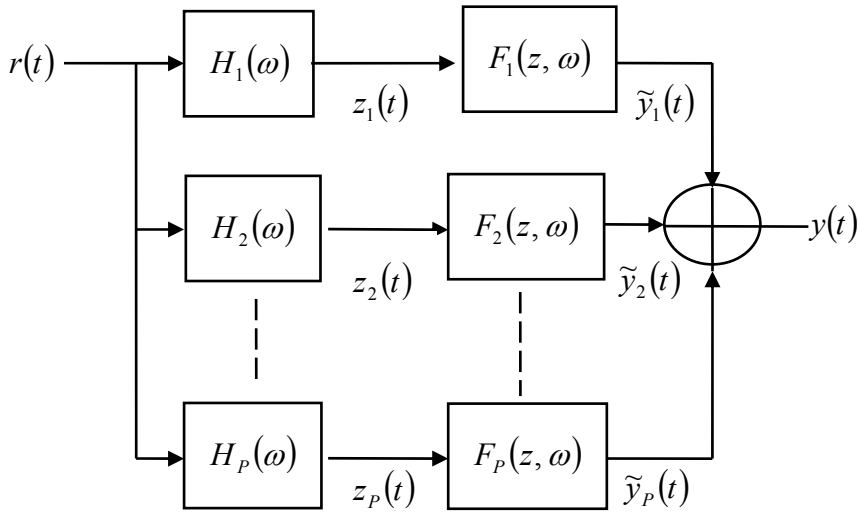

Figure 2-8 Parallel Wiener model in [18]

Each subsystem has a linear time invariant (LTI) system with function of $H()$, followed by frequency-dependent complex power series with function of $F()$.

Suppose the envelope frequency is ω_m, and the input signal is z, the functions of $F()$ is:

$$F(z,\omega_m) = a_1(\omega_m)z + a_3(\omega_m)z^3 + \ldots + a_{2n-1}(\omega_m)z^{2n-1} \tag{2.13}$$

where $a(\omega_m)$ are the coefficients of the frequency-dependent complex polynomial.

The LTI system $H()$ has the following characteristic function:

$$H_i(\omega_m) = |H_i(\omega_m)| e^{j\Omega_i(\omega_m)} \tag{2.14}$$

When an input signal $A\cos(\omega_m t)$ is applied, the output is:

$$\begin{aligned} y_p(t) &= \sum_{i=1}^{p} \tilde{y}_i(t) \\ &= \sum_{i=1}^{p} F_i(z_i) \\ &= \sum_{i=1}^{p} a_{1,i}(\omega_m) z + a_{3,i}(\omega_m) z^3 + \ldots + a_{2n-1,i}(\omega_m) z^{2n-1} \\ &= \sum_{i=1}^{p} \left\{ \begin{array}{l} a_{1,i}(\omega_m)\left(A|H_i(\omega_m)|\cos(\omega_m t + \Omega_i(\omega_m))\right) \\ + a_{3,i}(\omega_m)\left(A|H_i(\omega_m)|\cos(\omega_m t + \Omega_i(\omega_m))\right)^3 + \\ \ldots + a_{an-2,i}(\omega_m)\left(A|H_i(\omega_m)|\cos(\omega_m t + \Omega_i(\omega_m))\right)^{2n-1} \end{array} \right\} \\ &= \sum_{i=1}^{p} \sum_{k=1}^{n} a_{2k-1,i}(\omega_m)\left(A|H_i(\omega_m)|\cos(\omega_m t + \Omega_i(\omega_m))\right)^{2k-1} \end{aligned} \tag{2.15}$$

where p is the number of parallel branches and n is the order of polynomial.

The parameters of $H()$ can be acquired using cross-correlation function of the input. The complex coefficients $a_{2k-1,i}$ are determined to minimize the mean square error between the outputs from simulation system and samples from the real device.

A memory polynomial model is proposed in [15], which is shown in Fig. 2-9. When compared with the Wiener model in [18], this model uses sparse delay taps on each parallel subsystem instead of LTI, and the functions are memory polynomials.

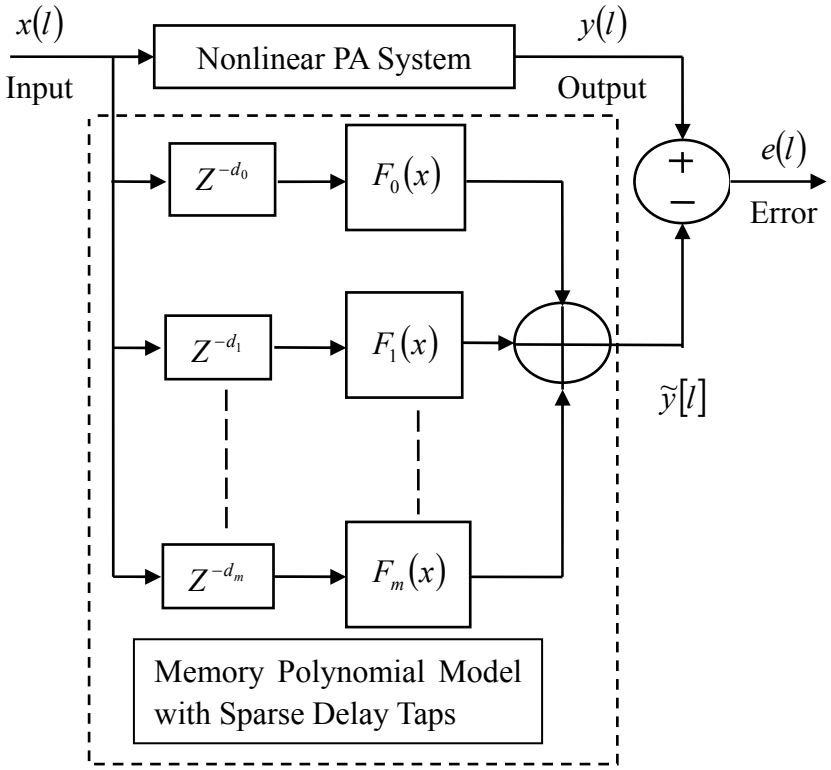

Figure 2-9 Memory polynomial model with sparse delay taps in [15]

Suppose the discrete complex input is *x[l]*, the function of *F*() is:

$$F_q(x[l]) = \sum_{k=1}^{n} a_{2k-1,q} \left| x[l] \right|^{2k-2} x[l] \tag{2.16}$$

where *n* is the order of the polynomials. The total output of the memory model is:

$$y[l] = \sum_{q=0}^{m} F_q(x[l-q]) = \sum_{q=0}^{m} \sum_{k=1}^{n} a_{2k-1,q} \left| x[l-q] \right|^{2k-2} x[l-q] \tag{2.17}$$

where *m* is the number of branches, and it also represents the length of memory effects.

2.1.3.4 Neural network based model

In [19], Ahemed *et al.* propose a new artificial neural network (ANN) model for power amplifiers. It is shown in Fig. 2-10. The inputs for this model are current input signal and optimum (sparse) delayed input signal. The ANN uses back propagation (BP) (described in 2.2.4.1) for modifying the weights to approximate the nonlinearities and memory effects of real amplifiers.

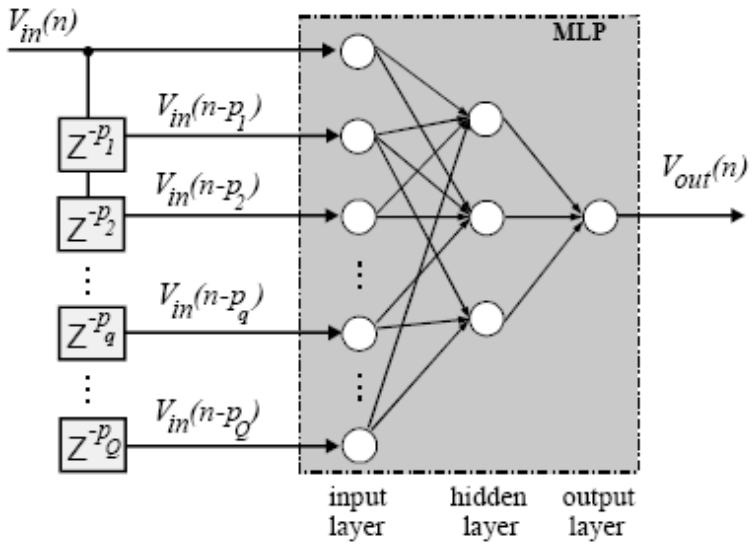

Figure 2-10 Time-delay neural network for PA model in [19]

2.2 Predistortion for power amplifiers

Efficiency is a primary concern for the PA designers. However, the trade off for high efficiency is normally a decrease in linearity, and the decreasing linearity contributes to spectral interference outside the intended bandwidth. Fortunately, there are linearization techniques that allow PAs to be operated at high power efficiency while with satisfying linearity requirements. There are many linearization techniques, such as predistortion [16], feedback [1, 2] and feed-forward[2]. Among them, predistortion promises better efficiency and lower cost. Because an ideal predistorter (PD) would

be an inverse function of the PA model, there are various PD models relative to the different PA models.

2.2.1 AM/AM and AM/PM conversion

The simplest concept for the predistorter is to generate the inverse of the AM/AM and AM/PM functions.

In 1983, J. Namiki proposed a nonlinear compensation technique (predistorter and prerotation) and its controller in [20]. The predistorter uses a cubic law device and phase shifter to compensate AM/AM and AM/PM distortion in PA. Experiment in [20] shows that the spectral regrowth has been reduced by 10dB. This kind of predistortion has been improved thereafter.

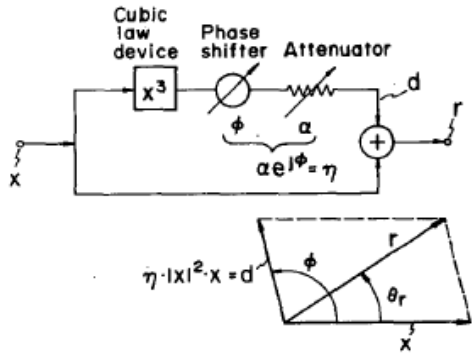

Figure 2-11 Predistorter proposed in [20]

As shown in Fig. 2-12, log amps and phase detectors are used at the input and output of the PA to estimate the instantaneous complex PA gain. This information is fed back to a voltage controlled variable attenuator and phase shifter, which is for AM/AM and AM/PM conversion [21]. Simulation of this predistortion has showed a 10 dB improvement on ACPR.

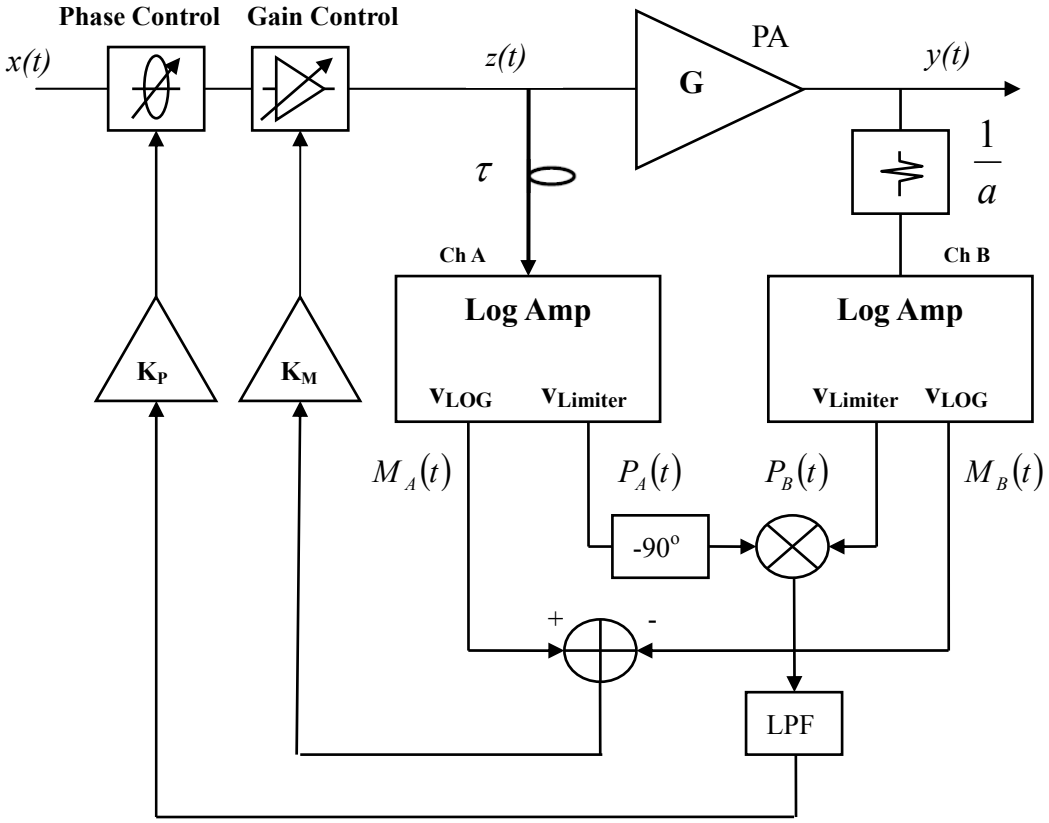

Figure 2-12 Envelope linearization in [21]

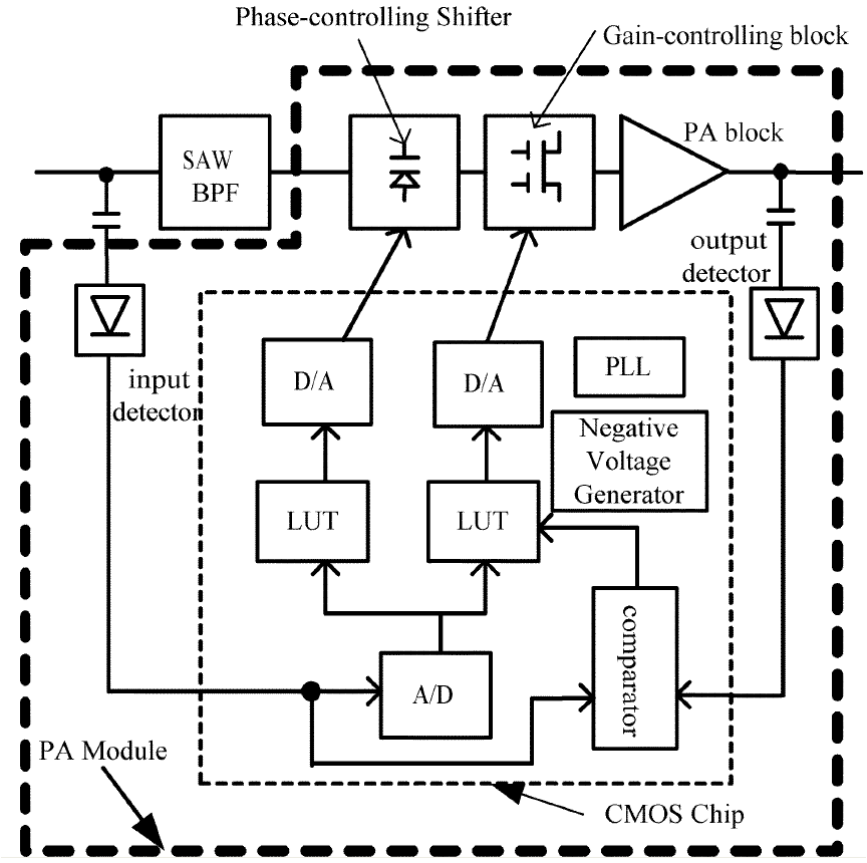

Figure 2-13 PDPA module in [22]

Instead of log amps and phase detectors, a Look-up Table (LUT) method can be used to control the gain and phase shift for the PD [22], as shown in Fig. 2-13. This LUT is a CMOS IC chip using a 0.25-μm process, which can be attached to the PA. By integrating all functions together, this PDPA module is applicable to handset terminals. A 7 dB improvement of ACPR is achieved in [22]. A similar example is also proposed in [9], with the block diagram shown in Fig. 2-14. There is a 12 dB improvement of ACPR in [9].

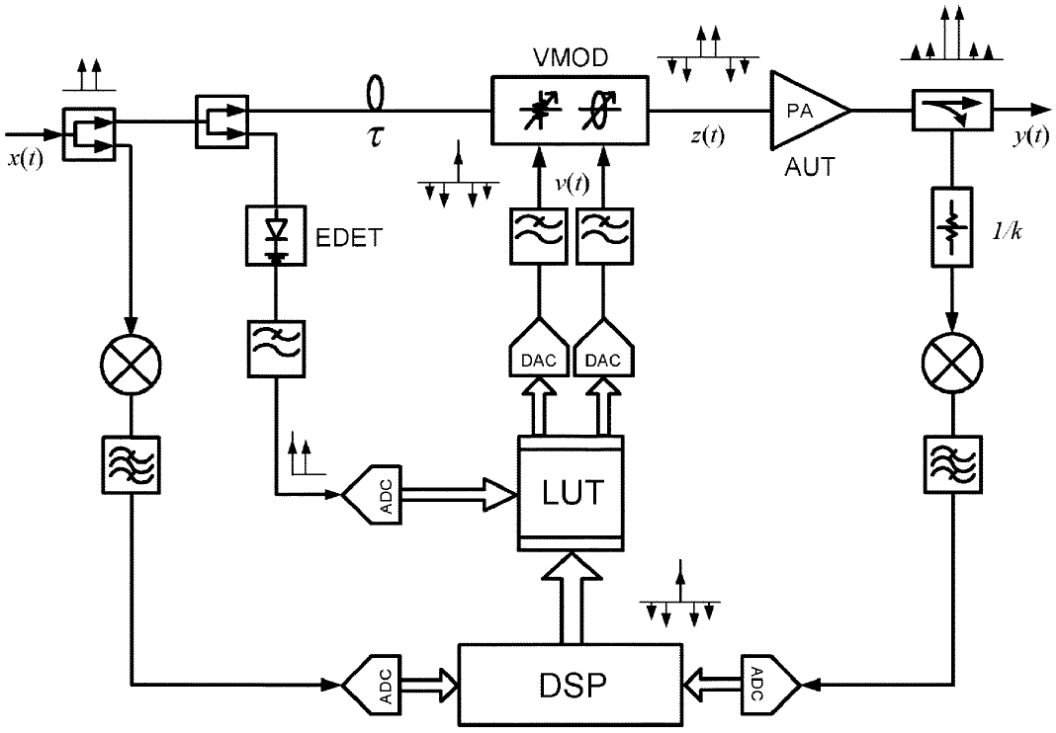

Figure 2-14 RF envelope predistortion system in [9]

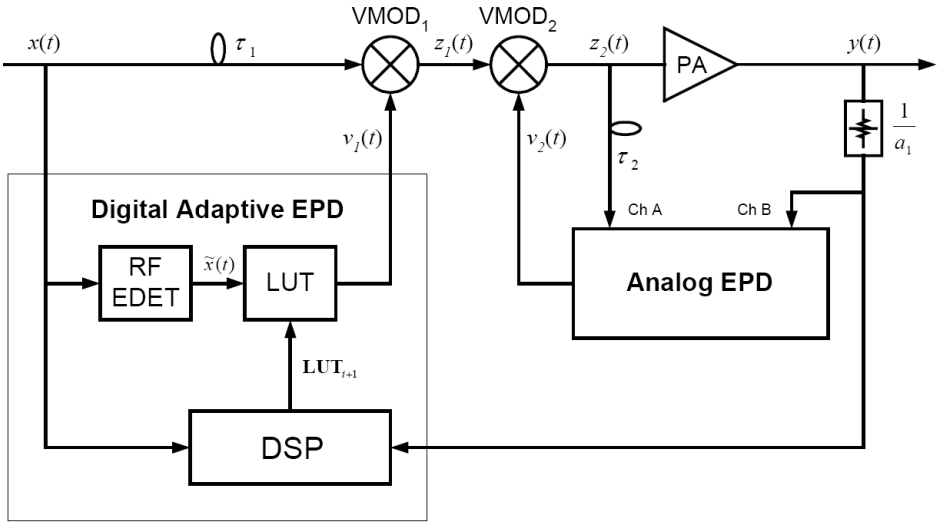

Figure 2-15 Combine digital/analogue cooperation predistortion in [23]

An upgraded predistorter which combines Fig. 2-12 and Fig. 2-14 is shown in Fig. 2-15 [23]. In this two-stage structure, the analogue envelope predistorter is used as an inner loop to correct slowly varying changes in gain, effectively compensating for long time constant memory effects, while the digital envelope predistorter forms the outer loop that corrects the distortion over a wide bandwidth. A 16 dB improvements on ACPR is achieved in [23].

2.2.2 Adjacent channel emissions

S. P .Stapleton, et al. proposed a slowly adapting predistorter in [24]. The structure is shown in Fig. 2-16. The approach is to use a filter and a power detector to extract intermodulation terms, and use these intermodulation products or complex spectral convolutions to control the parameters of predistorter.

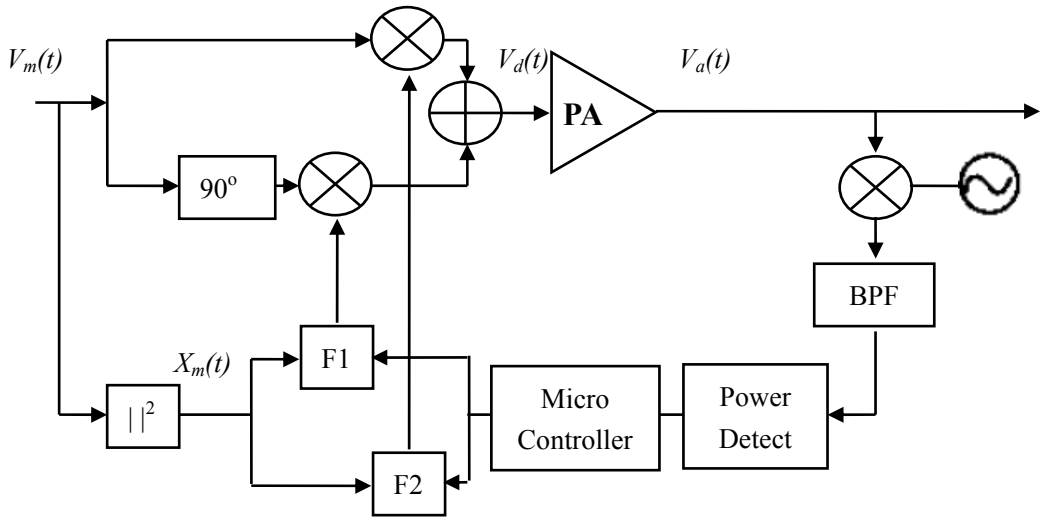

Figure 2-16 Predistorter proposed in [24]

Suppose the input signal for the entire system is $V_m(t)$, the input signal for the function F in the lower branch is $x_m(t)=|V_m(t)|^2$, and the function of F are:

$$F_1(x_m(t)) = \alpha_{11} + \alpha_{13}x_m(t) + \alpha_{15}x_m^2(t)$$
$$F_2(x_m(t)) = \alpha_{21} + \alpha_{23}x_m(t) + \alpha_{25}x_m^2(t) \quad (2.18)$$

So the complex gain of the predistorter can be expressed as:

$$F(x_m(t)) = F_1(x_m(t)) + jF_2(x_m(t)) = \alpha_1 + \alpha_3 x_m(t) + \alpha_5 x_m^2(t) \quad (2.19)$$

And the predistorter's output signal $V_d(t)$ now can be written as:

$$V_d(t) = V_m(t) \cdot F(x_m(t)) = \alpha_1 V_m(t) + \alpha_3 |V_m(t)|^2 V_m(t) + \alpha_5 |V_m(t)|^4 V_m(t) \quad (2.20)$$

By choosing appropriate values of α, the third- and fifth-order components can be cancelled at the PA output port. In the experiment of [24], a 15 dB improvement is obtained in the IM3 product in a two-tone test. Similar ideas are also proposed in [25].

2.2.3 Inverse Volterra model

Because memory effect plays a significant part in wideband communication, the predistorter based on the Volterra Model is popular nowadays. Again, the Volterra model needs a large number of coefficients, so the inverse function of a Volterra system is difficult to construct. As mentioned before, Wiener and memory polynomials are substitutes for the Volterra model. As a result, there are two corresponding predistorter models: the Hammerstein system [26, 27] and the inverse polynomial [13, 17, 28, 29]. Their relationships are shown in figure 2-17.

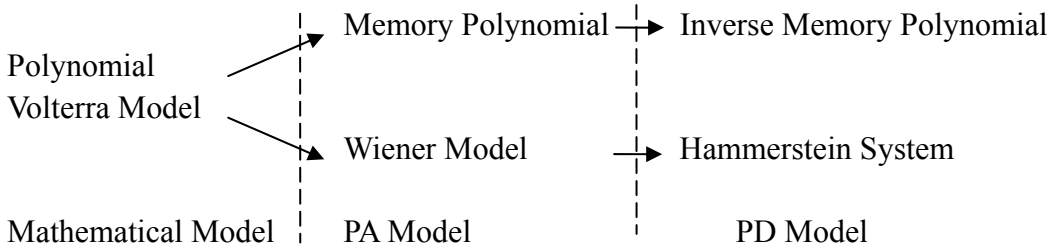

Figure 2-17 Relation between Volterra model and its PA/PD model

2.2.3.1 Inverse memory polynomial model

The Volterra series in (2.12) can be expressed in discrete time as:

$$\begin{aligned} y(n) = & \sum_{k=0}^{N} h_k^1 x(n-k) + \sum_{k=0}^{N}\sum_{l=0}^{N} h_{k,l}^2 x(n-k)x(n-l) \\ & + \sum_{k=0}^{N}\sum_{l=0}^{N}\sum_{m=0}^{N} h_{k,l,m}^3 x(n-k)x(n-l)x(n-m) + \ldots \end{aligned} \tag{2.21}$$

where N is the discrete system memory length, $x(n)$ and $y(n)$ are input and output.

Paper [13] applies the indirect learning architecture [30] to help to embed the Volterra model into the PD, which is shown in Fig. 2-18.

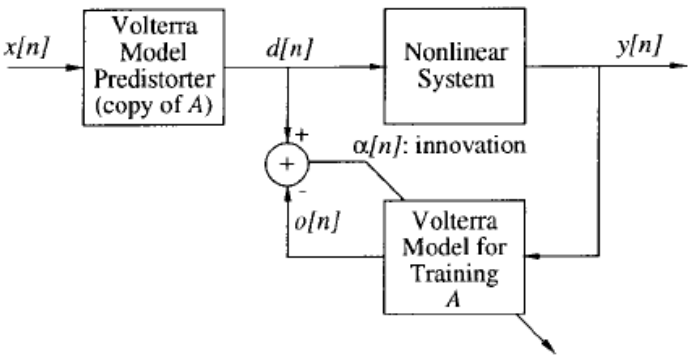

Figure 2-18 Indirect learning architecture for the predistorter

The idea in this paper is to uses two identical Volterra models (2.21) for the predistorter and training. The training process applies a recursive least squares algorithm. After the training, the innovation α*[n]* approaches zero, the output *y[n]* approaches the input *x[n]*, which means the overall system become linear. Similar polynomial models have been proposed, but with different ways to calculate the coefficients, such as Newton method[28], genetic algorithms[29] and least-squares solution[17].

2.2.3.2 Hammerstein model

Paper [26] proposes a Hammerstein predistortion structure shown in Fig. 2-19.

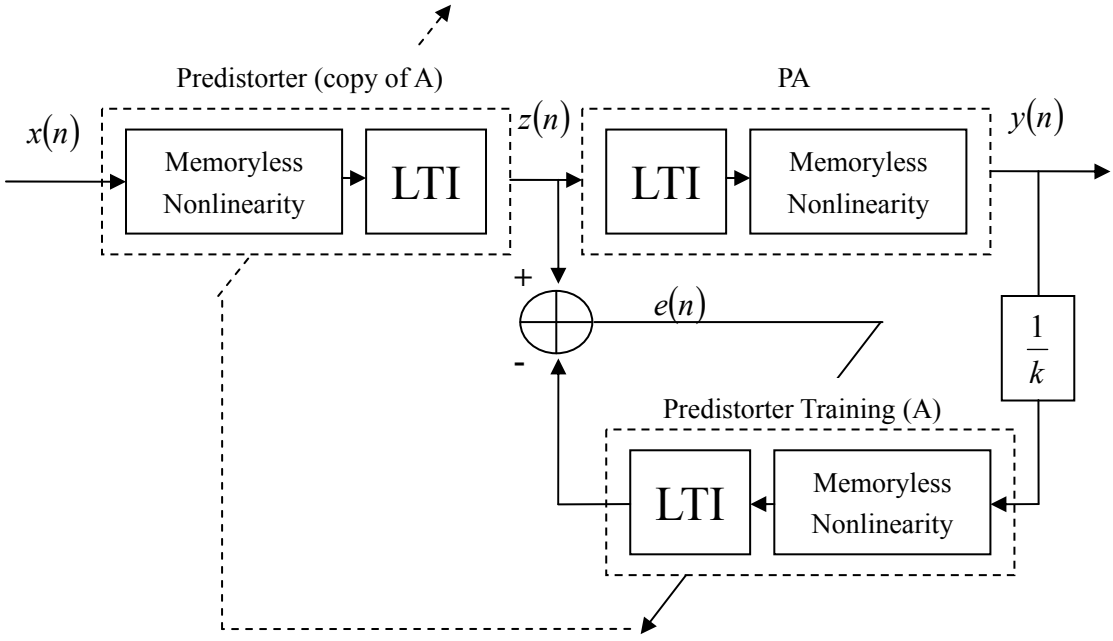

Figure 2-19 Hammerstein predistorter in indirect learning architecture in [26]

Suppose the input is *x(n)*, the output for the odd-order memoryless block is:

$$v(n)=\sum_{k=0}^{K} c_{2k+1}x(n)\left|x(n)\right|^{2k} \tag{2.22}$$

And the output *z(n)* from LTI system is:

$$z(n)=\sum_{p=1}^{P} a_p z(n-p)+\sum_{q=0}^{Q} b_q v(n-q) \tag{2.23}$$

So the entire relationship between input *x(n)* and output *z(n)* is:

$$z(n)=\sum_{p=1}^{P} a_p z(n-p)+\sum_{q=0}^{Q} b_q \sum_{k=0}^{K} c_{2k+1} x(n)\left|x(n)\right|^{2k} \tag{2.24}$$

The coefficients can be optimized by using Narendra-Gallman algorithm [26], and the simulation result has shown a 38 dB ACPR reduction.

Paper [27] proposed a similar Hammerstein predistorter, shown in Fig 2-20.

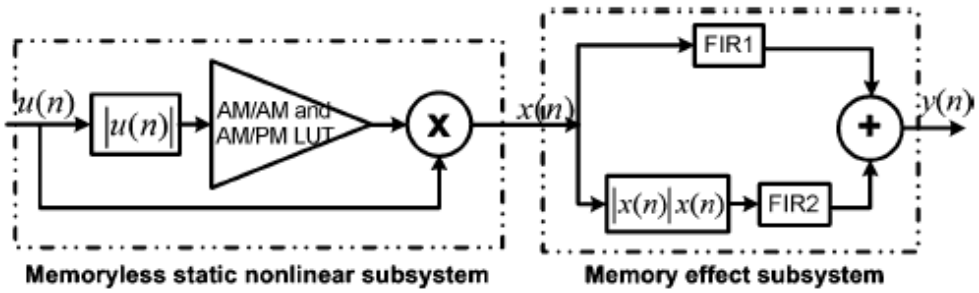

Figure 2-20 Augmented Hammerstein predistorter in [27]

When compared with [26], this model uses LUT instead of polynomial in (2.22), and finite impulse response (FIR) filter instead of recursive LTI in (2.24).

2.2.4 Computational method

Besides the traditional ideas, computational methods such as neural network [31] and adaptive neuro-fuzzy inference system (ANFIS) [32, 33] are brand new techniques. With its self-learning capabilities, a neural network could generate an inverse amplifier function after being trained.

2.2.4.1 Neural network

Neural networks are modeled after the physical architecture of human brains and they can use simple processing elements to perform complex nonlinear behaviors. Normally, a neural network is constructed by input signals, weights, neurons and their activation functions. Fig. 2-21 shows a simple neural network example.

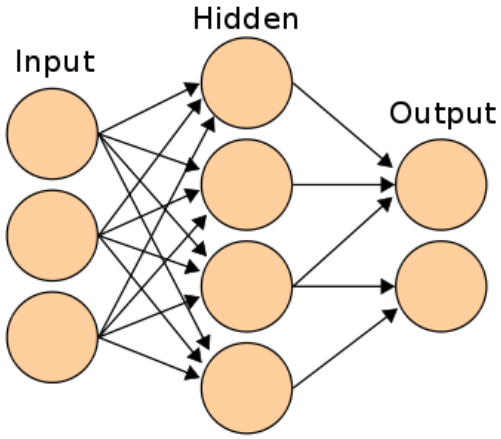

Figure 2-21 A simple neural network example

A neural network contains input ports ($X(x_1\ x_2\ x_3\ ...)$) and output ports ($O(o_1\ o_2\ o_3\ ...)$), which can be described as:

$$o_k = f^2\left(\left(\sum_j w_{jk} f^1\left(\left(\sum_i w_{ij} \times x_i\right) + b_j\right)\right) + b_k\right) \tag{2.25}$$

where W denote the weights, B denote the thresholds and f denote the activation functions. Typically, the activation functions are Sigmoid functions (2.26), as plotted in Fig.2-22.

$$f(x) = \frac{1}{1+e^{-x}} \tag{2.26}$$

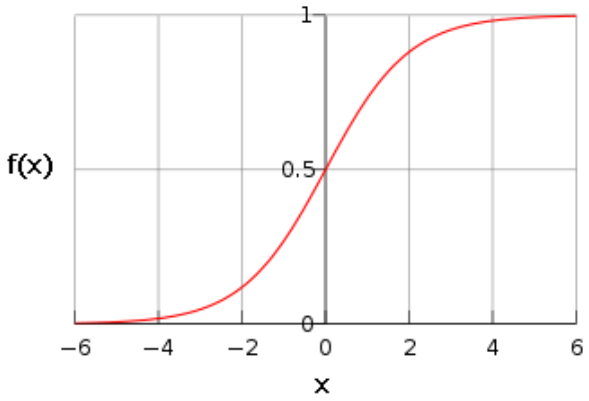

Figure 2-22 Sigmoid function

Back-propagation (BP) learning algorithm [34, 35] can be applied to adjust the weights. Suppose the training input output date sets are $X(x_1\ x_2\ x_3\ ...)$ and $Y(y_1\ y_2\ y_3\ ...)$, and the neural network are two-layer structure (2.25) with the Sigmoid function (2.26), the adjustment for weights are:

$$\Delta w_{jk} = \alpha o_k (y_k - o_k)(1 - o_k) o_j$$
$$\Delta w_{ij} = \alpha \left(\sum_k o_k (1 - o_k)(y_k - o_k) w_{jk} \right) o_j (1 - o_j) \qquad (2.27)$$

In (2.27), o means what we get from the layers of neural network, while y means what we want from the neural network, and α is the learning rate.

2.2.4.2 Fuzzy system and Fuzzy inference system

Two-valued or Boolean logic is a well-known theory. But it is impossible to solve all problems by mapping all kinds of situation into two-valued variables. Most real-world problems are characterized by a representation language to process incomplete, imprecise, vague or uncertain information. Fuzzy logic gives the formal tools to reason about such uncertain information. A fuzzy system is one which employs fuzzy logic [36].

A form of *if-then* rule in fuzzy system is shown as below:

if x is A then y is B

where A and B are linguistic values defined by fuzzy sets on the ranges x and y, respectively. The *if*-part of the rule "*x is A*" is called the antecedent or premise, while the *then-part* of the rule "*y is B*" is called the consequent or conclusion.

The Fuzzy Inference System (FIS) [37] is a system formed from the *if-then* rules. For example, we have two-input (x, y), two-rules, and defined the rules as:

Rule 1 if x is A_1 and y is B_1, then $f_1=p_1x+q_1y+r_1$

Rule 2 if x is A_2 and y is B_2, then $f_2=p_2x+q_2y+r_2$

The steps of fuzzy reasoning performed by Sugeno-type FIS is:

- Compare the input variables with the membership functions on the antecedent part to obtain the membership values of each linguistic label, shown as μ_{A1}, μ_{A2}, μ_{B1}, μ_{B2},. This step is called fuzzification.
- Combine the membership values on the antecedent part to get weight of each rule. For example: $w_1=\mu_{A1}\times\mu_{B1}$
- Generate the qualified consequent of each rule depending on the weight, i.e., $w_1\times f_1$ and $w_2\times f_2$
- Aggregate the qualified consequents to produce a final output (2.28). This step is called defuzzification.

$$f = \frac{w_1 f_1 + w_2 f_2}{w_1 + w_2} \tag{2.28}$$

All the steps are shown in fig. 2-23.

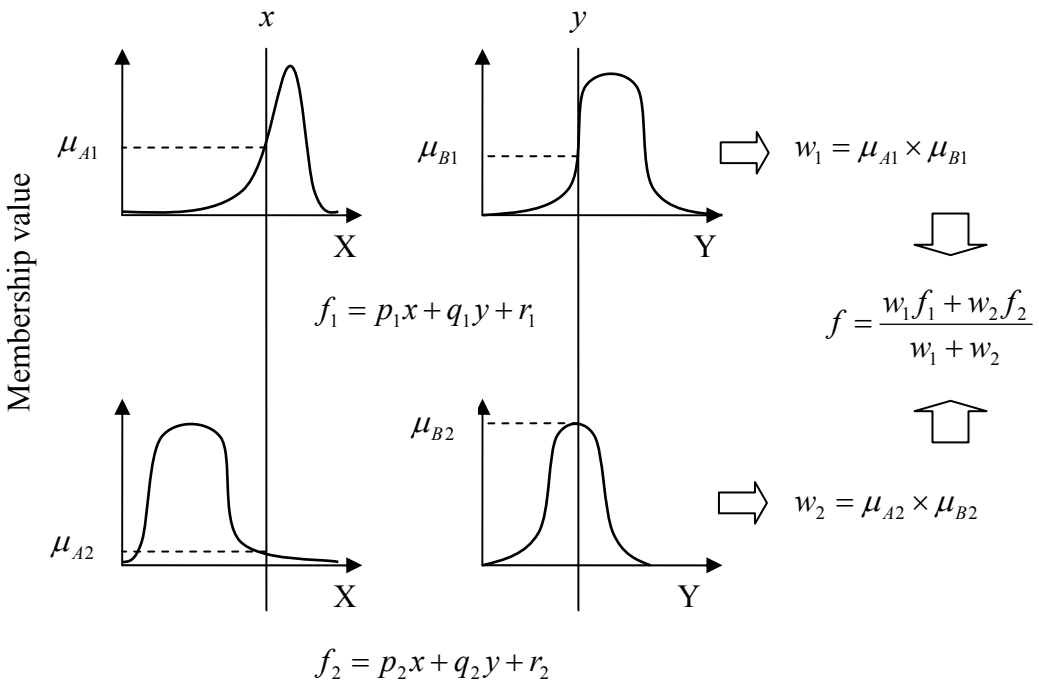

Figure 2-23 Sugeno fuzzy model

2.2.4.3 Neuro-Fuzzy system

Perhaps the most important advantage of neural networks is their capability for adaptation. Fuzzy logic performs an inference mechanism under cognitive uncertainty. Neuro-fuzzy networks are based on the combination of neural networks and fuzzy logic. Papers [37, 38] propose adaptive-network-base fuzzy inference system (ANFIS).

Fig. 2-24 is an equivalent ANFIS for the fuzzy model of Fig.2-23.

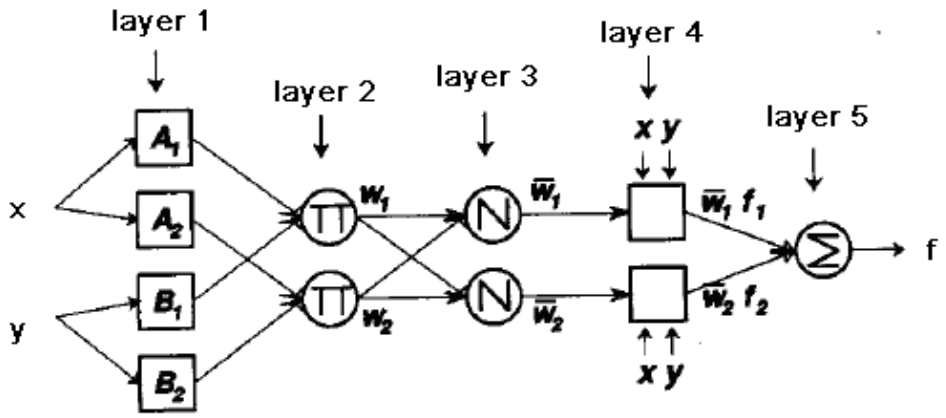

Figure 2-24 Equivalent ANFIS for Sugeno fuzzy model

The relationship between Fig.2-23 and Fig.2-24 is explained by the functions of layers:

Layer 1: The node function is:

$$O_i = \mu_{Ai}(x) \tag{2.29}$$

where x is the input of node i, and A_i is the linguistic label associated with this node function. In other words, O_i is the membership function of A_i. For example, the membership function can be the Gaussian function with maximum of 1 and minimum of 0, such as:

$$\mu_{Ai}(x) = \exp\left(\frac{-x^2}{2}\right) \tag{2.30}$$

Layer 2: This layer multiplies the incoming signals to obtain the weights:

$$w_i = \mu_{Ai} \times \mu_{Bi} \tag{2.31}$$

Layer 3: This layer calculates the ratio of the rules:

$$\overline{w_i} = \frac{w_i}{w_1 + w_2}, \quad i = 1,2 \tag{2.32}$$

Layer 4: This layer calculates the output for each consequent and multiplies its ratio in (2.32):

$$\overline{w_i} f_i = \overline{w_i}\left(p_i x + q_i y + r_i\right) \quad i = 1,2 \tag{2.33}$$

Layer 5: The single node in this layer gives the overall output as the summation of all incoming signals:

$$f = \sum \overline{w_i} f_i = \frac{w_1 f_1 + w_2 f_2}{w_1 + w_2} \tag{2.34}$$

It will get the same result as (2.28).

2.2.4.4 ANFIS predistortion

Paper [32] proposed a new predistortion technique employing an ANFIS system, shown in Fig. 2-25.

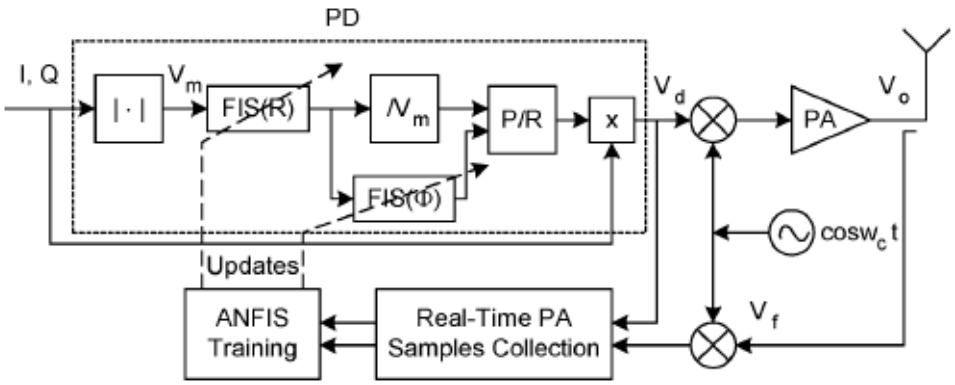

Figure 2-25 ANFIS for predistortion in [32]

The ANFIS systems are used for amplitude and phase corrections for the predistorter.

The membership functions for this ANFIS are Gaussian functions. Experimental results showed that with optimization, this ANFIS system can have a 26.3 dB reduction on the third order IMD products in a two-tone test, or a 13 dB ACPR reduction on wideband signals.

2.2.5 Injection predistortion

Injection is another simple type of predistortion. The idea is to add frequency components at the input port of PA, which generate the same amplitudes but opposite phases of the original intermodulation products at the output port, to counteract the distortions.

2.2.5.1 Injection in two-tone test

The main target for injection in a two-tone test signal is to cancel the third-order intermodulation products (IM3). There are different types of mechanisms to generate IM3 at the output port of PAs.

Paper [39] uses the linear gain of the PA to remove the unwanted spectral lines, shown in Fig. 2-26.

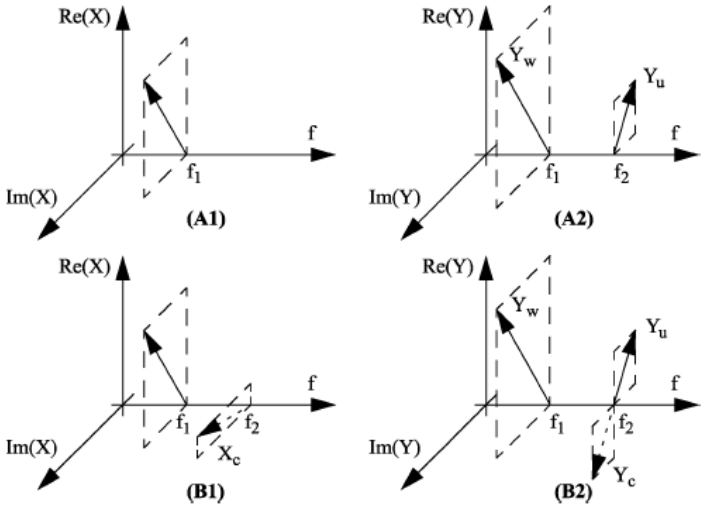

Figure 2-26 Basic idea of correction

The input signal X in (A1) is fed into the nonlinear device and the output signal Y is shown in A2. The output contains an unwanted component Y_U at frequency of f_2. It can not be created by the linearity of the system, since $X(f_2)=0$. So it must originate from the nonlinearities of the device. For the correction, an extra input component X_C is added at the frequency f_2, as shown in B1. The system is assumed to be predominantly linear, and this will create a new output component Y_C at frequency f_2. If Y_C has the same amplitude but opposite phase as Y_U, the unwanted contribution Y_U will be cancelled, as shown in B2. A similar idea with a different hardware implementation can be found in [8, 40-44].

Another injection technique is to inject difference frequencies into PAs [45].
Suppose the nonlinear PA model is written as:

$$V_o = g_1 V_{in} + g_2 V_{in}^2 + g_3 V_{in}^3 + \ldots \tag{2.35}$$

Considering a two tone signal with different frequency fed into the PA:

$$V_{in} = A_1 \cos(\omega_1 t) + A_2 \cos(\omega_2 t) + A_{21} \cos(\omega_2 t - \omega_1 t + \phi_{21}) \tag{2.36}$$

Substitution of (2.36) into (2.35) gives all the relevant components in output spectrum. Among these intermodulation products, the IM3 ($2\omega_2$-ω_1) will be:

$$V_{out}(2\omega_2-\omega_1)=\frac{3}{4}A_1A_2^2g_3\cos(2\omega_2t-\omega_1t)+\frac{3}{4}A_2A_{21}^2g_3\cos(2\omega_2t-\omega_1t+2\phi_{21}) \tag{2.37}$$

Equation (2.37) shows that by proper selection of phase and amplitude of the injected signal, it is possible to make the IM3 disappear. Similar ideas with different hardware implementation can be found in [46-49].

The last injection technique introduced here is the second harmonic injection predistortion [49]. Instead of the difference frequency, we inject second harmonic components as:

$$V_{in}=A_1\cos(\omega_1t)+A_2\cos(\omega_2t)+A_{11}\cos(2\omega_1t+\phi_1)+A_{22}\cos(2\omega_2t+\phi_2) \tag{2.38}$$

The IM3 ($2\omega_2$-ω_1) will be:

$$V_{out}(2\omega_2-\omega_1)=\frac{3}{4}A_1A_2^2g_3\cos(2\omega_2t-\omega_1t)+A_1A_{22}g_2\cos(2\omega_2t-\omega_1t+\phi_2) \tag{2.39}$$

Equation (2.39) also shows that the IM3 can be removed by choosing the appropriate phase and amplitude for the injected signal. Similar ideas with different hardware implementation can be found in [43, 44, 50]. The published injection techniques in two-tone tests can reduce the IM3s down to the noise floor, which vary from 20 dB [41] to 40 dB [48].

2.2.5.2 Injection in wideband signals

Besides two-tone test, the injection technique has also been applied to wideband communication signals. Paper [51] injects the third- and fifth-order distortion components in the baseband block to eliminate the fundamental distortion. It assumes that the amplifier nonlinearity can be expressed in a power series up to the fifth degree:

$$v_o = g_1 v_i + g_2 v_i^2 + g_3 v_i^3 + g_4 v_i^4 + g_5 v_i^5 \tag{2.40}$$

And the input digital modulation which has magnitude $c(t)$ and phase $\varphi(t)$ and carrier frequency ω:

$$\begin{aligned} v_i(t) &= c(t)\cos(\omega t + \phi(t)) \\ &= v_s\left(I\cos(\omega t) - Q\sin(\omega t)\right) \end{aligned} \tag{2.41}$$

where

$$I = \cos(\phi(t))c(t)/v_s \qquad Q = \sin(\phi(t))c(t)/v_s$$

and v_s is the average of $|c(t)|$. Therefore, average $(I^2+Q^2)=1$.

By substituting (2.41) into (2.40), the distorted output voltage appearing at the fundamental frequency is:

$$\begin{aligned} v_{funt}(t) = {} & g_1 v_s\left(I\cos(\omega t) - Q\sin(\omega t)\right) + \frac{3}{4} g_3 v_s^3\left(I^2+Q^2\right)\left(I\cos(\omega t) - Q\sin(\omega t)\right) \\ & + \frac{5}{8} g_5 v_s^5\left(I^2+Q^2\right)^2\left(I\cos(\omega t) - Q\sin(\omega t)\right) \end{aligned} \tag{2.42}$$

In (2.42), the second term is the third-order distortion, and the third term is the fifth-order distortion. Now the cube of the desired signal is added into (2.41) as the third-order distortion component:

$$v_i(t) = v_s\left(I\cos(\omega t) - Q\sin(\omega t)\right)\left\{1 + a\left(I^2 + Q^2\right)\right\} \tag{2.43}$$

Equation (2.42) will change to

$$\begin{aligned} v_{funt}(t) = {} & g_1 v_s\left(I\cos(\omega t) - Q\sin(\omega t)\right) \\ & + g_1 v_s a\left(I^2 + Q^2\right)\left(I\cos(\omega t) - Q\sin(\omega t)\right) \\ & + \frac{3}{4} g_3 v_s^3\left(I^2 + Q^2\right)\left(I\cos(\omega t) - Q\sin(\omega t)\right) \\ & + \frac{4}{9} g_3 v_s^3 a\left(I^2 + Q^2\right)^2\left(I\cos(\omega t) - Q\sin(\omega t)\right) \\ & + \frac{4}{9} g_3 v_s^3 a^2\left(I^2 + Q^2\right)^3\left(I\cos(\omega t) - Q\sin(\omega t)\right) \end{aligned} \tag{2.44}$$

In the calculation, the term that has a^3 is ignored because it is too small. The third term in (2.44) is the original third-order distortion. The second, fourth and fifth terms are generated by the injected distortion component. In a weakly nonlinear region, the input voltage v_s is small, the fourth and fifth terms can be ignored, which makes (2.44) become:

$$\begin{aligned} v_{funt}(t) = {} & g_1 v_s\left(I\cos(\omega t) - Q\sin(\omega t)\right) \\ & + g_1 v_s a\left(I^2 + Q^2\right)\left(I\cos(\omega t) - Q\sin(\omega t)\right) \\ & + \frac{3}{4} g_3 v_s^3\left(I^2 + Q^2\right)\left(I\cos(\omega t) - Q\sin(\omega t)\right) \end{aligned} \tag{2.45}$$

The second and third terms in (2.45) can cancel each other by choosing appropriate a:

$$a = -\frac{3g_3}{4g_1}v_s^2 \tag{2.46}$$

The relevant block diagram is shown in Fig. 2-27, and the ACPR reduction is around 20 dB in [51].

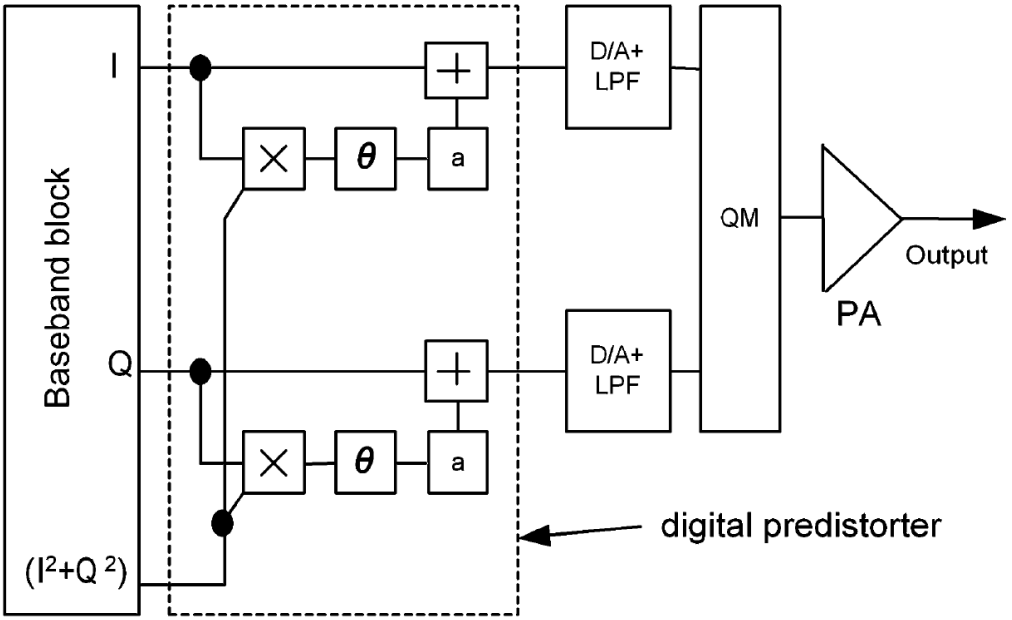

×: multiplexer +: adder QM: quadratic modulator

a: amplitude modulator θ: phase modulator

Figure 2-27 Injection predistorter in [51]

2.3 Summary

Firstly, we have outlined different types of PA models. They can describe either nonlinearities, like AM/AM and AM/PM conversion, memoryless polynomial, frequency-independent Saleh model, or both nonlinearities and memory effects, like frequency-dependent nonlinear quadrature model, ARMA model, Volterra model including memory polynomial and Wiener model, and neural network model. These models can explain how the nonlinearities generate intermodulation products in the

output spectrum, and how the memory effects cause asymmetries between the upper and lower side band of these intermodulation products.

Secondly, according to these PA models, their inverse models are also depicted in this chapter, such as AM/AM and AM/PM conversion, inverse Volterra model including inverse memory polynomial and Hammerstein model, and the neural network model. Besides these inverse PA models, the alternative technique, named injection, is also presented here. This technique addresses the amplitude and phase of the unwanted frequencies, and generates the same but with anti-phase phasors to counteract with the originals. Such kind of technique can reduce the IM3 in two-tone tests.

However, the published predistortion techniques have different drawbacks. The inverse memoryless PA predistortion can not deal with memory effects, which limits its operation in wideband signal cases. The Volterra and its derivated models can handle both nonlinearities and memory effects, but it is complicated to understand and extract its coefficients. The neural network types have the similar problem that, we can not explain what the coefficients mean. The injection can reduce IM3 products in two-tone tests, but its reduction on spectral regrowth in wideband signals is not completely down to the noise floor, as shown in the published papers.

New predistortion techniques which can deal with both nonlinearities and memory effects, and easy to understand and implement is needed. In my research work, I chose the injection as the fundamental predistortion technique. Improvements to the published injection techniques are given in Chapter 3, 4 and 5. We focus its application in the two-tone test in Chapter 3. It will reveal what the new problems injection causes and how to solve them. Experimental results in different signal conditions will be shown in the end of Chapter 3. In Chapter 4, such kind of injection technique will be upgraded in order to work in wideband signals. In Chapter 5, after analyzing LUT and injection working in wideband signal, a new predistortion technique, which combines both LUT and injection, is proposed. It inherits the

advantages from both LUT and injection. We have also used a cascaded PA system which has both significant nonlinearities and memory effects, to demonstrate its abilities.

CHAPTER 3

IMPROVEMENTS OF INJECTION TECHNIQUES IN TWO-TONE TESTS

Firstly, we will introduce a general two-tone test and demonstrate both nonlinearities and memory effects in a PA through a two-tone test. Secondly, we will discuss the published techniques for measuring and reducing third-order intermodulation (IM3) products in a two-tone test. Finally, we propose our improvements of these techniques.

3.1 Introductions of two-tone tests

The two-tone test is a universally recognized technique in assessing amplifier nonlinearities and memory effects [52]. Firstly, it is simple and easy to generate. Secondly, it can vary the envelope throughout a wide dynamic range to test the amplifier's transfer characteristic. Thirdly, it is possible to vary the tone spacing, which is the envelope base band frequency, to examine the amplifier's memory effects[9]. All these advantages mean it is considered to be the most severe test of power amplifiers.

The normal format of a two-tone test is:

$$\begin{aligned} V_{in} &= A\cos(\omega_1 t) + A\cos(\omega_2 t) \\ \omega_1 &= \omega_c - \omega_m \\ \omega_2 &= \omega_c + \omega_m \end{aligned} \tag{3.1}$$

In (3.1), A is the amplitude for a single carrier, ω_1 and ω_2 are the two carriers' frequencies, ω_c is the centre frequency of the signal while ω_m is half of the tone-spacing. Using the trigonometric identity, (3.1) can also be written as:

$$V_{in} = 2A\cos(\omega_c t)\cos(\omega_m t) \tag{3.2}$$

Equation (3.2) shows us that the two-tone test signal can also be treated as a sine wave with frequency of ω_c, modulated by an envelope which is another sine wave with frequency of ω_m. The overall maximum amplitude is 2A. Normally in RF research, $\omega_c >> \omega_m$, ω_c is in the RF frequency range of the PA, and ω_m is in the baseband frequency range that will causes memory effects. The reason is as follows. The impedance seen by the input of the transistor varies with frequency in the baseband range, because the bias decoupling circuit is required to behave low impedance at low frequency but high impedance at carrier frequency. There are baseband currents flowing in the bias circuit due to the second and higher order nonlinearities of the transistor. These currents will result voltages that are frequency-dependant [53]. Therefore, while the two-tone test is applied to a PA, the difference frequency ω_m voltage on the gate terminal modulates the gain and generates nonlinearity products whose levels are dependent on this difference frequency. In other words, these nonlinearities products will vary as the difference frequency varies, which are memory effects. All the information of A, ω_c , ω_m in a two-tone waveform is shown in Fig. 3-1.

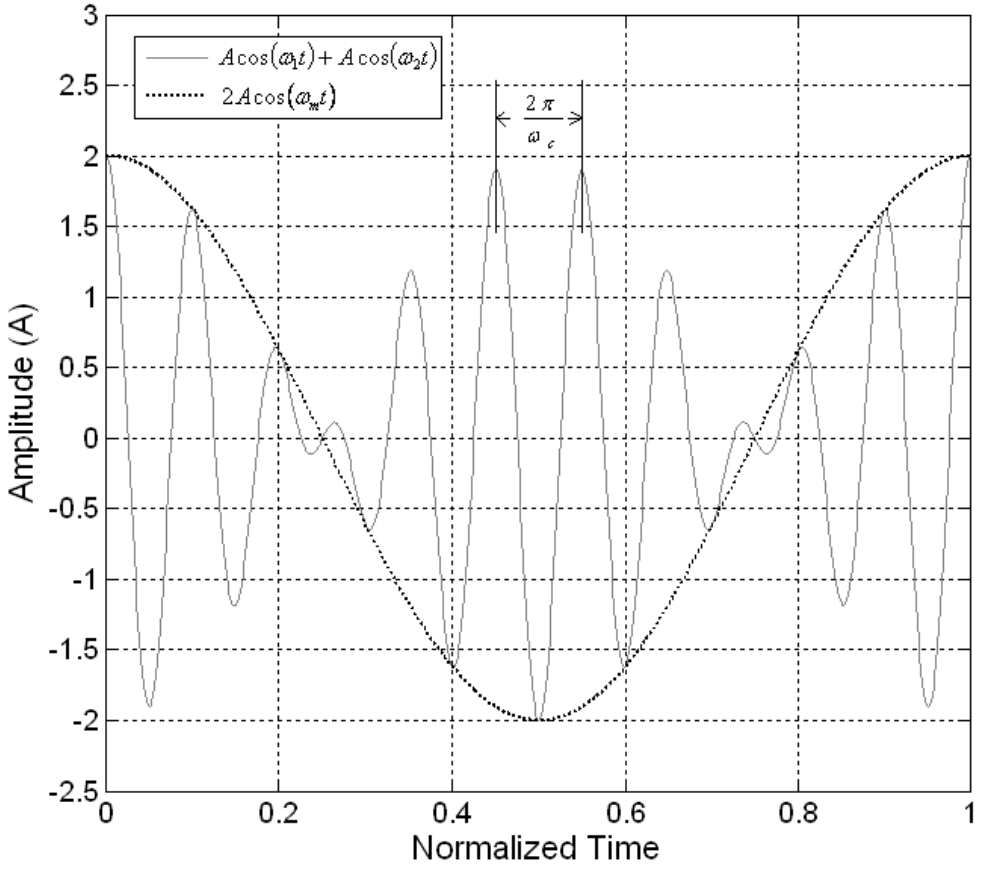

Figure 3-1 A two-tone test signal

When this two-tone signal is applied to a PA, the signal will be amplified, with some new intermodulation products created by the PA nonlinearities. This can be simply explained by memoryless polynomial model. Suppose the characteristic of the PA is:

$$y(x) = a_1 x + a_2 x^2 + a_3 x^3 + a_4 x^4 + a_5 x^5 + \ldots \tag{3.3}$$

We substitute (3.1) into (3.3), we will get the output:

$$\begin{aligned} y(V_{in}) = {} & a_1 A[\cos(\omega_1 t)+\cos(\omega_2 t)] + a_2 A^2[\cos(\omega_1 t)+\cos(\omega_2 t)]^2 \\ & + a_3 A^3[\cos(\omega_1 t)+\cos(\omega_2 t)]^3 + a_4 A^4[\cos(\omega_1 t)+\cos(\omega_2 t)]^4 \\ & + a_5 A^5[\cos(\omega_1 t)+\cos(\omega_2 t)]^5 + \ldots \end{aligned} \tag{3.4}$$

Take the third order intermodulation products (IM3) for example, (3.4) will yield:

$$\begin{aligned} y_{IM3}(V_{in}) &= C_{3\omega 1}\cos(3\omega_1 t) + C_{3\omega 2}\cos(3\omega_2 t) \\ &\quad + C_{2\omega 1-\omega 2}\cos((2\omega_2 - \omega_1)t) + C_{2\omega 2-\omega 1}\cos((2\omega_1 - \omega_2)t) \\ &\quad + C_{2\omega 1+\omega 2}\cos((2\omega_2 + \omega_1)t) + C_{2\omega 2+\omega 1}\cos((2\omega_1 + \omega_2)t) \\ C_{3\omega 1} &= C_{3\omega 2} = \frac{1}{4}a_3 A^3 \\ C_{2\omega 1-\omega 2} &= C_{2\omega 2-\omega 1} = C_{2\omega 1+\omega 2} = C_{2\omega 2+\omega 1} = \frac{3}{4}a_3 A^3 \end{aligned} \tag{3.5}$$

In (3.5), we can see that there are six IM3 products. Among them, only $C_{2\omega 1-\omega 2}$ and $C_{2\omega 2-\omega 1}$ will affect the in band spectrum since others are at frequencies far above ω_1 or ω_2. And these two IM3 products mainly cause spectral interference in real-world communication signals, which are the objects of linearization techniques.

3.2 Published measurements and injections for IM3 products in two-tone tests

Equation (3.5) is a simple case of using memoryless PAs. However, once the PA shows a significant degree of memory effects, the coefficient a_3 would change to be a frequency-dependent parameter, so that the more complicated models listed in Section 2.1.3 are required. Thus, memory effects shown in IM3 in two-tone tests [52, 54, 55] is an interesting and important topic for linearization techniques. Recent research mainly focuses on the measurement and elimination of IM3 products. One of the common ways to measure the IM3 in two-tone tests, is to vary the input power and the tone spacing [15, 18]. Injection is a procedure that can be based on measurement results, to remove these IM3 products, since the basic idea for injection is to generate IM3 products at the output port, which have identical amplitudes but opposite phases to the original ones.

3.2.1 Measurements on IM3 products

Since the power of IM3 products can be directly observed from spectrum analyzers, the only problem is measurement of IM3 phases. IM3 phases are varying with time, so we can not identify them with any particular values. One of the common ways to evaluate IM3 phases is to define or create a reference sine wave with the same frequency, and measure the phase difference.

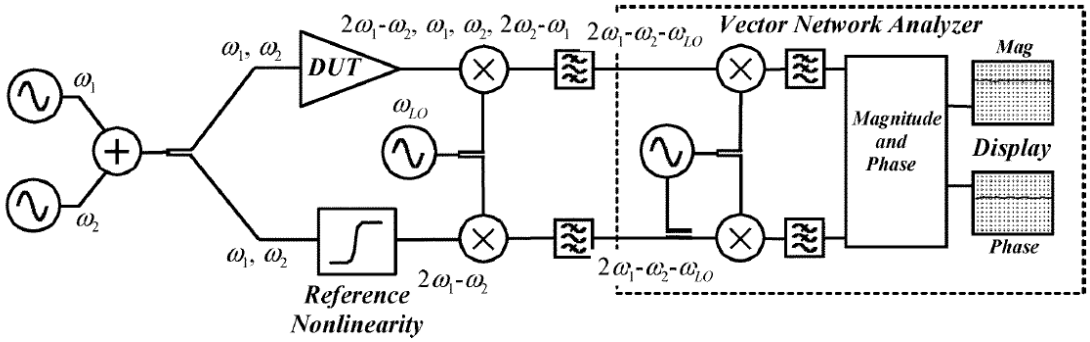

Figure 3-2 IM3 phase measurement in [56]

An IM3 phase measurement technique was proposed in [56-58], as shown in Fig. 3-2. The two-tone signal will go through two branches: one with the nonlinear device under test (DUT) and the other one with a reference nonlinearity device. The system down-converts these two outputs to IF, selects the sought mixing product by a narrow band pass filter and measures their relative phases in a vector network analyzer.

Compared with Fig. 3-2, [59] proposed a similar structure for measurement but with only one branch, shown in Fig. 3-3.

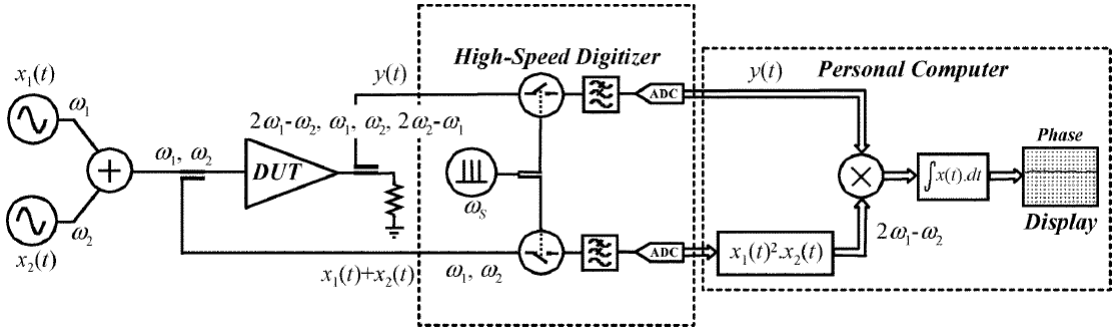

Figure 3-3 IM3 phase measurement in [59]

Suppose the input two frequencies are:

$$x_1(t) = \cos(\omega_1 t)$$
$$x_2(t) = \cos(\omega_2 t) \tag{3.6}$$

The idea behind this setup is to synchronously digitize the DUT's input and output waveforms and calculate the correlation between output signal $y(t)$ and $x_1(t)^2 x_2(t)$ at frequency of $2\omega_1-\omega_2$, to extract the phase difference, shown in (3.7).

$$S_{yx}(2\omega_1 - \omega_2) = \frac{1}{T}\int_{-\frac{T}{2}}^{\frac{T}{2}} y(t) e^{-j(2\omega - \omega_2)t} dt \tag{3.7}$$

Instead of using an extra branch or mathematical calculation, [60] proposed another way of generating IM3 references. As shown in Fig. 3-4, it uses a driver amplifier to create a small amount of IM3 products at the input port of the main power amplifier.

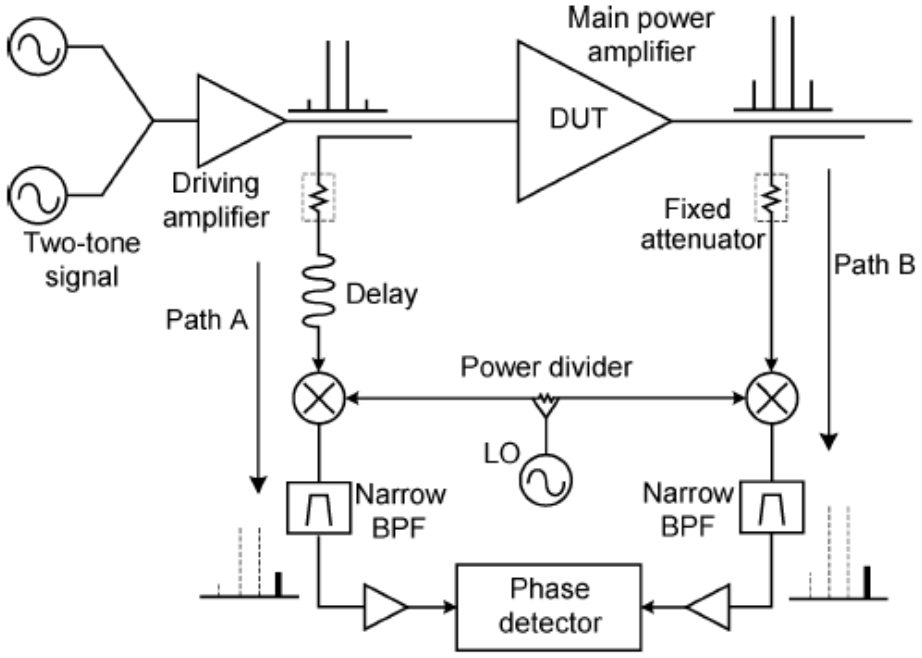

Figure 3-4 IM3 phase measurement in [60]

Suppose the phase in path A and path B (Fig. 3-4) are $\psi(A)$, and $\psi(B)$, the phase transfer function of DUT is simply expressed by:

$$\psi = \psi(B) - \psi(A) \tag{3.8}$$

Alternatively, [41] directly adds IM3 references into the input with the two-tone signal by software. The PC in Fig. 3-5 generates input as:

$$A\cos(\omega_1 t) + A\cos(\omega_2 t) + A_I \cos[(2\omega_1 - \omega_2)t + \Phi_I] \tag{3.9}$$

The procedure is to adjust the amplitude A_I and phase Φ_I to make the IM3 ($2\omega_1$-ω_2) at output port disappear. This Φ_I can indirectly represent the phase of IM3 at output port.

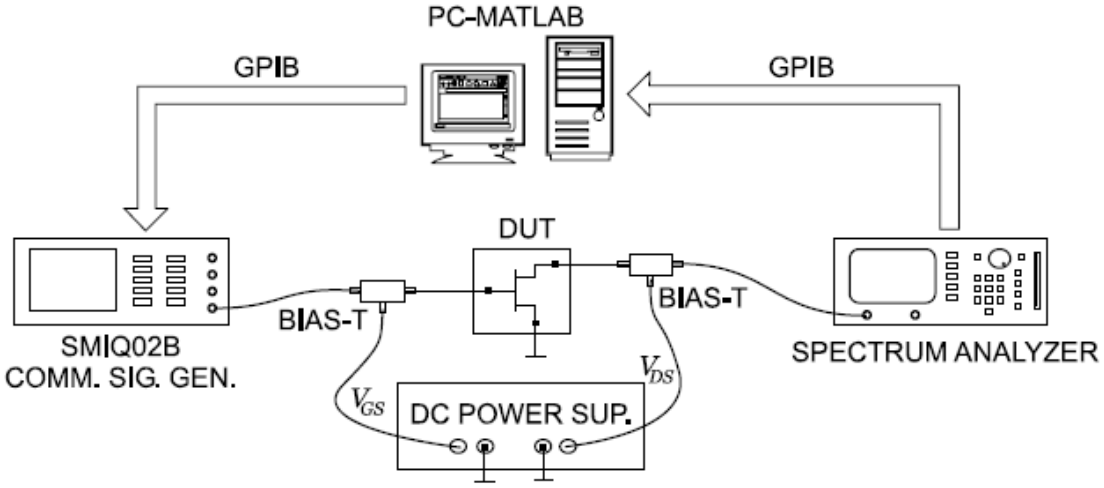

Figure 3-5 IM3 phase measurement in [41]

3.2.2 Injections on IM3 products

The aim for injection is to add new frequency components at the input port of the PA, to counteract IM3 at the output port. There are lots of choices for the frequency components to complete the same work, such as second harmonic, difference-frequency and third order injection. Their detailed theories can be found in Section 2.2.5. This part sums up their published experiment results. Second harmonic frequency injection has been shown to decrease the IM3 level more than 40dB in [43, 44, 48, 50, 61]. The difference-frequency approach [40, 45, 46, 48] produces similar results but it needs no RF circuitry and can be implemented at baseband frequencies. The third-order injection can eliminate one of the IM3 products by injecting **Error! Bookmark not defined.**$2\omega_2$-ω_1 or $2\omega_1$-ω_2, [40, 44] or both IM3 products. [41, 42]

3.3 Improvements for the measurements and injections in two-tone tests

However, the published injection techniques have different drawbacks. For example,

in [42], good results were achieved but with the PA working somewhat below the compression point. The injection technique described in [39] needs a large number of measurements. There are three novel improvements to third-order injection techniques in our work.

1) A new way of generating a reference against which to measure IM3 products.

A completed two-tone IM3 characterization requires magnitude and phase measurements [52, 54, 62]. Finding an IM3 reference is a general and useful approach. We propose a virtual calculated IM3 reference which only comes from the output two main tones. The technique produces accurate measurement results without the extra hardware [56-58] or complicated mathematical functions [52, 55, 59].

2) A new mathematical description of the relationship between injected and output IM3 products, including their amplitude and phase.

The injection technique requires the generation of anti-phase phasors to cancel the IM3 products at the output port. In some published works, manual tuning is used to adjust these phases. We propose a mathematical description of the relationship between injected and output IM3 products, from which these anti-phase phasors can be precisely calculated. A similar description proposed in [39], was based on the measurement of power, while our work is based on the measurement of amplitude and phase. As a result, the earlier method can not reveal the interactions between upper and lower side band injected IM3 products, and hence needs large measurement times. This will be explained in Section 3.3.3.

3) A new view of the interaction between the lower and upper IM3 products, which affects the dual sideband injection.

Third-order injection uses input lower third-order intermodulation products (IM3L) to

eliminate output IM3L and input upper third-order intermodulation products (IM3U) to eliminate output IM3U, separately. However, when these two injected products are introduced together, they will affect each other at the output port because of the PA's nonlinearities. The frequency relationships can be written as: $2\omega_1-\omega_2=\omega_1+\omega_2-(2\omega_2-\omega_1)$ and $2\omega_2-\omega_1=\omega_1+\omega_2-(2\omega_1-\omega_2)$. We define these to be interactions in our work. The significance of the interaction depends on the third-order nonlinearity of the PA. When the PA is working well below compression point, dual sideband predistortion can be achieved perfectly without considering the interaction. For example, [42] shows a perfect IM3 elimination without detecting interactions. In that work, the IM3s are -30dBc relative to the two-tone carriers before predistortion, suggesting that the PA is not driven hard, and the IM3s are only 20dB above the noise floor which limits the observation range. If the PA is driven harder and the spectrum analyzer is working with higher sensitivity to have a wider observation range, the effects of interactions will become more apparent. In our work, the PA is operated beyond the 1dB compression point, thus a completed matrix for both IM3 products suppression is proposed in Section 3.3.3.

3.3.1 IM3 reference

Injection can achieve perfect distortion correction or it can make the result worse, depending on whether the correct phase in used. Hence measuring the phases of output IM3s plays an important role in injection. One solution is to generate an IM3 reference and define the IM3 phase as the difference between the reference and the IM3 product. We will describe the experimental setup and introduce a new method of generating the IM3 reference.

3.3.1.1 Experimental setup

Practically, the centre frequency ω_c of two-tone test is at RF band, up to 2-3 GHz. The sample rate of the digital devices for analysis is 200 MHz at most, which is far below RF band. Therefore, we employ I-Q modulation/demodulation in our experiments. The signals we produce and analyze are in baseband, before the up-converter or after the down-converter, while the PA is operated in the RF band, after the up-converter. The measurement set up is shown in Fig. 3-6. The PC generates one period of a two-tone digital signal which is transferred to the memory of a waveform generator (Rohde and Schwarz AMIQ, appendix B). The AMIQ (Rohde and Schwarz SMIQ, appendix C) outputs the analogue signal repeatedly (the program to control AMIQ and the output power dynamic range is described in Appendix D, the program to generate the signal is in Appendix E). These signals are up-converted to RF by a signal generator with a built in modulator (Rohde and Schwarz SMIQ). The RF signal is amplified by a 40dB gain commercial PA (ZHL-4240 in Appendix A). Finally, the output signals are sampled and analyzed by the vector signal analyzer with a built in demodulator (VSA) after a 20dB attenuator.

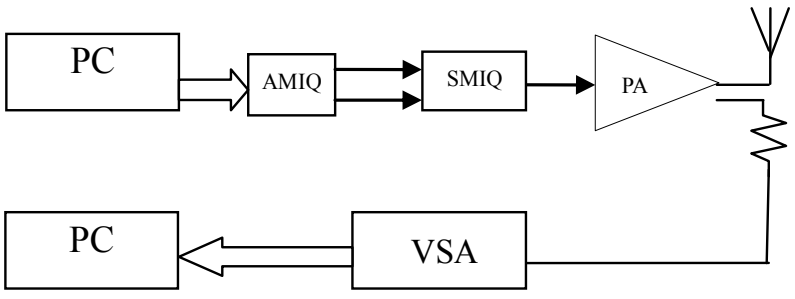

Figure 3-6 Experimental set up

3.3.1.2 Data organization

Specifically, the PC generates complex numbers representing in-phase and quadrature

signals, while the SMIQ performs an I-Q modulation.

In the following analysis, the amplitude of each carrier of a two-tone input signal is normalized. The baseband signal in the AMIQ is:

$$\begin{aligned} I &: \cos(-\omega_m t) + \cos(\omega_m t) \\ Q &: \sin(-\omega_m t) + \sin(\omega_m t) \end{aligned} \tag{3.10}$$

The RF signal from the output of the SMIQ, fed to the PA directly is:

$$\begin{aligned} v_{in} &= I \times \cos(\omega_c t) - Q \times \sin(\omega_c t) \\ &= [\cos(-\omega_m t) + \cos(\omega_m t)] \times \cos(\omega_c t) \\ &\quad - [\sin(-\omega_m t) + \sin(\omega_m t)] \times \sin(\omega_c t) \\ &= 2\cos(\omega_m t) \times \cos(\omega_c t) - 0 \times \sin(\omega_c t) \\ &= \cos(\omega_1 t) + \cos(\omega_2 t) \end{aligned} \tag{3.11}$$

where $\omega_{1,2}=\omega_c \pm \omega_m$ are the two input carrier frequencies.

The base band signals will be written as complex numbers ($I+jQ$), instead of I and Q channel. Accordingly, the amplitude and phase are:

$$Amplitude = \sqrt{I^2 + Q^2} \qquad Phase = \tan^{-1}\left(\frac{Q}{I}\right) \tag{3.12}$$

The VSA will measure the phase and amplitude of the distorted signal including the IM3 components:

$$\begin{aligned} v_{out} &= C_1 + C_2 + C_{lower} + C_{upper} \\ &= |C_1| \exp(j\angle C_1) + |C_2| \exp(j\angle C_2) \\ &\quad + |C_{lower}| \exp(j\angle C_{lower}) + |C_{upper}| \exp(j\angle C_{upper}) \end{aligned} \tag{3.13}$$

3.3.1.3 Test details

Following is an example of our experiments. The tone spacing for this test is set to 1 MHz. So the two base band frequencies are -0.5MHz and 0.5MHz. In order to output this baseband signal:

- Two carrier frequencies are set to be -0.5 and 0.5 in software. Hence the period of the combination of two carriers is 2.
- Each period has 200 digital samples. We feed these samples into the AMIQ and set its sample rate as $10^8 s^{-1}$. Hence the actual frequencies of the two output carriers are -0.5 MHz and 0.5 MHz in baseband.

The signal is up-converted by the SMIQ with a central frequency of 2GHz, and down-converted by the VSA. This means that the PA operates at RF frequency, but we record the data in baseband. The measurement is achieved in frequency domain, so we manipulate frequency span and resolution bandwidth for spectrum observation, instead of sample rate and number of samples. In this test, the frequency span is 80 MHz and the resolution bandwidth is 100 kHz in the VSA. Additionally, we apply a flat-top window function to measure particular frequency components with great accuracy. In this case, the phasors C_1, C_2, C_{lower}, C_{upper} in (3.13) can be obtained from sub-frequency numbers of -5, 5, -15 and 15, when we define the centre frequency to be zero. Alternatively, we can use a demodulator and ADC, applying a Fourier transform to get the same measurement results.

3.3.1.4 Theory and experimental analysis for IM3 reference

When we record the spectrum and extract the phasors from the particular sub-frequencies, the amplitudes $|C_1|$, $|C_2|$, $|C_{lower}|$, $|C_{upper}|$ are constants, but the phases $\angle C_1$, $\angle C_2$, $\angle C_{lower}$, $\angle C_{upper}$ vary with time. This makes extracting phases

meaningless. There are different techniques to solve this problem. In [59], the authors sample the input signal to generate an IM3 reference and compare with the output signal. In [60], a driving amplifier is used to create IM3 references and in [41] an input signal is generated by software to define a zero initial phase to characterize all the IM3 phases. Indeed, we can find the phase relationship between the two output IM3s and the two output carriers, and apply a simpler and more efficient way to create IM3 reference which is based on that relationship.

Firstly, the phase relation between carriers and IM3s can be expressed by:

$$\begin{cases} \angle C_1 = (\omega_1 t) \bmod 2\pi \\ \angle C_2 = (\omega_2 t) \bmod 2\pi \\ \angle C_{lower} = (2\omega_1 t - \omega_2 t + \angle C_{lower-distortion}) \bmod 2\pi \\ \angle C_{upper} = (2\omega_2 t - \omega_1 t + \angle C_{upper-distortion}) \bmod 2\pi \end{cases} \tag{3.14}$$

Where, $\angle C_{lower\text{-}distortion}$ and $\angle C_{upper\text{-}distortion}$ represent phase distortion for IM3L and IM3U.

So the ideal reference IM3 phases can be constructed by the phases of two carriers, which can be obtained from the VSA directly:

$$\begin{aligned} \angle C_{lower-reference} &= (2\omega_1 t - \omega_2 t) \bmod 2\pi = (2\angle C_1 - \angle C_2) \bmod 2\pi \\ \angle C_{upper-reference} &= (2\omega_2 t - \omega_1 t) \bmod 2\pi = (2\angle C_2 - \angle C_1) \bmod 2\pi \end{aligned} \tag{3.15}$$

And the phase distortion can be calculated by:

$$\begin{aligned} \angle C_{lower-distortion} &= \angle C_{lower} - \angle C_{lower-reference} \\ &= (\angle C_{lower} - (2\angle C_1 - \angle C_2)) \bmod 2\pi \\ \angle C_{upper-distortion} &= \angle C_{upper} - \angle C_{upper-reference} \\ &= (\angle C_{upper} - (2\angle C_2 - \angle C_1)) \bmod 2\pi \end{aligned} \tag{3.16}$$

From (3.15), knowledge of C_1, C_2 is enough to create an IM3 reference, and knowing C_{lower}, C_{upper}, we can characterize the phase distortion in (3.16). We don't need to add additional hardware [60], to use two channels to sample the input/output signal [59], to sample at different times [10] or to define a zero initial phase [41]. Practically, we use the complex number defined in (3.13), to calculate the normalized IM3L and IM3U references:

$$\begin{cases} \exp\left(j\angle C_{lower-reference}\right) = \exp\left[j\left(2\angle C_1 - \angle C_2\right)\right] = \dfrac{C_1^2 C_2^*}{\left|C_1^2 C_2\right|} \\ \exp\left(j\angle C_{upper-reference}\right) = \exp\left[j\left(2\angle C_2 - \angle C_1\right)\right] = \dfrac{C_2^2 C_1^*}{\left|C_2^2 C_1\right|} \end{cases} \tag{3.17}$$

3.3.1.5 IM3 measurement and results

After introducing a suitable IM3 reference in Section 3.3.1.4, we can use (3.18) to characterize amplitudes and relative phases for both IM3L and IM3U.

$$\begin{cases} \left|C_{lower}\right| \exp\left(j\angle C_{lower-distortion}\right) = \dfrac{C_{lower}}{\exp\left(j\angle C_{lower-reference}\right)} = \dfrac{C_{lower}\left|C_1^2 C_2\right|}{C_1^2 C_2^*} \\ \left|C_{upper}\right| \exp\left(j\angle C_{upper-distortion}\right) = \dfrac{C_{upper}}{\exp\left(j\angle C_{upper-reference}\right)} = \dfrac{C_{upper}\left|C_2^2 C_1\right|}{C_2^2 C_1^*} \end{cases} \tag{3.18}$$

Each of the equations in (3.18) uses only three parameters, so it represents a simpler description compared with published approaches. For example: [52], applies second-order and base band effects to calculate a gain function; [55] proposes a multislice behavioral model to generate IM3 estimation; and [42] applies a simplified Newton method to calculate IM3 phases.

The measured amplitude and phase distortion for IM3L and IM3U are shown in Fig.3-7 (a), (b), (c) and (d), respectively. The results in Fig. 3-7 (a) and (c) show that

the amplitudes of IM3 increase as we increase the input power level, as expected. But the variation of the IM3 products with tone spacing is not obviously seen in the amplitude plot. On the other hand, Fig.3-7 (b) and (d) show that the variation of phase distortions $\Delta C_{lower\text{-}distortion}$ and $\Delta C_{upper\text{-}distortion}$ with frequency is bigger at low power levels than at high power levels.

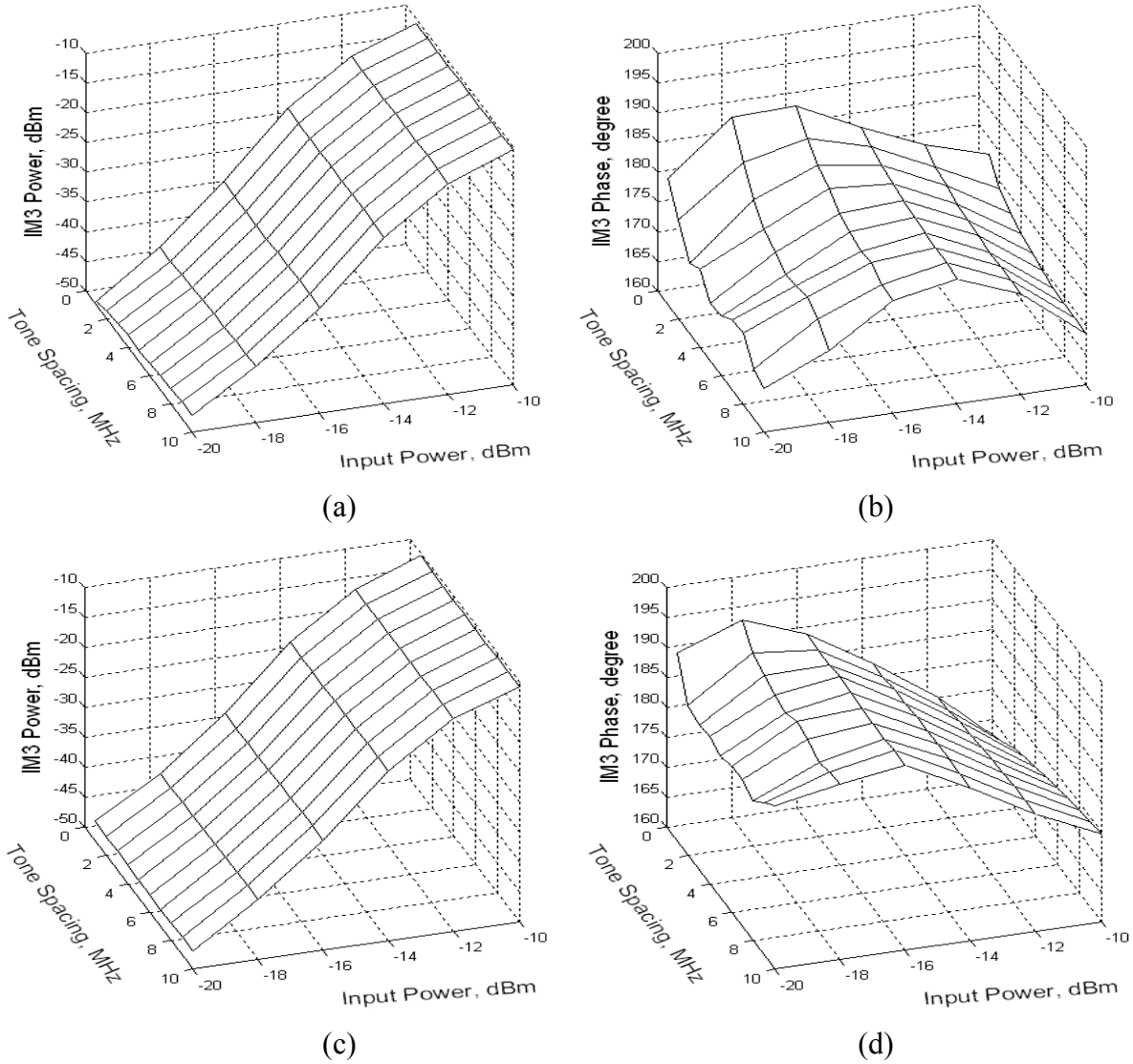

Figure 3-7 Measured IM3 amplitudes and phases

(a) Measured amplitudes of IM3L

(b) Measured phase distortion of IM3L

(c) Measured amplitudes of IM3U

(d) Measured phases distortion of IM3U

3.3.2 Model for single sideband injection

Based on the measurement mentioned previously in Section 3.3.1, this section proposes a new mathematical description of the relationship between injected IM3L and output IM3L. The advantage of this mathematical description is that it can clearly and quickly predict the injection signal required for single sideband predistortion, instead of tuning the input phase and amplitude manually, or measuring the power repeatedly. We discuss IM3L injection in detail. The result for IM3U injection follows analogously.

The input signal is changed to a two-tone with IM3L injection:

$$v_{in} = \exp(j\omega_1 t) + \exp(j\omega_2 t) + k_1 e^{j\Phi_1} \exp(j\omega_{lower} t) \tag{3.19}$$

In (3.19), k_1 and Φ_1 are used to set the amplitude and phase of the injected IM3L.

We define a new parameter:

$$R_{lower} = \frac{C_{lower}}{\exp(j\angle C_{lower-reference})} = C_{lower} \div \frac{C_1^2 C_2^*}{|C_1^2 C_2|} \quad (Input \quad IM3L) \tag{3.20}$$

Equation (3.20) is similar to (3.18), but with different input signals: (3.18) implies a two-tone test while (3.20) implies a two-tone test with IM3L injection. This parameter describes the ratio between output IM3L and reference IM3L. It is simply calculated from the output phasors at three sub-frequencies C_1, C_2, C_{lower}.

Figure 3-8 shows different R_{lower} with respect to different pairs of (k_1, Φ_1). The dashed lines indicate contours of constantΦ_1, with k_1 varying. The solid closed contours represent constant k_1 withΦ_1 varying. They are approximately circular.

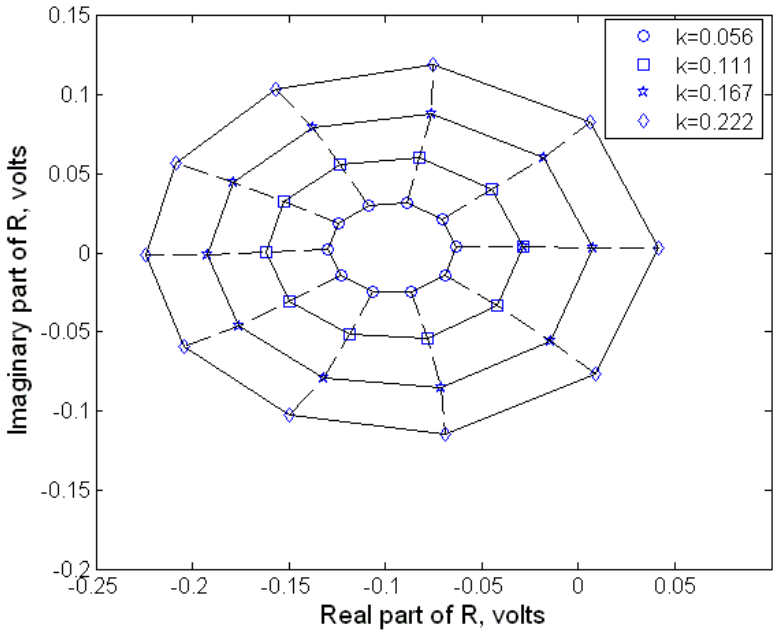

Figure 3-8 Plots of R_{lower}

We can explain the approximately circular contours in Fig.3-8 by analyzing C_{lower}. It consists of two parts: the original IM3L produced by two carriers; and the injected IM3L component multiplied by $G_{linear\text{-}lower}$, the linear gain of the PA, as shown in (3.21):

$$C_{lower} = G_{3-lower} \times \exp(j\omega_{lower}t) + G_{linear-lower} \times k_1 e^{j\Phi_1} \exp(j\omega_{lower}t) \quad (3.21)$$

Equation (3.22) is obtained by substituting (3.21) into the numerator of (3.20):

$$\begin{aligned} R_{lower} &= \frac{G_{3-lower} \times \exp(j\omega_{lower}t) + G_{linear-lower} \times k_1 e^{j\Phi_1} \exp(j\omega_{lower}t)}{\exp(j\omega_{lower}t)} \\ &= G_{3-lower} + G_{linear-lower} \times k_1 e^{j\Phi_1} \end{aligned} \quad (3.22)$$

Using (3.22) to interpret Fig.3-8, the centre of these circles is indicated by $G_{3\text{-}lower}$ and the radius is given by $G_{linear\text{-}lower} \times k_1$. The single sideband predistortion can be

achieved by choosing appropriate (k_1, Φ_1) such that (3.22) becomes zero:

$$k_1 e^{j\Phi_1} = -\frac{G_{3-lower}}{G_{linear-lower}} \tag{3.23}$$

With the appropriate choice of k_1, the circle touches the origin in Fig.3-8 for some value of Φ_1. This corresponds to perfect cancellation. These circles help to explain the input and output IM3L relation and the meanings of $G_{3\text{-}lower}$, $G_{linear\text{-}lower}$. In the predistortion process, we only need two measurements to obtain $G_{3\text{-}lower}$ and $G_{linear\text{-}lower}$, to determine the required (k_1, Φ_1) for perfect cancellation. The first one has k_1=0, i.e a two-tone test with no injection, so that R_{lower} =$G_{3\text{-}lower}$. The second measurement uses an input two tone signal with IM3L injection using an arbitrary pair of (k_1, Φ_1). The $G_{linear\text{-}lower}$ can be calculated from (3.22) using the known (k_1, Φ_1) and $G_{3\text{-}lower}$. The measurements need both amplitude and phase, but this predistortion process is faster than [39].

Similarly, the relation for IM3U and its predistortion are:

$$\begin{aligned} R_{upper} &= \frac{C_{upper}}{\exp\left(j\angle C_{upper-reference}\right)} = C_{upper} \div \frac{C_2^2 C_1^*}{\left|C_2^2 C_1\right|} \quad (Input \quad IM3U) \\ &= G_{3-upper} + G_{linear-upper} \times k_2 e^{j\Phi_2} \end{aligned} \tag{3.24}$$

$$k_2 e^{j\Phi_2} = -\frac{G_{3-upper}}{G_{linear-upper}} \tag{3.25}$$

The original two-tone test and these two single sideband predistortion results are shown in Fig.3-9 (a), (b) and (c).

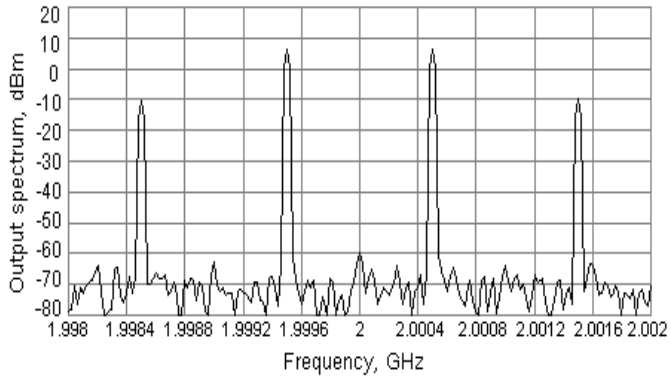

(a)

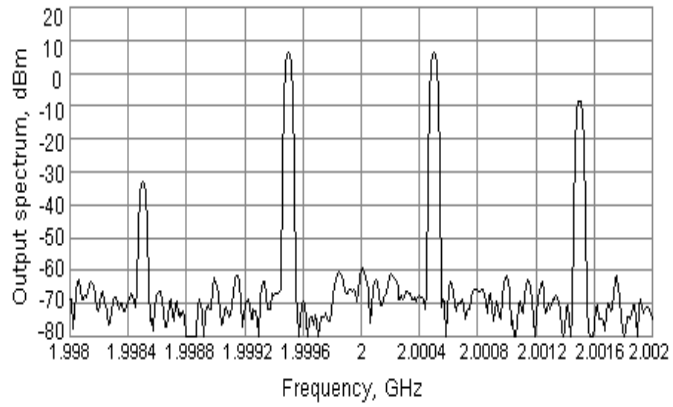

(b)

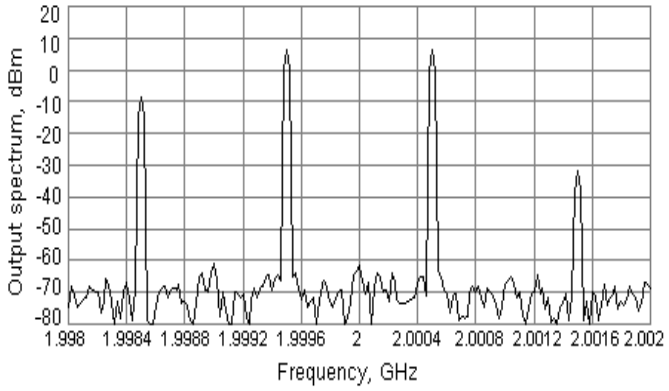

(c)

Figure 3-9 (a) Two-tone test

(b) Lower Sideband Injection

(c) Upper Sideband Injection

Figure 3-9 (a) shows the output spectrum of a two-tone test while the PA is working

beyond its 1dB compression point. It can be seen that the IM3L is -16.9dBc relative to carriers and IM3U is -16.4dBc relative to carriers. After a single sideband injection, the IM3L is reduced to -39.7dBc in Fig.3-9 (b) or IM3U is reduced to -37.5dBc in Fig.3-9 (c). Each of the IM3 products has more than 20dB improvement. These injections can be further improved by the following sections.

3.3.3 Interaction and dual sideband predistortion

Figure 3-10 shows the output spectrum when IM3 injection signals calculated from (3.23) and (3.25) are input simultaneously. IM3s are reduced to -34.9dBc (IM3L) and -35.9dBc (IM3U). Compared with the result in Fig.3-9 (b) and Fig.3-9 (c), the IM3s are increased by 4.8dB and 1.6dB. The comparison shows that new IM3 products are generated, when both of the lower and upper sideband injections are introduced simultaneously.

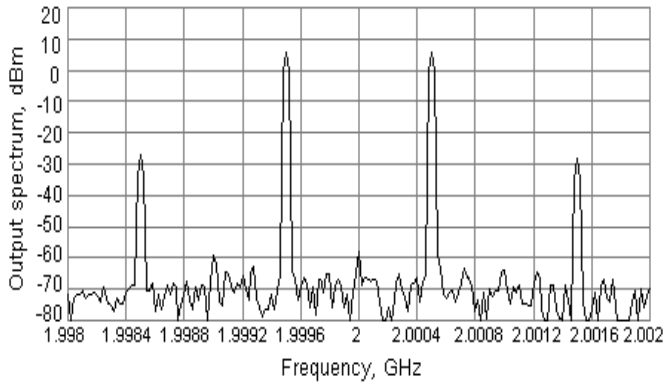

Figure 3-10 Injection without considering interactions

3.3.3.1 Interaction

Figure 3-10 indicates that the injected IM3L affects the output at not only IM3L but also at IM3U. Similarly, injection at IM3U also affects the output at IM3L. This could be caused by a third order nonlinearity acting on the input signals, since

$$\omega_{lower} = \omega_1 + \omega_2 - \omega_{upper}$$
$$\omega_{upper} = \omega_1 + \omega_2 - \omega_{lower} \tag{3.26}$$

In other words, if we introduce both IM3 components indicated by (3.23) and (3.25), the original pair of IM3s is partially cancelled, but another new pair of third-order distortion products at the same IM3 frequencies is generated again by these interactions. This is the reason why the power levels of IM3 in Fig.3-10 rise up again compared with the predistorted IM3L in Fig.3-9 (b) and IM3U in Fig.3-9 (c). However, the IM3s in Fig.3-10 still have been reduced compared with the uncorrected two-tone test in Fig.3-9 (a). The reason is that, the original IM3s result from high amplitude two-tone signals while the new IM3s result from the two carriers and a lower amplitude injected component, so the amplitudes of the original IM3s are bigger than the new IM3s. If the noise floor level is higher than the power level of IM3s in Fig.3-10, the difference caused by these interactions will not be observed. This is one of the reasons that the two-tone injection papers have not reported such effects. On the other hand, the correction algorithm in [39] focuses on one particular frequency every time so it can not compensate this interaction. That is partially why its proposed technique needs a large number of measurements: once one unwanted frequency is reduced, the other predistorted frequency components rise up again.

In order to characterize these interactions, we define another new parameter to reveal how the injected IM3L affects output IM3U:

$$R_{lower-upper} = \frac{C_{upper}}{\exp\left(j\angle C_{upper-reference}\right)} = C_{upper} \div \frac{C_2^2 C_1^*}{\left|C_2^2 C_1\right|} \quad (Input \quad IM3L) \tag{3.27}$$

Equation (3.27) is similar to (3.24) but they are based on different sideband injection. Equation (3.24) shows how injected IM3U (k_2, Φ_2) affects output IM3U. Equation (3.27) shows how IM3L (k_1, Φ_1), which is intended to control IM3L, affects IM3U.

Figure 3-11 shows the measured $R_{lower\text{-}upper}$ with the respect to different pairs of (k_1, Φ_1). The dashed lines indicate contours of constant Φ_1, with k_1 varying. The solid closed contours represent constant k_1 with Φ_1 varying. They are approximately circular like Fig.3-8.

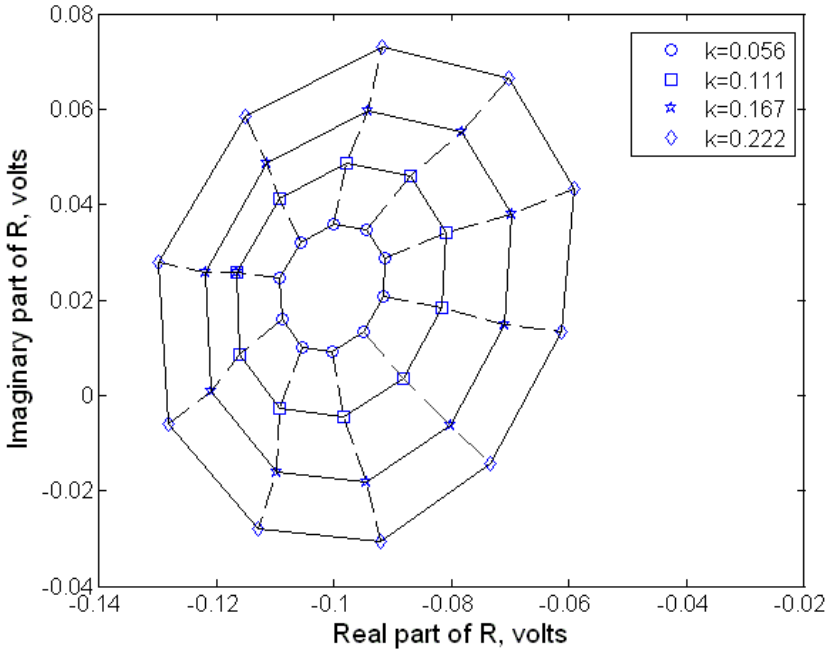

Figure 3-11 Plots of $R_{lower\text{-}upper}$

Similarly to the lower single sideband injection analysis, we can decompose the numerator in (3.27) and get:

$$R_{lower-upper} = \frac{\left\{ G_{3-upper} \times \exp\left(j\omega_{upper}t\right) + G_{lower-upper} \times e^{j\omega_1 t} \times e^{j\omega_2 t} \times \left[k_1 e^{j\Phi_1} \exp\left(j\omega_{lower}t\right)\right]^* \right\}}{\exp\left(j\omega_{upper}t\right)} = G_{3-upper} + G_{lower-upper} \times k_1 e^{-j\Phi_1} \quad (3.28)$$

where $G_{3\text{-}upper}$ is the third-order nonlinearity of the IM3U of the PA, while $G_{lower\text{-}upper}$ is the interaction gain which describes how the input IM3L interacts with the two carriers to generate another new IM3U contribution through the third-order nonlinearity of the PA. Because the interaction is contributed by the conjugation of IM3L, the phase of the second term in (3.28) is negative. Equation (3.28) is similar to

(3.22), but the sign of Φ_1 is opposite. This can be also observed in the experiments: as Φ_1 increases with constant k_1, R_{lower} in Fig.3-8 rotates anti-clockwise, while $R_{lower\text{-}upper}$ in Fig.3-11 rotates clockwise. The radius of the circle in Fig.3-11 is much smaller than the one in Fig.3-8, but it is significant enough to affect dual sideband predistortion. To the authors knowledge, no paper has proposed this term before. In the predistortion process, $G_{3\text{-}upper}$ is obtained as in the previous section. $G_{lower\text{-}upper}$ can be calculated from one more measurement using any single pair of (k_1, Φ_1) in (3.28). By analogy with (3.28), the interaction between the injected IM3U and the carriers, producing another contribution to IM3L, can be characterized by:

$$\begin{aligned} R_{upper-lower} &= \frac{C_{lower}}{\exp\left(j\angle C_{lower-reference}\right)} = C_{lower} \div \frac{C_1^2 C_2^*}{\left|C_1^2 C_2\right|} \quad (Input \quad IM\,3U) \\ &= G_{3-lower} + G_{upper-lower} \times k_2 e^{-j\Phi_2} \end{aligned} \tag{3.29}$$

3.3.3.2 Dual sideband predistortion

To sum up, the equation for describing dual sideband injected IM3s and output IM3s considering the interaction is:

$$\begin{cases} C_{lower} = \left(G_{3-lower} + G_{linear-lower} k_1 e^{j\Phi_1} + G_{upper-lower} k_2 e^{-j\Phi_2}\right)\exp\left(j\omega_{lower} t\right) \\ C_{upper} = \left(G_{3-upper} + G_{linear-upper} k_2 e^{j\Phi_2} + G_{lower-upper} k_1 e^{-j\Phi_1}\right)\exp\left(j\omega_{upper} t\right) \end{cases} \tag{3.30}$$

When we want to eliminate both IM3s completely at the output using injection, we need to satisfy this requirement:

$$\begin{aligned} G_{3-lower} + G_{linear-lower} k_1 e^{j\Phi_1} + G_{upper-lower} k_2 e^{-j\Phi_2} &= 0 \\ G_{3-upper} + G_{linear-upper} k_2 e^{j\Phi_2} + G_{lower-upper} k_1 e^{-j\Phi_1} &= 0 \end{aligned} \tag{3.31}$$

It can be organized and re-written in matrix form:

$$\begin{bmatrix} G_{3-lower} \\ G^*_{3-upper} \end{bmatrix} + \begin{bmatrix} G_{linear-lower} & G_{upper-lower} \\ G^*_{lower-upper} & G^*_{linear-upper} \end{bmatrix} \begin{bmatrix} k_1 e^{j\Phi_1} \\ k_2 e^{-j\Phi_2} \end{bmatrix} = 0 \qquad (3.32)$$

With the values of G_{lower}, G_{upper}, $G_{linear\text{-}lower}$, $G_{linear\text{-}upper}$, $G_{upper\text{-}lower}$, $G_{lower\text{-}upper}$ measured in (3.22), (3.24), (3.28) and (3.29), the solution for dual sideband predistortion would be:

$$\begin{bmatrix} k_1 e^{j\Phi_1} \\ k_2 e^{-j\Phi_2} \end{bmatrix} = -\begin{bmatrix} G_{linear-lower} & G_{upper-lower} \\ G^*_{lower-upper} & G^*_{linear-upper} \end{bmatrix}^{-1} \begin{bmatrix} G_{3-lower} \\ G^*_{3-upper} \end{bmatrix} \qquad (3.33)$$

From this completed matrix description, we can see that perfect dual sideband predistortion cannot be achieved simply by adding IM3s which have the same amplitudes but in anti-phase with the original IM3. The trade-off between linear gain $G_{linear\text{-}lower}$, $G_{linear\text{-}upper}$ and the interactions $G_{upper\text{-}lower}$, $G_{lower\text{-}upper}$ needs to be considered as well. Therefore, a complete dual sideband predistortion would be very hard to optimize by manual tuning.

The parameters for dual sideband predistortion, $G_{linear\text{-}lower}$, $G_{linear\text{-}upper}$ and $G_{upper\text{-}lower}$, $G_{lower\text{-}upper}$ are obtained from four measurements. Dual sideband injection using parameters calculated from Equation (3.33) gives reductions of -38.8dBc for IM3L and -37.5dBc for IM3U when applied to the same amplifier, as shown in Fig.3-12. Compared with Fig.3-10, these IM3s have been reduced by 3.9dB (IM3L) and 1.6dB (IM3U). This injection can be further improved by iterations where both of the IM3s are reduced to the noise floor, as shown in the next section.

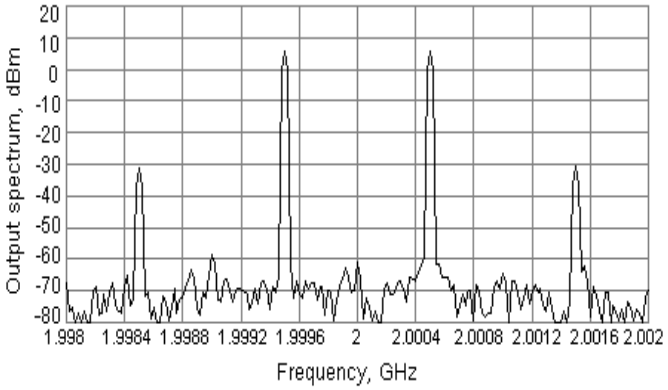

Figure 3-12 Measured dual sideband injection predistortion considering interactions

3.3.4 Improvement by iteration

3.3.4.1 Reasons for iteration

There are several issues that affect the accuracies of G_{lower}, G_{upper}, $G_{linear\text{-}lower}$, $G_{linear\text{-}upper}$, $G_{upper\text{-}lower}$, $G_{lower\text{-}upper}$:

1) The injected IM3s interact non-linearly with the two carriers. The IM3 references are constructed from the two carriers. These two aspects will lead to a distortion of measurement of R_{lower}, R_{upper}, $R_{upper\text{-}lower}$, $R_{lower\text{-}upper}$ and hence affect the calculations of G_{lower}, G_{upper}, $G_{linear\text{-}lower}$, $G_{linear\text{-}upper}$, $G_{upper\text{-}lower}$, $G_{lower\text{-}upper}$.

2) The resolution of the DAC in the AMIQ and the ADC in the VSA will generate a certain degree of inaccuracy which will affect the measurement.

3) The fifth-order nonlinearities will affect the performance as well. Take measuring R_{lower} in a single sideband predistortion for example. The input signal can be judged as a three tone input signal: $C_1+C_2+C_{lower}$. There are a lot of fifth-order intermodulation products generated by the combination of these three carriers. Among these

intermodulation products, some will be located at the frequency of C_{lower}:

$$\omega_{lower} = \omega_2 - 2\omega_1 + 2\omega_{lower} \tag{3.34}$$

This fifth-order intermodulation product will turn the circles (e.g. see Fig.3-8 and Fig.3-11) into ellipse-like shapes with a small ellipticity. The algorithm for calculating the required injection is based on the assumption that the new output component has a circular locus when injecting components with varying phase but fixed amplitude. Fig.3-13 shows the distance from the centre to the perimeter plotted against angle, demonstrating the slight deviations from a true circular shape. The reason is as follows. When adding the fifth-order nonlinearity (3.34) into (3.22):

$$\begin{aligned} R_{lower} &= \frac{\left\{ \begin{array}{l} G_{3-lower} \times e^{j\omega_{lower}t} + G_{linear-lower} \times k_1 e^{j\Phi_1} e^{j\omega_{lower}t} \\ + G_5 \times e^{j(\omega_2 - 2\omega_1)t} \times \left[k_1 e^{j\Phi_1} e^{j\omega_{lower}t} \right]^2 \end{array} \right\}}{\exp(j\omega_{lower}t)} \\ &= G_{3-lower} + G_{linear-lower} \times k_1 e^{j\Phi_1} + G_5 \times k_1^2 e^{2j\Phi_1} \end{aligned} \tag{3.35}$$

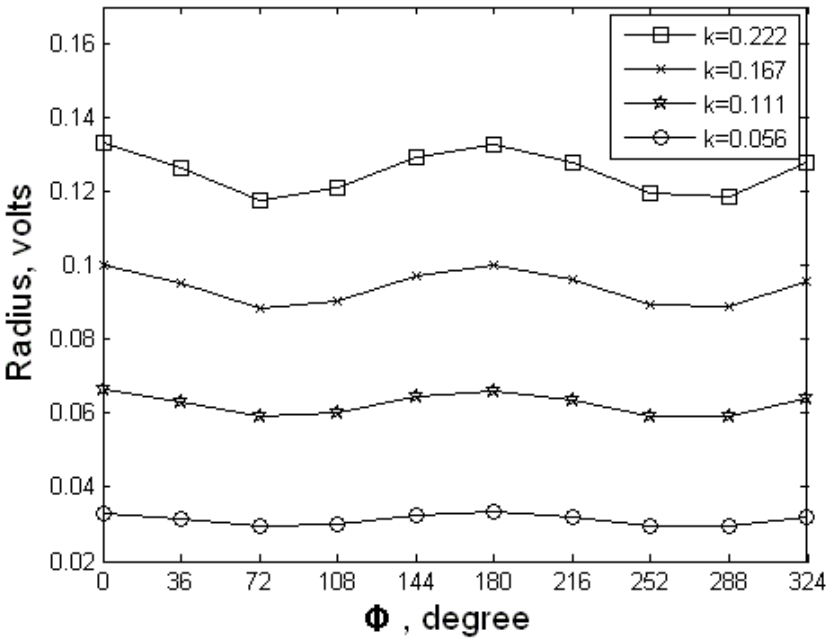

Figure 3-13 Variation of radius with angle from Fig. 3-8

The relationship between (3.35) and Fig.3-8 is explained as follows:

- The first term represents the centre of the circle.
- The linear gain $G_{linear\text{-}lower}$ is much bigger than the fifth-order nonlinearity G_5. As a result, the second term determines the average radius while the third term modulates the radius with two periods per revolution.
- The bigger the value of k is in (3.35), the more apparent the radius variation becomes in Fig.3-13.

This fifth order distortion also affects R_{upper}, $R_{upper\text{-}lower}$, $R_{lower\text{-}upper}$, affecting in turn the injection accuracy of predistortion in highly nonlinear PAs. They are similar to R_{lower}, and we list the frequency relationships in (3.36).

$$\begin{aligned} \omega_{upper} &= \omega_1 - 2\omega_2 + 2\omega_{upper} \\ \omega_{upper} &= 3\omega_1 - 2\omega_{lower} \\ \omega_{lower} &= 3\omega_2 - 2\omega_{upper} \end{aligned} \tag{3.36}$$

The above factors limit the accuracy of calculations for (k_1, Φ_1) and (k_2, Φ_2), and weaken the predistortion as demonstrated by the incomplete cancellation in Fig.3-9 and Fig.3-12.

3.3.4.2 Iteration algorithm and feasibility

In order to demonstrate the feasibility of further improvement by iteration, we discuss the relation between injected IM3s and output IM3s. Following the format of Equation (3.32), Equation (3.30) can be written in matrix form:

$$B = \begin{bmatrix} G_{3-lower} \\ G_{3-upper} \end{bmatrix} + \begin{bmatrix} G_{linear-lower} & G_{upper-lower} \\ G^*_{lower-upper} & G^*_{linear-upper} \end{bmatrix} A$$

where

$$\mathrm{A} = \begin{bmatrix} k_1 e^{j\Phi_1} \\ k_2 e^{-j\Phi_2} \end{bmatrix} \quad B = \begin{bmatrix} \dfrac{C_{lower}}{\exp(j\omega_{lower}t)} \\ \dfrac{C_{upper}}{\exp(-j\omega_{upper}t)} \end{bmatrix} \tag{3.37}$$

Equation (3.37) describes the transformation from injected IM3s (A) to output IM3s (B), $f: A \rightarrow B$. The linearity of the relationship described by (3.37) should ensure that in an iterative process, the predistortion result will converge to an optimum. The iteration steps are:

1. Measure G_{lower}, G_{upper}, $G_{linear\text{-}lower}$, $G_{linear\text{-}upper}$, $G_{upper\text{-}lower}$, $G_{lower\text{-}upper}$
2. Substitute them into (23) to determine the injection phasors $k_1e^{j\Phi 1}$, $k_2e^{j\Phi 2}$.
3. Change the input signals to:

$exp(j\omega_1 t)+exp(j\omega_2 t) + k_1e^{j\Phi 1}exp(j\omega_{lower}t)+k_2e^{j\Phi 2}exp(j\omega_{upper}t)$

4. Measure new G_{lower}, G_{upper}, $G_{linear\text{-}lower}$, $G_{linear\text{-}upper}$, $G_{upper\text{-}lower}$, $G_{lower\text{-}upper}$ again.
5. Substitute them into (3.33) and find out new $k^*_1e^{j\Phi *1}$, $k*_2e^{j\Phi *2}$
6. Add $k^*_1e^{j\Phi *1}$ and $k*_2e^{j\Phi *2}$ to the injection phasors.
7. Repeat steps 3 to 6 until the IM3 at output is reduced to the noise floor.

3.3.4.3 Experimental results

Figure 3-14 shows single sideband injection in (a) and (b). The improvement, by over 30 dB, between Fig. 3-9 (b) and Fig. 3-14 (a), and between Fig. 3-9 (c) and Fig. 3-14 (b), is brought about by iteration. Using simultaneously the same injection parameters as in Fig. 3-14 (a) and Fig. 3-14 (b), but without considering interactions, gives the dual sideband result shown in Fig. 3-14 (c). The result of dual sideband injection, considering interactions and with 2 iterations is shown in Fig. 3-14 (d). It can be seen

that the IM3 can be reduced to around -70dBm, near the noise floor, where further measurements of G_{lower}, G_{upper}, $G_{linear\text{-}lower}$, $G_{linear\text{-}upper}$, $G_{upper\text{-}lower}$, $G_{lower\text{-}upper}$ for further iterations become impractical. The dual sideband injection predistortion in Fig. 3-14 (d) has reduced IM3s by 60dB compared with the original two-tone test output spectrum in Fig. 3-9 (a).

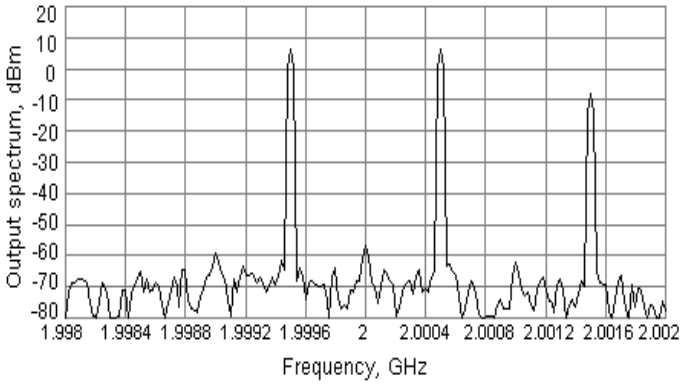

(a)

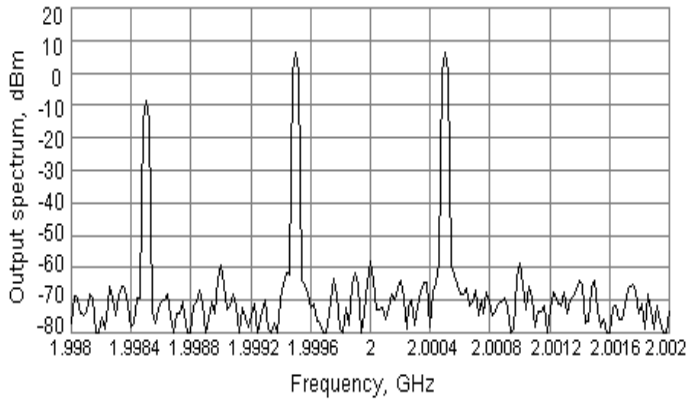

(b)

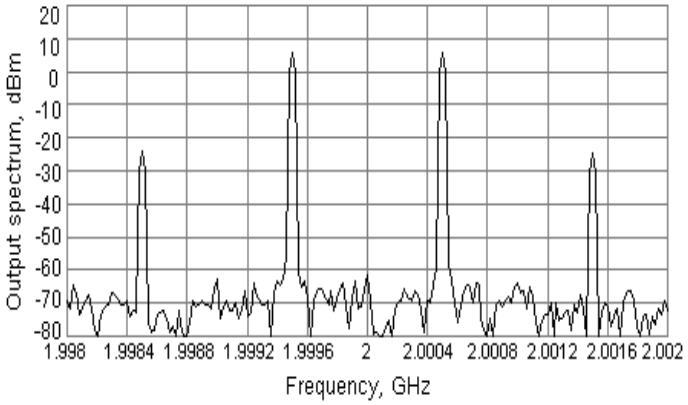

(c)

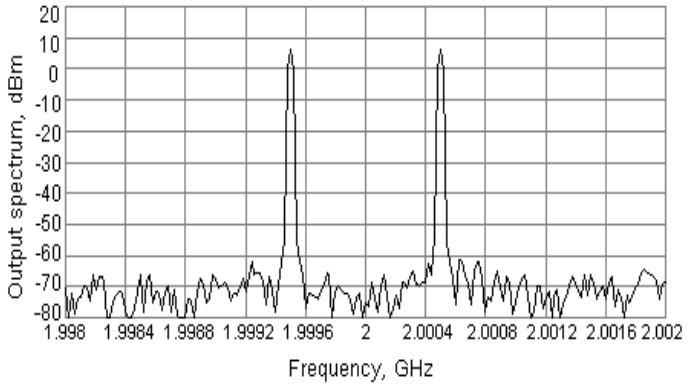

(d)

Figure 3-14 (a) Lower sideband injection with 2 iterations

(b) Upper sideband injection with 2 iterations

(c) Dual sideband injection without considering interactions

(d) Dual sideband injection considering interactions with 2 iterations

3.3.5 Injection predistortion in different signal conditions

In these experiments, the PA used is a commercial power amplifier: ZHL-4240. The gain of this PA is around 40dB. It has a maximum input power restriction of -5dBm. The 1dB compression point is -11dBm at the input. In a two-tone test, the maximum voltage of the signal is twice the maximum voltage of one carrier, so the peak envelope input power is 6dB higher than the power of one carrier. Therefore the

peak envelope power reached the maximum specified input power when each input carrier was at -11dBm. The peak envelope power reached the 1dB compression point when each input carrier was at -17dBm. Fig.3-15 shows the result of dual sideband injection predistortion with the input power per carrier varied from -18dBm to -10dBm, which therefore spans the 1dB compression point and the maximum specified input power, and with the tone-spacing varied from 1MHz to 10MHz.

The injected signals at each tone-spacing and power level were determined by the methods discussed in Section 3.3.4. The IM3 powers before and after predistortion are shown in Fig.3-15 (a), the injected IM3 amplitudes and phases are shown in Fig.3-15 (b) and Fig.3-15 (c). All of the injection parameters were determined in only two iterations.

In Fig.3-15 (a), the upper planes in both IM3L and IM3U represent the original IM3 powers, while lower planes represent IM3 powers after injection predistortion. All these power levels are relative to the output carrier power. The small fluctuations occur because the IM3 powers are reduced to the noise floor. Comparing the phase plots of IM3L and IM3U in Fig.3-7 (b) and (d), with the phases of the injected IM3L and IM3U signals in Fig.3-15 (c), the shapes are similar, with approximately 180^{o} offset. An offset of exactly 180^{o} would be expected for perfect cancellation if there were no interaction between upper and lower IM3s, and the deviation from 180^{o} is due to the interactions.

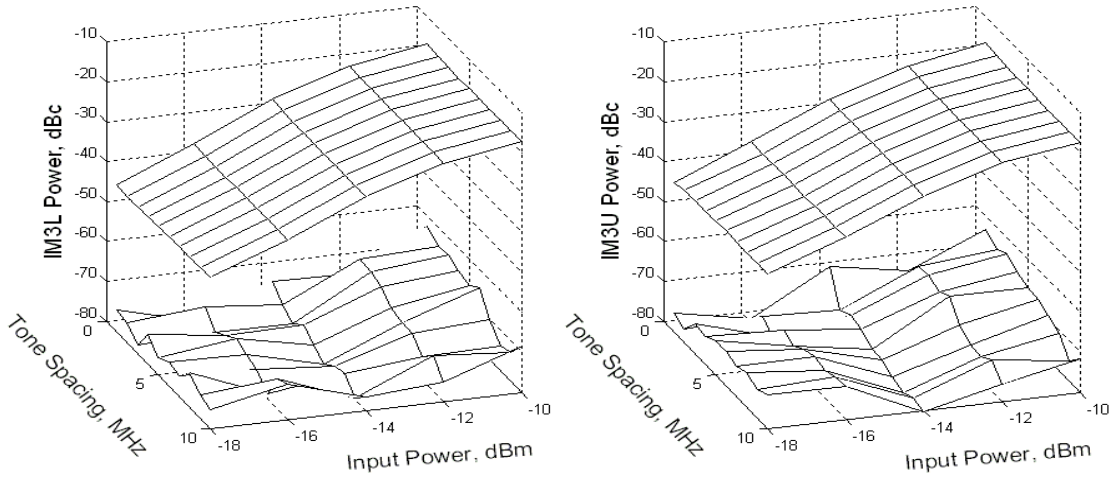

(a)

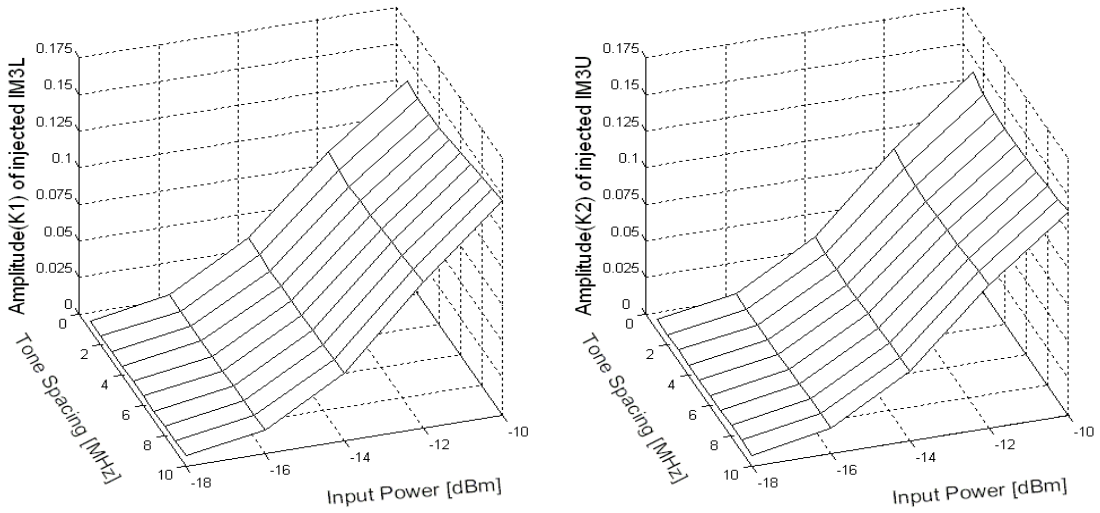

(b)

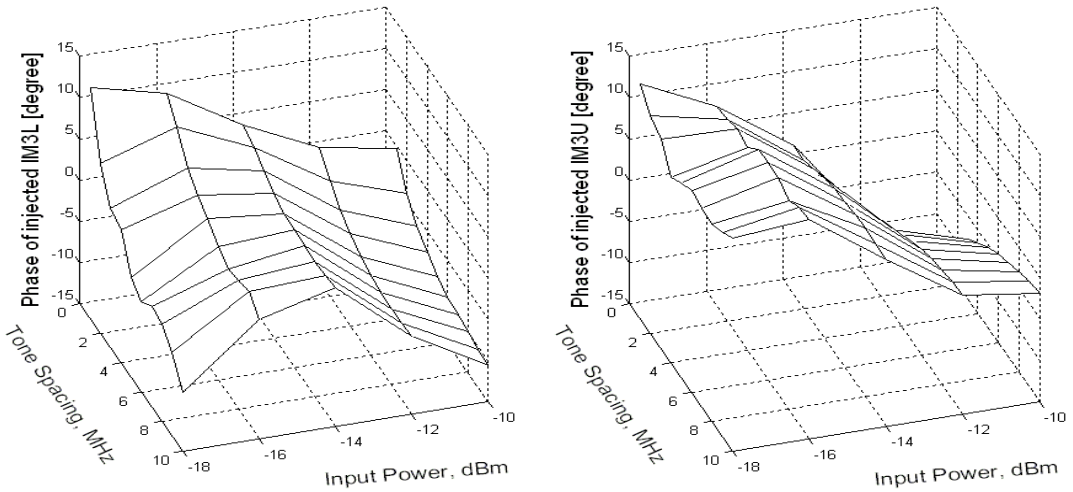

(c)

Figure 3-15 (a) IM3s power level before/after injection

(b) Amplitude of injected IM3s

(c) Angle of injected IM3s

3.4 Summary

In this chapter, we have briefly introduced two-tone tests, and implemented new measurement and injection predistortion techniques in two-tone tests.

The new measurement is to calculate the ratio between output IM3 products and novel

IM3 references which are created by the two main output tones. With these results, we can clearly describe the relationship between injected and output IM3 products. Based on this relationship, a correct injection for either lower or upper sideband IM3 can be easily calculated instead of manual tuning. Additionally, interaction between lower and upper sideband IM3 products has been revealed during the research. To our knowledge, this interaction has not been proposed in published papers before. As a result, further IM3 reductions have been achieved considering these interactions. The advantage of injection compared with a look-up table approach is that it can address each intermodulation product separately, making it more capable of handling memory effects in PAs.

CHAPTER 4

APPLICATION OF INJECTION PREDISTORTION TECHNIQUES IN 16 QAM SIGNALS

After applying injection predistortion in two-tone tests in Chapter 3, here we will apply the similar methods to a PA subjected to a 16 QAM signals. In this chapter, we will firstly review the injection results in the published papers, and then introduce our different injection techniques. Furthermore, we will demonstrate how this injection predistortion deals with memory effects.

4.1 Published injection predistortion result for wideband signal

Since injection linearization has been proved to work in two-tone tests, it is reasonable to apply similar techniques in a PA subjected to 16 QAM signals. The principles are explained in Chapter 2, so in this section, we just review their performances.

Paper [48] has shown a harmonic injection technique applied to a 28 dBm PA with a 1.23 MHz channel bandwidth offset-QPSK CDMA signal, in Fig. 4-1. An average improvement in adjacent channel power ratio (ACPR) of 6 dB is obtained.

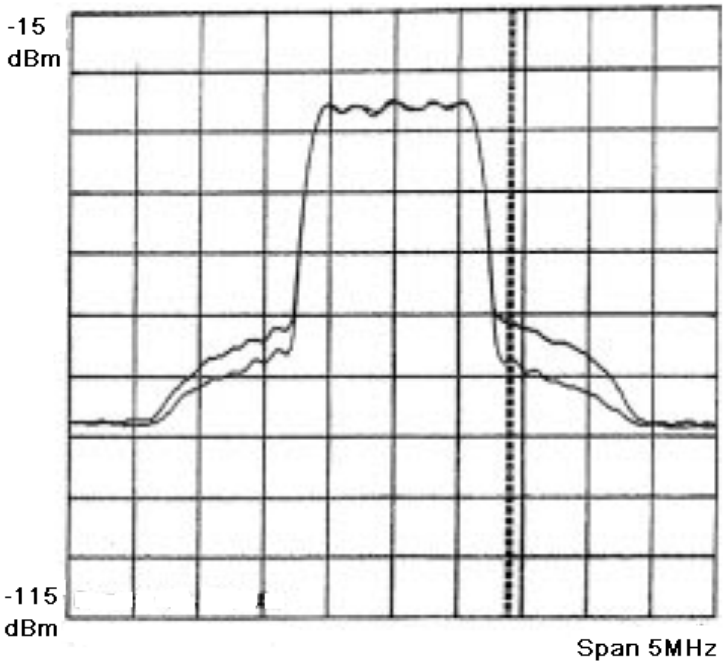

Figure 4-1 Second harmonic injection in wideband signal in [48]

Third- and fifth-order baseband component injection [51] is analyzed in Section 2.2.5.1. It has around 10 dB reduction on spectral regrowth, shown in Fig. 4-2.

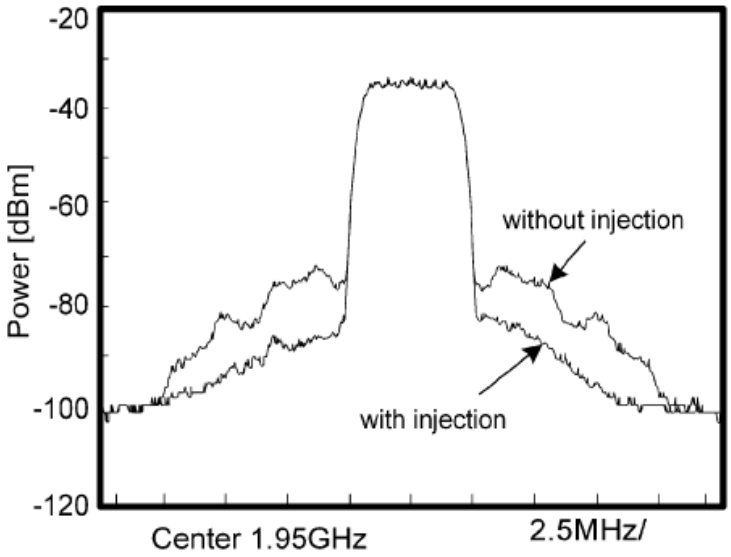

Figure 4-2 Third- and fifth-order injection in W-CDMA in [51]

A simultaneous harmonic and baseband signal injection is proposed in [47]. Fig. 4-3 shows the comparisons between the combined injection and single injection. Among these predistortions, the combined harmonic and baseband signal injection has a 25

dB reduction in the spectral regrowth.

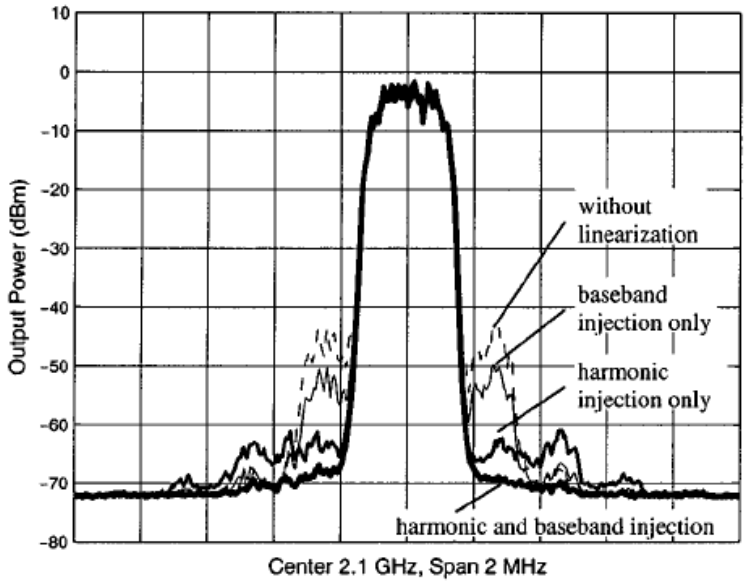

Figure 4-3 Simultaneous harmonic and baseband signal injection [47]

The injection can selectively suppress a small number of intermodulation products, for example, IM3 products in a two-tone test. However, when used in wideband communication systems, the injection methods proposed in the last three papers only control the magnitude and phase of the entire set of injected signals. It is not possible by these methods to control the relative phases and amplitudes of the individual injected sub frequency component. As a result, their ACPR reduction doesn't work well. In the third example, the combined injection has a better performance, but the authors do not report the extent of the memory effects that existed in the experimental PA. Theoretically, it would be better to control each sub-frequency instead of the entire signal in injection predistortion, especially applied in PA with significant memory effects.

4.2 Proposed digital baseband injection

We propose a novel injection technique for a power amplifier subjected to 16 QAM

signals. It allocates every sub-frequency, defining their amplitudes and phases individually, to counteract the output spectral regrowth.

4.2.1 Experimental setup

Suppose a wideband digital communication signal in baseband is written as

$$I(t) + j \times Q(t) \tag{4.1}$$

After modulation in RF domain with centre frequency of ω_c:

$$I(t) \times \cos(\omega_c t) - Q(t) \times \sin(\omega_c t) \tag{4.2}$$

The digital injection is operated in baseband (4.1), while the PA is working in RF band (4.2). The experimental setup is shown in Fig. 4-4. The PC generates digital baseband signals added with injected signals and transfers them into memory of a waveform generator (Rhode and Schwarz AMIQ, Appendix B). The AMIQ outputs I and Q analogue signal repeatedly and these signals are modulated and up-converted to RF frequencies (2GHz) by a signal generator with a built-in modulator (the program to control AMIQ is in Appendix D and the program to generate the signal is in Appendix F). The RF signals go through a 40dB gain commercial PA (ZHL-4240, Appendix A) working in its saturation range where it achieves higher efficiency but lower linearity. Finally, the output signals are down-converted and demodulated to baseband I and Q signals and sampled inside a vector signal analyzer (VSA). There is an attenuator connected to the input of VSA to protect it from high power signal.

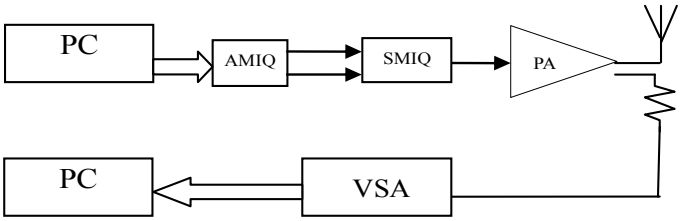

Figure 4-4 Experimental setup

4.2.2 Sub-frequency allocation and calculation

In this injection predistortion, we need to specify the frequency range of the injected sub-frequency components, and calculate the amplitudes and phases of these sub-frequencies. Supposing that the bandwidth of the signals is B Hz, the main spectral regrowth (also called adjacent channel intermodulation products) after a nonlinear PA will cover B Hz both in lower and upper sidebands, as shown in Fig. 4-5 (a).

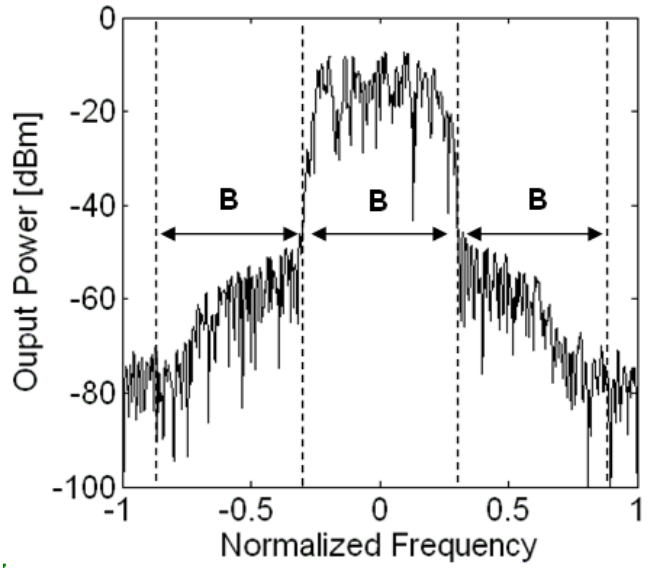

(a)

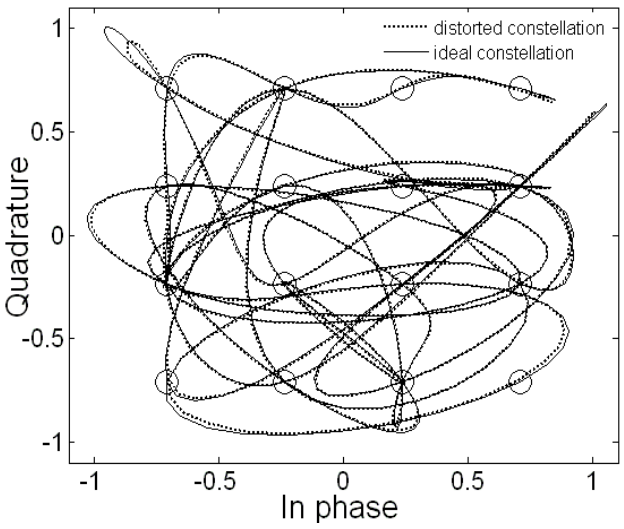

(b)

Figure 4-5 (a) Measured output spectrum of a 16 QAM signal

(b) Measured (normalized) and ideal constellation

Figure 4-5 (a) shows there is a -40dBc spectral regrowth relative to in band communication signals, which indicate that the PA is driven hard. Fig. 4-5 (b) shows the distorted constellation after demodulation, as well as an ideal constellation. The distorted constellation also shows that the PA is working in compression, because a reduction of amplitude is apparent at the highest amplitude regions of the trace.

Written in mathematical equations, the input base band 16 QAM signals (4.1) can be written as the sum of sine waves:

$$K_0 e^{j\omega t} + K_1 e^{j(\omega+1)t} + \ldots + K_N e^{j(\omega+N)t} = \sum_{i=0}^{N} K_i e^{j(\omega+i)t} \qquad (4.3)$$

where, ω is a normalized frequency, $\omega+i$ is the normalized frequency of sub-band i, N is the normalized bandwidth of the signal.

Accordingly, the sum of sine waves of i=-N to -1 can represent the lower sideband:

$$K_{-1}e^{j(\omega-1)t} + K_{-2}e^{j(\omega-2)t} + \ldots + K_{-N}e^{j(\omega-N)t} = \sum_{i=-N}^{-1} K_i e^{j(\omega+i)t} \qquad (4.4)$$

Similarly, the upper sideband spectral regrowth with sub-frequencies of $i=N+1$ to $2N$ would be:

$$K_{N+1}e^{j(\omega+N+1)t} + K_{N+2}e^{j(\omega+N+2)t} + \ldots + K_{2N}e^{j(\omega+2N)t} = \sum_{N+1}^{2N} K_i e^{j(\omega+i)t} \qquad (4.5)$$

The aim of injection predistortion is to choose appropriate values of K in (4.4) and (4.5), to counteract the output spectral regrowth. We define 10 groups of K values, shown in table 4-1. Each row in table 4-1 represents a set of experimental K values. And each set of K values will be applied to (4.4) and (4.5) as an injected signal to go through the PA. So we have ten output results.

TABLE 4-1
Values for K

	K_{-N}	...	K_{-2}	K_{-1}	K_{N+1}	K_{N+2}	...	K_{2N}
1	$e^{j\frac{1}{5}\pi}$	$e^{j\frac{1}{5}\pi}$	$e^{j\frac{1}{5}\pi}$	$e^{j\frac{1}{5}\pi}$	$e^{j\frac{1}{5}\pi}$	$e^{j\frac{1}{5}\pi}$	$e^{j\frac{1}{5}\pi}$	$e^{j\frac{1}{5}\pi}$
2	$e^{j\frac{2}{5}\pi}$	$e^{j\frac{2}{5}\pi}$	$e^{j\frac{2}{5}\pi}$	$e^{j\frac{2}{5}\pi}$	$e^{j\frac{2}{5}\pi}$	$e^{j\frac{2}{5}\pi}$	$e^{j\frac{2}{5}\pi}$	$e^{j\frac{2}{5}\pi}$
…	$e^{j1\frac{4}{5}\pi}$	$e^{j1\frac{4}{5}\pi}$	$e^{j1\frac{4}{5}\pi}$	$e^{j1\frac{4}{5}\pi}$	$e^{j1\frac{4}{5}\pi}$	$e^{j1\frac{4}{5}\pi}$	$e^{j1\frac{4}{5}\pi}$	$e^{j1\frac{4}{5}\pi}$
10	$e^{j2\pi}$	$e^{j2\pi}$	$e^{j2\pi}$	$e^{j2\pi}$	$e^{j2\pi}$	$e^{j2\pi}$	$e^{j2\pi}$	$e^{j2\pi}$

In our experiment, we are using 16-QAM modulations to encode a sequence of 50 symbols repeatedly, with a raised cosine filter with an up sample rate of 10. Thus each period of 50 symbols has 500 samples. When we apply a Fourier transform on one period of these signals, there are 500 different sub-frequencies in frequency domain. The wanted signal covers sub-frequencies from -29 to 30 as shown in Fig. 4-6 (a).

As in table 4-1, the lower and upper spectral regrowth will cover the sub-frequencies from -89 to -30 and from 31 to 90, respectively. We generate 10 different sets of injections (e.g. in Table 4-1), which have the identical amplitude as shown in Fig. 4-6 (a), but different phases, from 0^o to 360^o with an interval of 36^o as shown in Fig. 4-6 (b). The real measured input spectrum using one set of data is shown in Fig. 4-7. The injected components look like two "brick-walls".

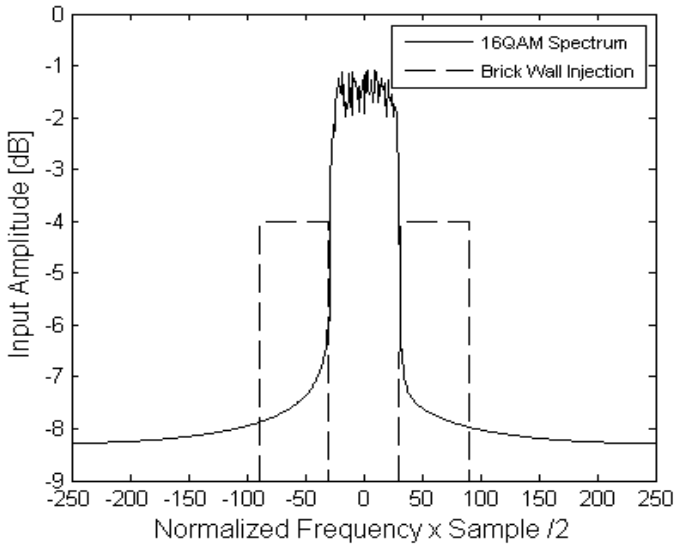

(a)

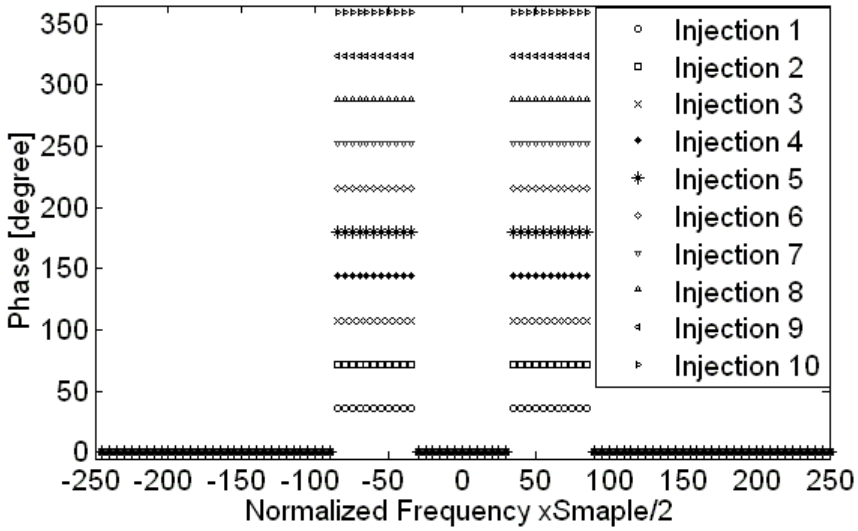

(b)

Figure 4-6 (a) Amplitude of 16 QAM signals and injection

(b) Phase of 10 different injections

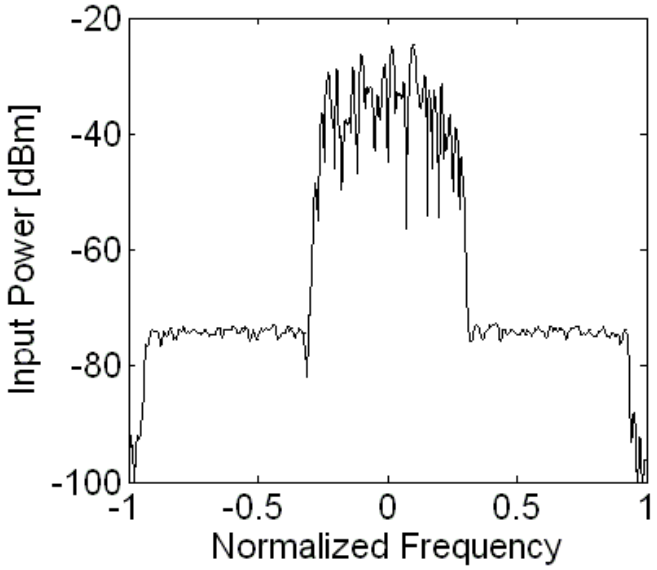

Figure 4-7 Input spectrum of injection

There are 10 different outputs relative to 10 different injections, which are demodulated and written as complex signals. With these 10 different complex signals, we synchronize them by their amplitudes, and pick up one period from each output for next step of analysis.

After synchronization in the time domain, we apply a Fourier transform to these 10 different signals and analyze them in the frequency domain. In each spectrum, each sub-frequency component in adjacent channel can be considered as the combination of intermodulation products and injections. When we compare 10 sub-frequency components from 10 different spectra but with the same frequency, they have the same intermodulation products but 10 different phases of injections. For example, Fig. 4-8 plots 50 different vectors which are collected from 5 different sub-frequencies of 10 output spectra.

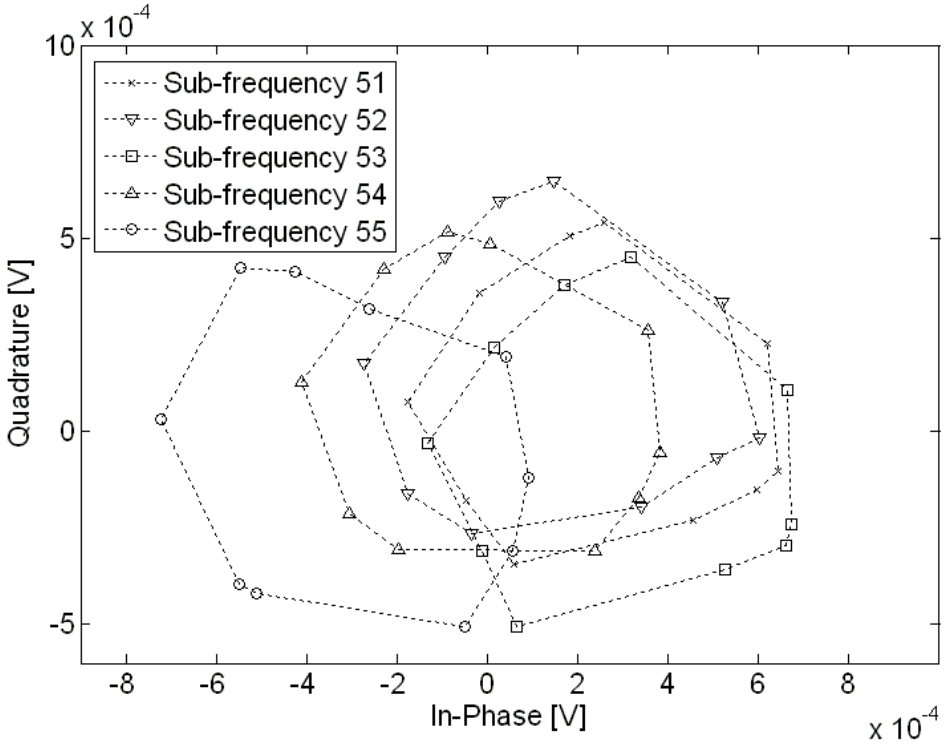

Figure 4-8 Sub-frequency from 51 to 55

In Fig. 4-8, among these 50 different vectors, we divide them into 5 groups by their sub-frequency numbers. In each group, we connect them successively by the order of the injections. The contours are approximately circles. In each circle, the centre is contributed by original intermodulation products and the radius is contributed by the injected vector. The ideal relation for one sub-frequency can be seen in Fig. 4-9.

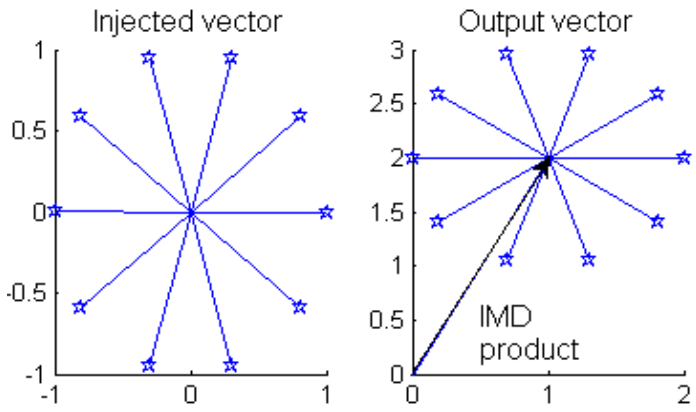

Figure 4-9 Ideal input output relation for each sub-frequency

The target for the injection is to generate a new vector which counteracts the original intermodulation products at every sub-frequency in the lower and upper side band. Note that the interactions in two-tone test injection also occur in the wideband signal injection. These can be observed by the distortions of the circles in Fig. 4-8. The equation for solving interactions in two-tone tests is written again here:

$$\begin{bmatrix} k_1 e^{j\Phi_1} \\ k_2 e^{-j\Phi_2} \end{bmatrix} = -\begin{bmatrix} G_{linear-lower} & G_{upper-lower} \\ G^*_{lower-upper} & G^*_{linear-upper} \end{bmatrix}^{-1} \begin{bmatrix} G_{3-lower} \\ G^*_{3-upper} \end{bmatrix} \tag{3.33}$$

A 2×2 matrix with 4 parameters is simple and effective for a two-tone test. However, when this matrix is applied to a wideband signal case, its size will increase dramatically. For example, there are 120 sub-frequencies in this 16 QAM signal, which indicates a 120×120 matrix. For each element of this matrix, we need to plot a circle to calculate its value. Even though we can measure 3 spots to identify the circle as the fastest way, there are still totally 120×120×3=43200 measurements to complete this matrix. This matrix method is unrealistic in wide band signal cases. Therefore, an alternative is needed.

In this case, we propose an iterative method to solve this interaction problem in wideband signal cases. Suppose the total number of sub-frequencies of the QAM signal is *N*, which means:

$$I(t) + jQ(t) = \sum_{i=0}^{N} K_i e^{j(\omega+i)t} \tag{4.6}$$

It also means that each of the lower and upper sideband spectral regrowth has *N* sub-frequencies, which is coordinate with (4.3), (4.4) and (4.5). With these assumptions, the iteration is shown and explained as follows:

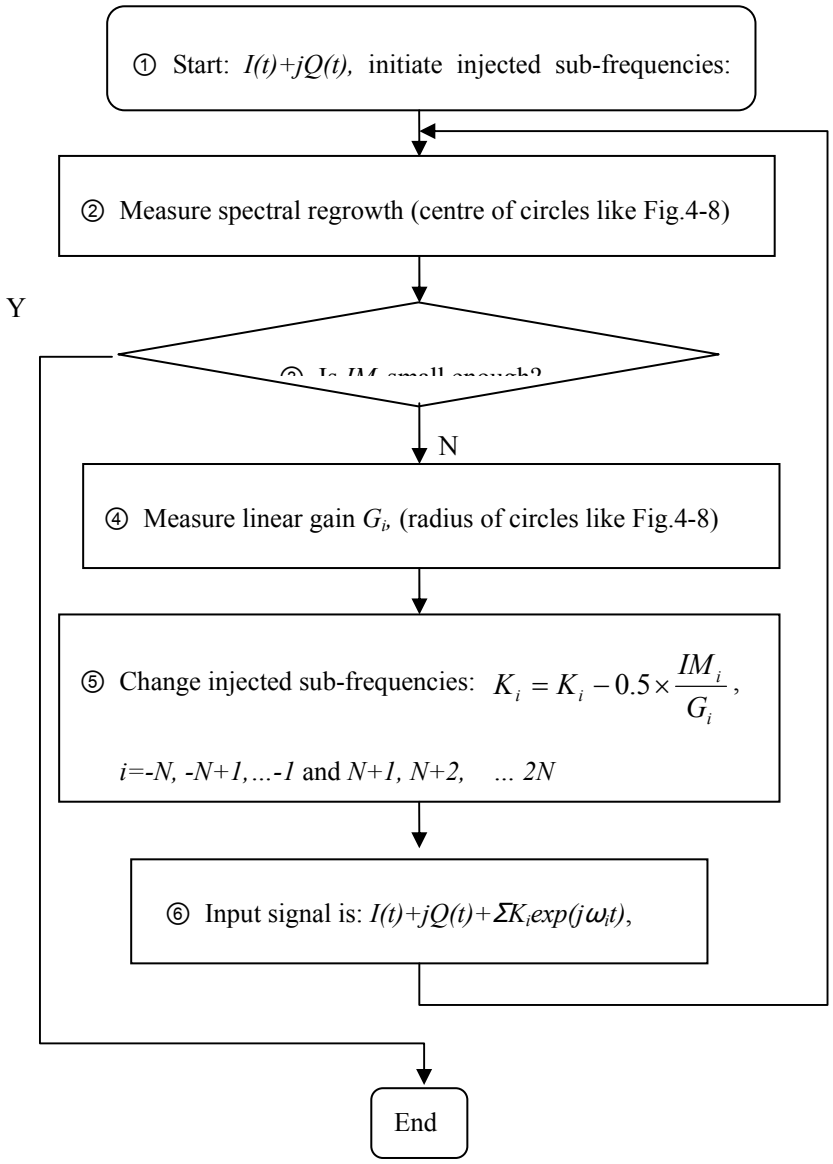

Figure 4-10 Flowchart for iterative computation of injection in 16 QAM

□ At the beginning, the initial injected sub-frequencies K_i are set to be zero. The input now only contains the 16 QAM signals.

□ We measure the residual intermodulation products (IM_i) at the spectral regrowth, which are the centre of the circles plotted in Fig. 4-8.

□ If IM_i are small which means the spectral regrowth are reduced to a satisfactory

range, we stop the process, otherwise we begin to calculate the injection K_i.

 We measure the linear gain of the PA (G_i), at different sub-frequencies, which can be determined from the radius of the circles in Fig. 4-8. The linear gains should be identical in a memoryless PA case. However, in a PA with memory effects, they vary with frequency, so we need to measure them separately.

 The injection without considering the interaction would be:

$$K_i = -\frac{IM_i}{G_i} \tag{4.7}$$

We put a negative sign in (4.7) because we need the opposite phases for injection. When (4.7) is applied to the procedure, we have two modifications. Firstly, a reduction to the injected components is needed in order to suppress the interaction between the in band signal and these injected components. In this case, we divide all the injected components by two. However, this suppression coefficient can be varied from zero to one, depending on the situation. For example, we can have a smaller coefficient if the interactions are substantial, or have a larger coefficient if the interactions are inconspicuous. Secondly, all of the injection results are accumulated in the iteration. So (4.7) is changed to:

$$K_i(new) = K_i - 0.5 \times \frac{IM_i}{G_i} \tag{4.8}$$

 All the injected sub-frequencies and the 16 QAM signal are added together as a new input signal. We then go to step again.

4.2.3 Experimental results

The injection results in this case are shown in Fig. 4-11. The ACPR before predistortion is around -40dBc relative to in band power. It has been reduced by more than 15dB at the first injection. A further 12dB reduction is achieved by the second iteration, giving a total of nearly 30dB improvement.

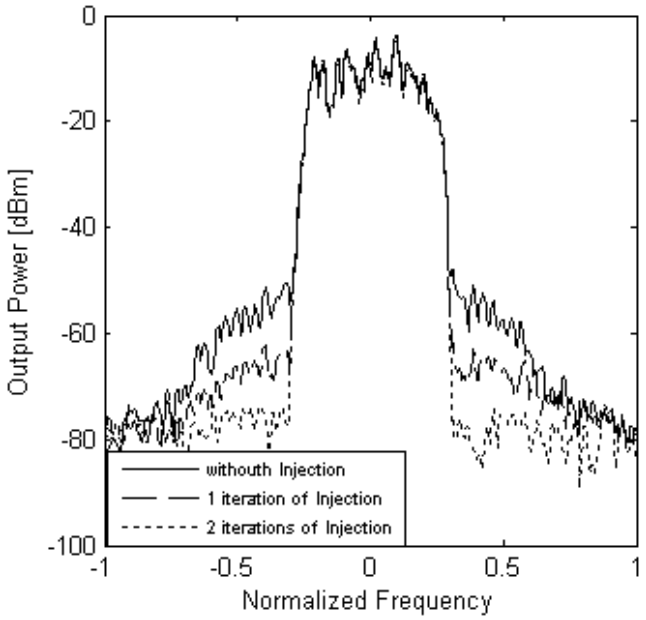

Figure 4-11 Output spectra in injection predistortion

Unlike the published techniques, this injection predistortion has taken account of the different frequency response of the PA, and gives different scales and different rotations for different sub-frequencies instead of manipulating them all together. Fig. 4-12 shows a single side band injection, which reduces the upper sideband of spectral regrowth. It shows that this injection technique is sensitive to each sub-frequency and more capable of handling memory effects.

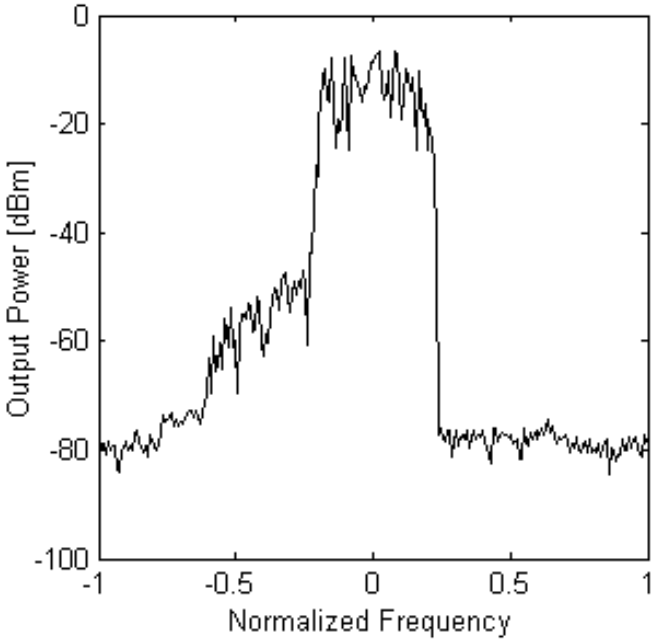

Figure 4-12 Upper sideband injection

4.3 Summary

In this chapter, we have applied the similar digital injection techniques to a 16 QAM wideband signal. Since the matrix approach is no longer practical in wideband signal cases, we use an iterative method to solve the interaction problem.

Unlike the published injection techniques, this new digital injection predistortion method can address the amplitude and phase for each sub-frequency in the spectral regrowth. In our experiment, this injection technique achieves a 30 dB reduction of spectral regrowth, which is better than the published papers. Additionally, we have also proved that this injection method can suppress the upper and lower spectral regrowth sidebands separately, thus demonstrating its capacity for dealing with memory effects.

It is easy to reduce the spectral regrowth by suppressing them to zero. However, it is more difficult to tell the correct values of amplitudes and phases of the

sub-frequencies in the in band range. Therefore, this injection technique can not reduce intermodulation products in the in band signal. Additionally, the interactions caused by the injected signal will be added to the in band signal. In Chapter 5, we will propose a combined technique, which can solve this problem.

CHAPTER 5

COMBINED LUT PLUS INJECTION PREDISTORTION

Firstly in this chapter, we will briefly review LUT based predistortion, and discuss the difference between LUT and injection mathematically. Secondly, we will compare their experimental performance mainly in terms of adjacent channel power ratio (ACPR) reduction, error vector magnitude (EVM) improvement. Thirdly, we propose an integrated predistorter: LUT plus injection (L+I) predistortion to inherit their advantages based on their comparisons, and verify its abilities by applying to a cascaded PA system having both nonlinearities and memory effects.

5.1 Mathematical relations between LUT and injection

The traditional LUT is a simple AM/AM and AM/PM predistortion technique. Fig. 5-1 shows a simple digital predistorter using AM/AM and AM/PM conversion: $F(|V_i|)$, and this conversion can be carried out by a LUT. There are many improvements [16] of this conversion to achieve better performance where there are memory effects in the PA, like Volterra, Wiener, Hammerstein and memory polynomials.

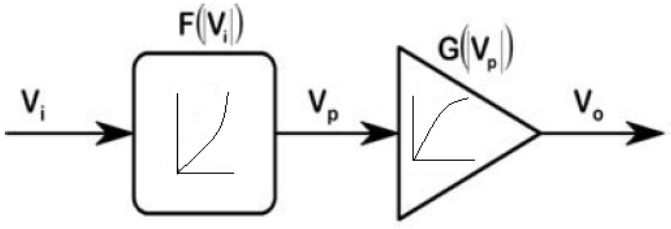

Figure 5-1 Digital predistortion for a power amplifier

The LUT mentioned in this chapter is referred to a simple AM/AM and AM/PM conversion. The LUT in our research is generated and implemented by Matlab, which can be found in Appendix G. We firstly analyze the relation and difference between LUT and injection mathematically before comparing their experimental results.

As shown in Fig. 5-1, $F(|V_i|)$ describes the AM/AM and AM/PM conversion, which can be written in a power series:

$$F(|V_i|) = A_1 V_i + A_2 |V_i| V_i + A_3 |V_i|^2 V_i + A_4 |V_i|^3 V_i + A_5 |V_i|^4 V_i + \ldots \qquad (5.1)$$

We denote

$$A = |A| . \exp[j \angle A]$$

for A_1, A_2, A_3, A_4, A_5.

In (5.1), A_1 represents the linear gain back-off, which can be observed in Fig. 5-2, the odd order coefficients representing the odd order distortions will determine the in-band distortion. And these terms $A_3|V_i|^2 V_i$, $A_5|V_i|^4 V_i$ in (5.1) can be judged as third- and fifth-order injections [51]. It is important to note that, unlike the LUT, the injection generally does not affect the linear gain.

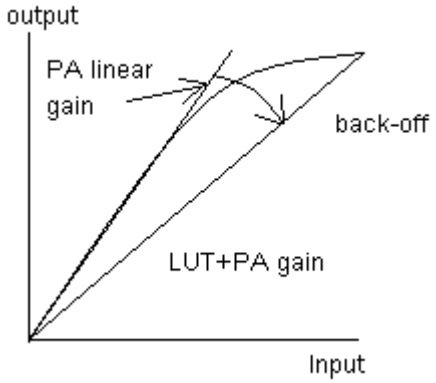

Figure 5-2 Explanation of linear gain back-off in LUT

We now analyze the differences among LUT, published injection and our proposed injection techniques.

Assume that the input V_i is written in the form of Fourier series as:

$$K_0 e^{j\omega t} + K_1 e^{j(\omega+1)t} + \ldots + K_N e^{j(\omega+N)t} = \sum_{i=0}^{N} K_i e^{j(\omega+i)t} \tag{5.2}$$

Equation (5.2) is the same as (4.3). The third-order power series of LUT, (i.e., $A_3|V_i|^2 V_i$) would be:

$$\begin{aligned} A_3 V_i^2 V_i^* = A_3 \left(K_0 e^{j\omega t} + K_1 e^{j(\omega+1)t} + \ldots + K_N e^{j(\omega+N)t}\right)^2 \times \\ \left(K_0 e^{-j\omega t} + K_1 e^{-j(\omega+1)t} + \ldots + K_N e^{-j(\omega+N)t}\right) \end{aligned} \tag{5.3}$$

There will be a lot of cross products in (5.3). Disregarding the coefficients A and K, and focusing on the exponential terms, we will find out that:

$$\begin{aligned} &\left(e^{j\omega t} + e^{j(\omega+1)t} + \ldots + e^{j(\omega+N-1)t}\right) \times e^{-j(\omega+N)t} \times e^{j\omega t} \\ &= e^{j(\omega-N)t} + e^{j(\omega-N+1)t} + \cdots + e^{j(\omega-1)t} \end{aligned} \tag{5.4}$$

These cross products will provide the lower sideband frequencies, the same as in (4.4). And we can find out the upper sideband frequencies in (5.3) similarly:

$$\begin{aligned} &\left(e^{j(\omega+1)t} + e^{j(\omega+2)t} + \ldots + e^{j(\omega+N)t}\right) \times e^{-j\omega t} \times e^{j(\omega+N)t} \\ &= e^{j(\omega+N+1)t} + e^{j(\omega+N+2)t} + \cdots + e^{j(\omega+2N)t} \end{aligned} \tag{5.5}$$

In other words, this third-order term has provided us both of the lower and upper sideband frequencies. The published injection [47, 48, 51] and LUT focus on verifying A_3, which is enough while the PA doesn't have strong memory effects. By contrast, our injection focuses on the lower and upper sideband of the sub-frequencies

and verifies their amplitude and phases to particularly deal with different frequency response or memory effects of the PA.

5.2 Experimental comparisons between LUT and injection

After the mathematical analysis, we will individually apply LUT and injection predistortion to a commercial PA having weak memory effects but strong nonlinearities, with a 16 QAM signal (The program to implement the LUT and L+I is in Appendix G). The comparisons include spectral regrowth, average output power, peak to average ratio and error vector magnitude (EVM), which is defined on page 100. All the measurements are shown from Fig. 5-3 to Fig. 5-7.

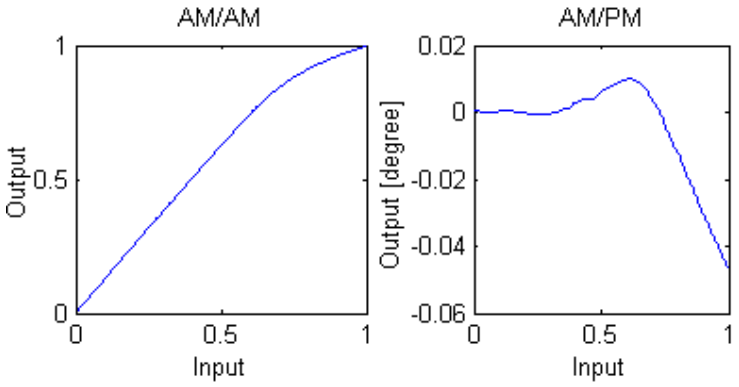

Figure 5-3 Normalized AM/AM and AM/PM measurement

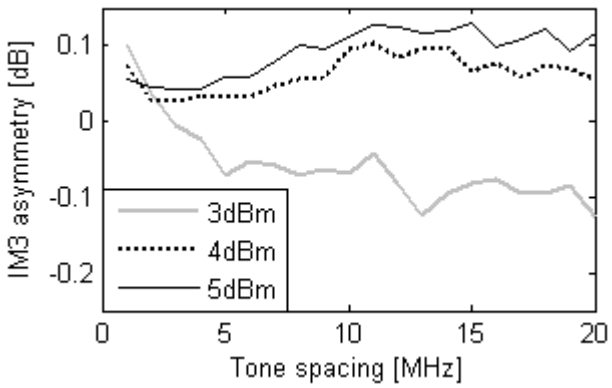

Figure 5-4 IM3 asymmetries at different two-tone input power

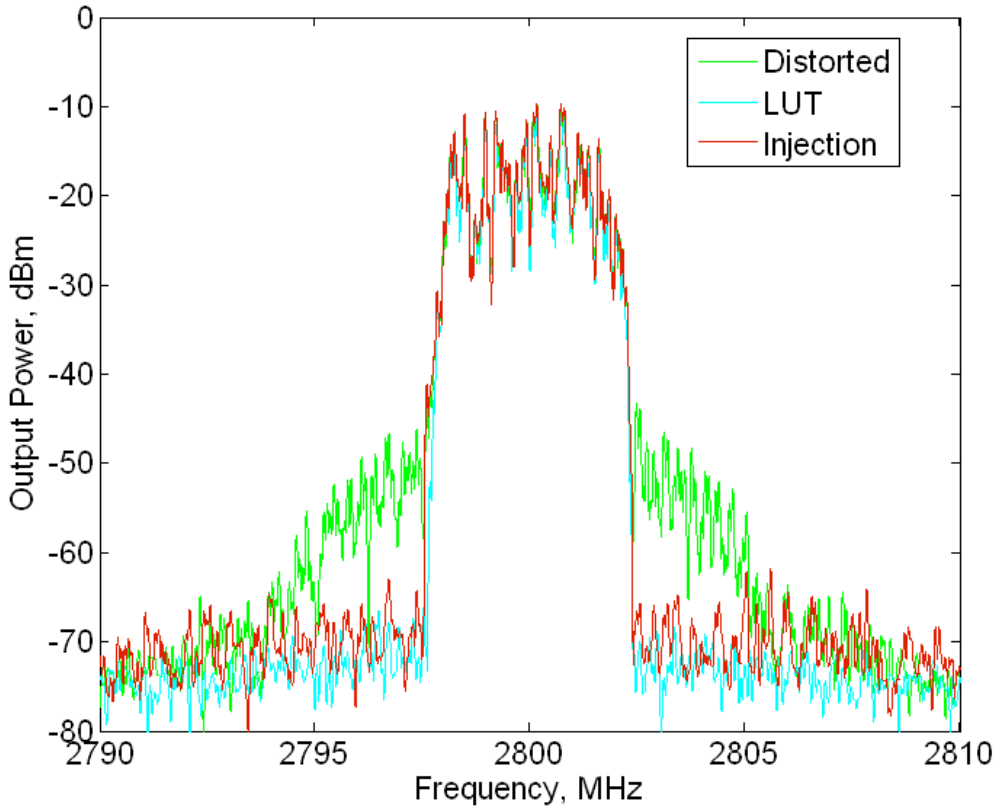

Figure 5-5 Comparison of power spectra

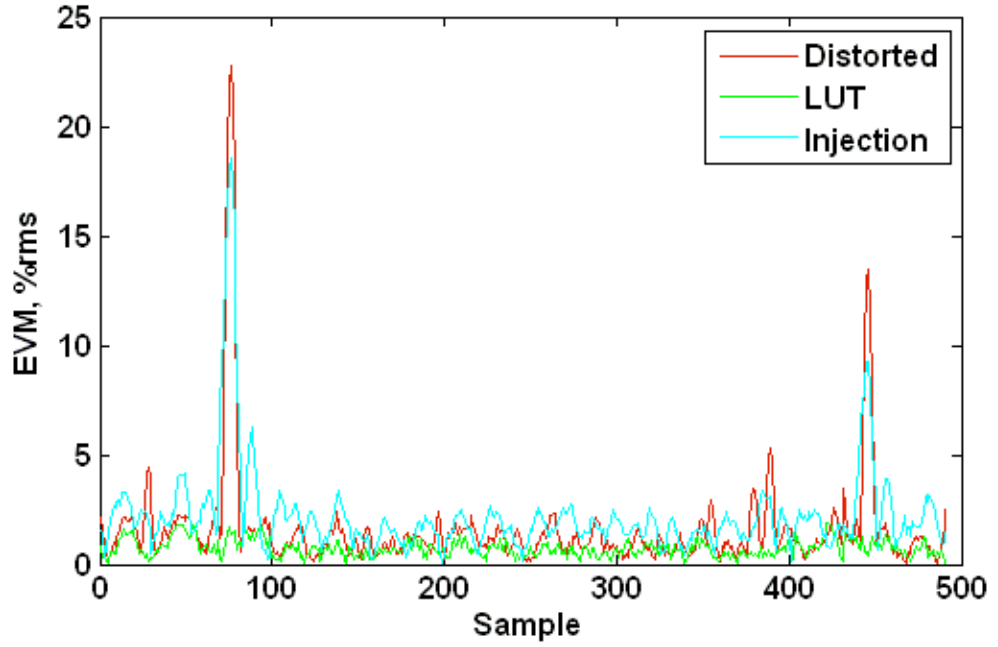

Figure 5-6 Comparison on EVM

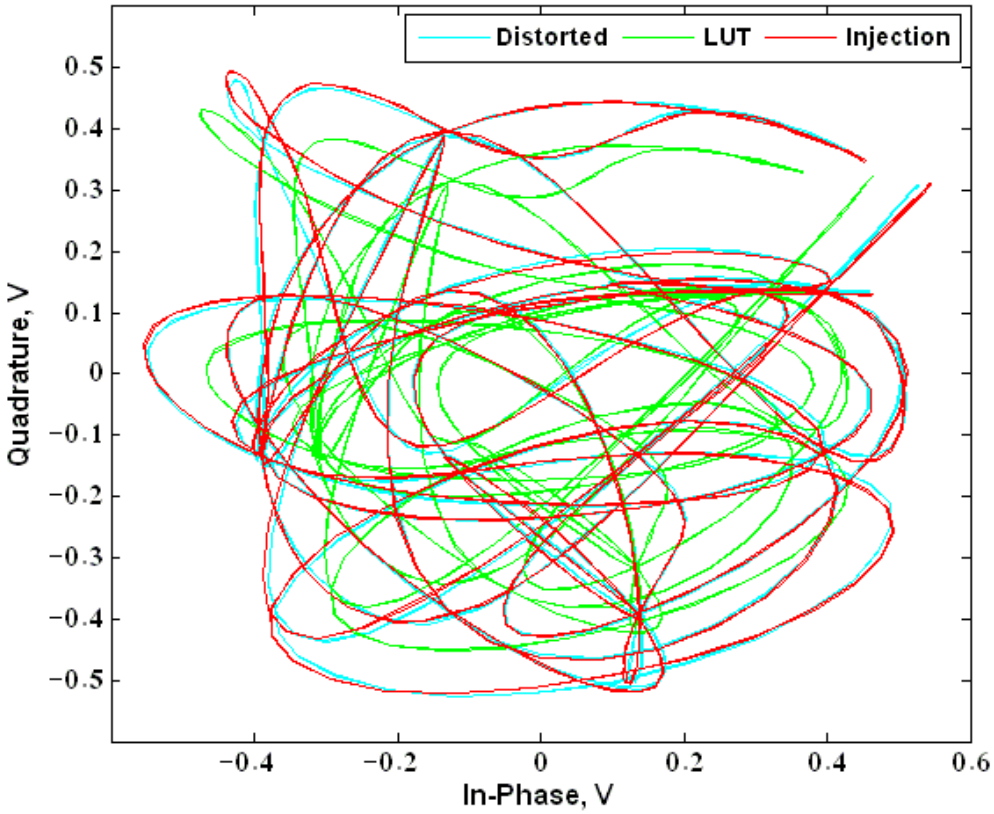

Figure 5-7 Comparison of output constellations

TABLE 5-1
EXPERIMENTAL MEASUREMENTS

	ACPR reduction (dBc)	Average EVM (%rms)	Average output magnitude (Volt)	Peak value (Volt)	Crest factor (input 2.075)
Distorted	N/A	1.6002	0.3678	0.6420	1.7455
LUT	23	0.7305	0.3054	0.6405	2.0974
Injection	23	2.1976	0.3669	0.6581	1.7936

Fig. 5-3 shows the AM/AM and AM/PM conversion occurring in a commercial memoryless PA. They are measured using sine wave envelope signals. The AM/AM conversion shows that the PA is working at its compression point. Fig. 5-4 plots the third order intermodulation (IM3) asymmetries measurements in a two-tone test, which shows that the PA has weak memory effects, comparing with the next experiments (the input maximum power for this experiment without predistortion is

4dBm). Fig. 5-5 shows the spectral regrowth reductions by LUT and injection. Fig. 5-6 shows the EVM improvements by LUT and injection. Fig. 5-7 shows the PA's distorted constellation compared with LUT and injection predistortion constellation. Table 5-1 shows a comparison of the detailed results. EVM is short for error vector magnitude. An error vector is the difference between the ideal constellation and the actual received constellation. The average power of the error vector, normalized to the signal power, is the EVM. The peak value is the maximum magnitude in the constellation of the signal. The crest factor (peak-to-average ratio or peak-to-average power ratio) is a measurement that calculated form the peak amplitude of the waveform divided by the root mean square value of the waveform.

From these comparisons, we can see that both LUT and injection reduce the spectral regrowth down to the noise floor. The difference is that LUT has a significant linear gain back-off, where $|A_1|<1$ in (5.1), while the injection technique has not. This can be observed either from their average output magnitudes in Table 5-1, or constellation routes in Fig. 5-7. However, their peak values are near to each other. The LUT generally has the same peak value as the distorted signal because they share the same maximum input amplitude in AM/AM conversion. Injection would be a little bigger or smaller than the distorted signal because the injection signal would enhance the original signal while the phase between them is smaller than 90^o at highest magnitude, or cancel each other while the phase between them is bigger than 90^o. On the other hand, due to the linear gain back-off, the shape of LUT output constellation is more similar to a standard 16 QAM signal, when compared with the output constellation using injection. This can be observed in the EVM plot in Fig. 5-7, or in the crest factor in table 5-1. Although these two predistortion techniques have similar impacts on spectral regrowth reduction, they result in different EVM values. The reason is as follows. EVM is contributed by both in-band distortion and spectral regrowth in the frequency domain. Injection reduces spectral regrowth and therefore improves the EVM. While at the same time, due to the nonlinearities of the PA, the side band injected signal and original in band signal will generate new intermodulation products

[8] and this will affect the in-band signal, which increases the EVM. Fig. 5-4 shows strong nonlinearities existing in the PA, which means the new in band intermodulation distortion is dominant for EVM. So the total EVM for injection predistortion is getting worse. However, we can still see certain EVM improvements appearing at the high magnitude points in the constellation.

5.3 L+I predistorter

Figure 4-12 has shown how well the injection technique deals with memory effects and Section 5.2 has clearly explained how well the LUT deals with nonlinearities. However, each of the techniques alone can not deal perfectly with a PA that has both nonlinearities and memory effects.

5.3.1. Basic idea of L+I

We propose a new predistortion method which combines LUT and injection. The objectives of this new combined technique are to use LUT to minimize the nonlinearities, and to use injection to eliminate the residual memory effects, so that both spectral regrowth and EVM can be improved. The LUT plus injection predistortion structure is shown in Fig. 5-8. The logical reason for applying LUT first then injection, rather than injection first then LUT, is that the LUT predistorter will first reduce the majority of the PA's nonlinearities and hence the new intermodulation products generated from the interaction of injection and pre-linearized signal [8] will be much less significant. With the linearity improvements from LUT, we do not need iterations like Fig. 4-10, in the injection part.

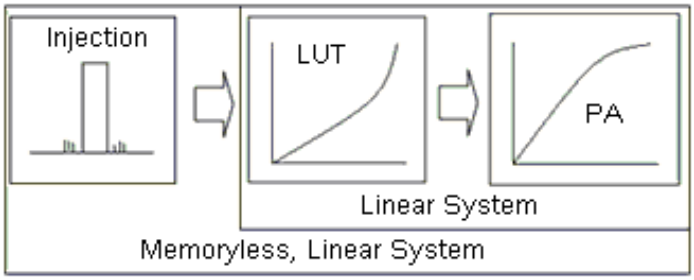

Figure 5-8 L+I predistorter

5.3.2 Experimental PA system and comparison results

In this section, we cascade the previous PA having high nonlinearities but weak memory effects, with a PA having both strong nonlinearities and memory effects. We then apply LUT, injection and L+I predistortion respectively. Fig. 5-9 plots the AM/AM, AM/PM conversion and Fig. 5-10 shows IM3 asymmetry measurement (Input maximum power for this experiment without predistortion is 4dBm). These two figures show that the cascaded PA system has both nonlinearities and significant memory effects compared with the single PA in Section 4.3.1.

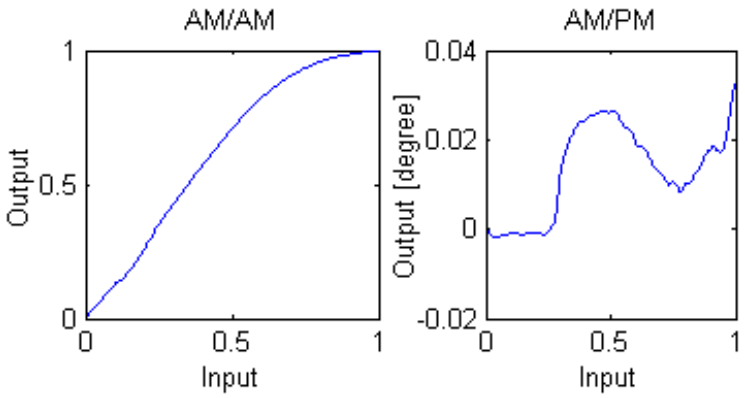

Figure 5-9 Normalized AM/AM, AM/PM measurements

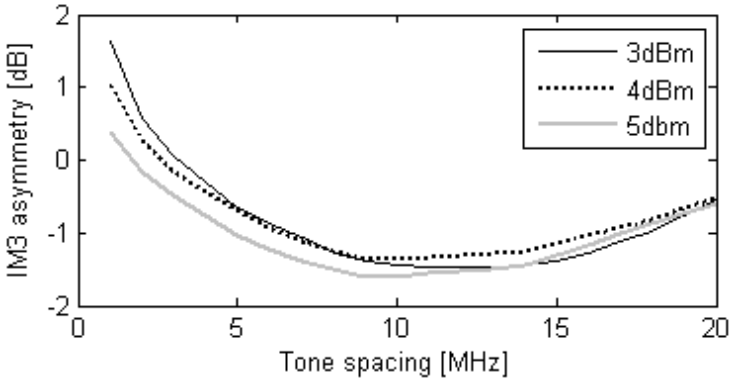

Figure 5-10 IM3 asymmetries at different two-tone input powers

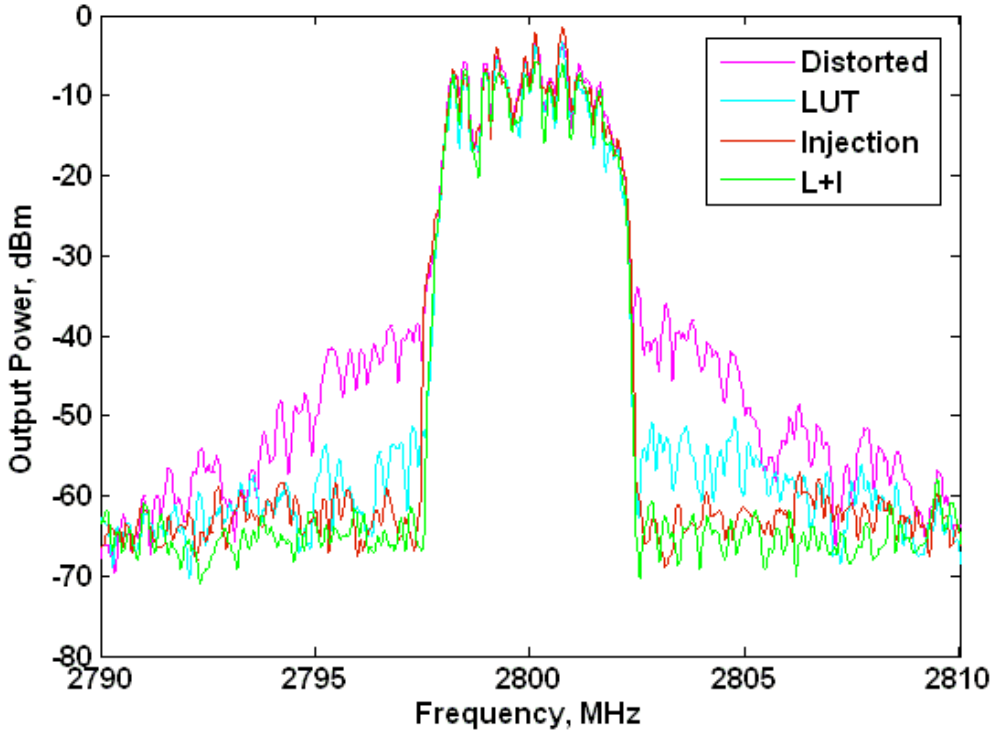

Figure 5-11 Comparison of power spectra

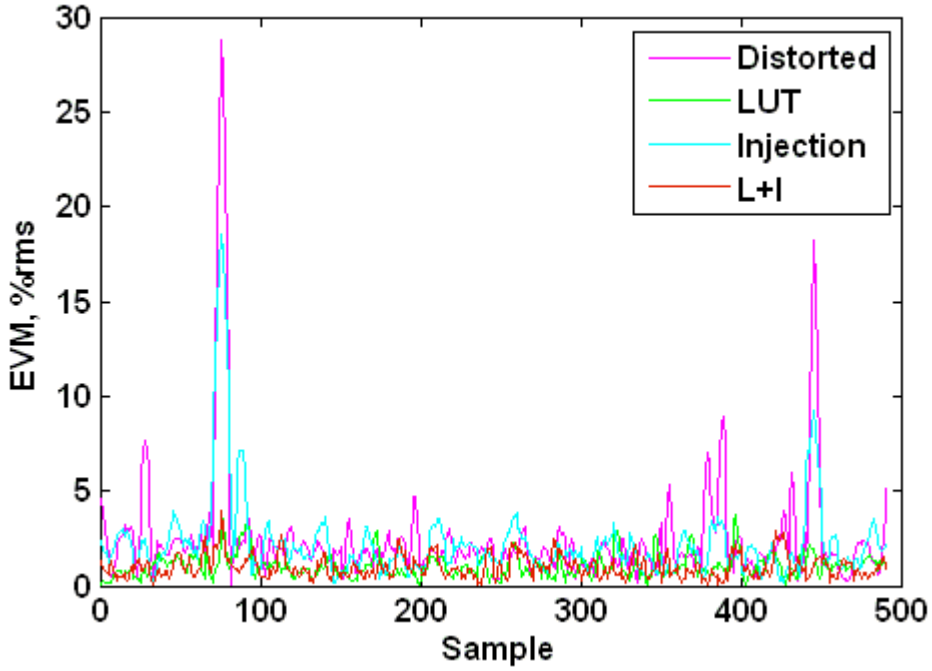

Figure 5-12 Comparison on EVM

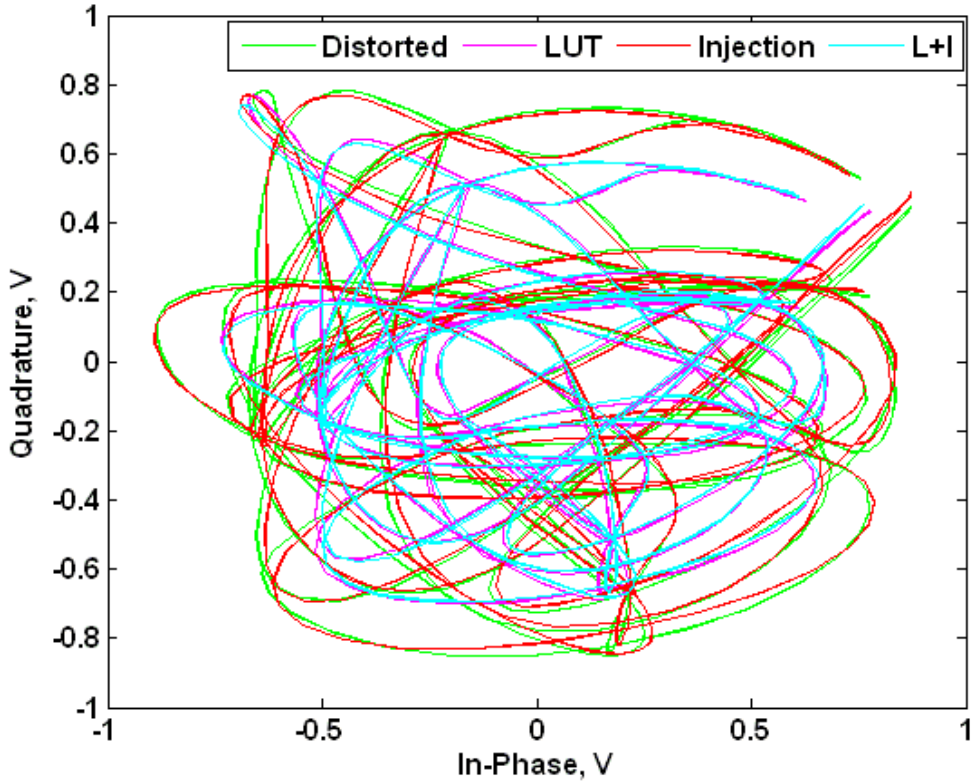

Figure 5-13 Comparison of output constellations

TABLE 5-2
EXPERIMENTAL MEASUREMENTS

	ACPR reduction (dBc)	Average EVM (%rms`)	Average output magnitude (Volt)	Peak value (Volt)	Crest factor (input 2.075)
Distorted	N/A	2.5330	0.6138	1.0147	1.6531
LUT	18	1.0399	0.4851	1.0143	2.0908
Injection	25	2.2688	0.5991	1.0277	1.7154
L+I	25	1.0041	0.4810	1.0119	2.1038

Fig. 5-11 shows the spectral regrowth, Fig. 5-12 shows the EVM and Fig. 5-13 shows the output constellation for all original distorted signals, LUT, injection and L+I predistortion. Table 5-2 lists the comparative results. As expected, L+I has a linear gain back-off to compensate the compression, which is similar to LUT, and it can address each sub-frequency to cancel the remaining memory effects, which is similar to injection. As a result, it can improve EVM effectively and reduce spectral regrowth down to the noise floor.

Another application of L+I is demonstrated in [63]. It is applied in a highly-efficient broadband Inverse Class E PA. Improvement of approximately 40 dB for spectral regrowth reduction (Fig. 5-14) and 0.7% EVM (rms) in a 16 QAM signal is achieved.

Compared with published memory polynomial models, L+I can reduce spectral regrowth and improve EVM as well. The advantage of L+I is that, the LUT is applicable to the nonlinearities while the injection is applicable to memory effects. This L+I predistortion may be useful for further research, such as using predistortion to separate nonlinearities and memory effects in a PA. In contrast, the coefficients in memory polynomial models do not obviously separate or indicate the extent of the nonlinearities and memory effects in PAs.

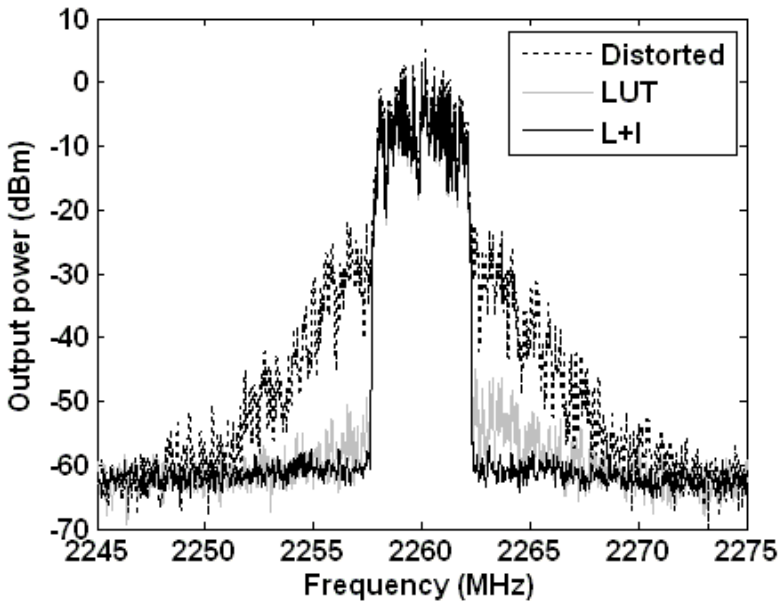

Figure 5-14 Application of L+I in an Inverse Class E PA

5.4 Summary

Although the injection technique in Chapter 4 was proven to work in the frequency domain, it results in inevitably poor EVM, as demonstrated in Section 5.2. Therefore, we propose a combined predistortion technique in this chapter, which applies both LUT and injection. The idea is that it can use LUT to reduce most of the nonlinearities and then apply injection to remove the residual spectral regrowth. This combined predistortion technique has two advantages compared with the single injection. First, it doesn't need a matrix (in two-tone tests) nor iterations (in wideband signals) to compensate the interactions. Secondly, it can reduce both ACPR and EVM, when the PA has both strong nonlinearities and memory effects, as demonstrated in Section 5.3.

CHAPTER 6

SUMMARY AND CONCLUSION

6.1 Summary

Due to the growing number of mobile users and the trend towards multi-band and multi-mode communication systems, high efficiency and high linearity power amplifiers are more and more desirable. Therefore, a high efficiency power amplifier with an integrated linearization technique is increasingly popular today. During the PhD research, we have analyzed and implemented a range of published and novel predistortion techniques. The range covers from memoryless AM/AM, AM/PM conversion to memory Volterra, and finally our proposed combined LUT plus injection. Meanwhile, the testing amplifiers varied from commercial memoryless power amplifier, inverse class E power amplifier, to a cascaded power amplifier system which contains both nonlinearities and memory effects.

This thesis began with a brief introduction of linearization techniques, and basic models of both analogue and digital predistortion, in Chapter 1. We chose digital predistortion as our main linearization technique, and begin to analyze numbers of power amplifier models and the corresponding digital predistortion techniques in Chapter 2.

In Chapter 2, we firstly discussed the power amplifiers models which are divided into two categories. The first category is memoryless models, which includes AM/AM, AM/PM conversion, memoryless polynomial, frequency-independent Saleh model. The second category considers both nonlinearities and memory effects, which contains a frequency-dependent nonlinear quadrature model, ARMA model, Volterra

model, memory polynomial model, Wiener model, and neural network model. Most of their inverse models are also depicted later in the same chapter, which are AM/AM, AM/PM conversion, inverse Volterra, inverse memory polynomial, Hammerstein, and neural network model. All of the inverse models are implemented in the digital predistorter. Further, we introduced digital injection predistortion. Unlike the traditional digital predistortions which are inverse power amplifier models, this injection technique generates phasors in anti-phase to those representing the intermodulation products, in order to cancel each other at the output port. This is attractive because it is good at dealing with memory effects in two-tone tests. Some novel improvements for the injection are described in the following Chapter 3 and 4.

In Chapter 3, we proposed and demonstrated novel methods on measurement and injection for intermodulation products in two-tone tests, which were subsequently published in [8]. We brought several innovations to the published techniques. The new measurement can clearly and easily describe the relationship between injected and output intermodulation products. Based on this discovered relationship, either lower or upper sideband IM3 injection can be calculated instead of manual tuning. Interaction between lower and upper sideband IM3 products has been discovered for the first time with this new measurement. To our knowledge, this interaction has not been proposed or discussed in published papers before. As a result, further IM3 reductions have been achieved while considering these interactions. In order to maximize its merit, we attempt to apply the same technique in wideband 16 QAM signal in Chapter 4.

In Chapter 4, the same injection technique is applied to a 16 QAM signal. However, the matrix approach proposed in Chapter 3 is no longer practical since what we reduce are not lower and upper IM3 products, but the whole spectral regrowth. As we know, the interaction is caused by the third order nonlinearities of the power amplifier while the cancellation of spectral regrowth is through the linear gain of the power amplifier. So the amplitudes of anti-phase phasors are bigger than those of the new interactions.

We can adjust the injection to become smaller in order to cancel part of the spectral regrowth while generating negligible interactions, step by step in the whole injection. Hence, an alternative iterative method is proposed to compensate interaction problems in 16 QAM injections. Since our injection can effectively control each sub-frequency, therefore, our results give much better spectral regrowth reduction compared with published works. In the end of this chapter, we have completely demonstrated its capacity for dealing with memory effects by showing that, as an extreme case, it can be used to suppress only the upper sideband of spectral regrowth. Although injection performs good spectral regrowth reduction even for power amplifiers that show significant memory effects, it still has a few disadvantages which limit its applications. Further discussions and a solution were presented in Chapter 5.

Communication signals not only require high spectrum efficiency, i.e. low frequency interference, but also high accuracy. A widely accepted measure applicable to this is the EVM in 16 QAM signal. In the published works on injection, authors typically focus on intermodulation products reduction in spectrum rather than I-Q signal precision. No relevant measurements such as EVM are given. Our measurement shows that injection will result in poor EVM compared with traditional LUT linearization. In Chapter 5, we firstly went back to a simple LUT using AM/AM and AM/PM conversion. And then we compare LUT and injection, regarding to their mathematical models, experimental results such as spectral regrowth reduction, output power, signal crest factor and EVM. With these analyses, we finally propose a new digital predistortion technique, which combine injection and LUT. The idea behind this combination is to use LUT to reduce most of the nonlinearities first, and then injection to reduce the rest of the spectral regrowth. This LUT plus injection predistortion is applied to a cascaded power amplifier system which has shown both significant nonlinearities and memory effects. With this predistortion method, both spectral regrowth and EVM show an improvement when compared with any single predistortion technique.

6.2 Major contributions and achievements

In the research, we have the following novel contribution on digital predistortion linearization techniques:

a. Improvements on traditional digital injection in two-tone test. Firstly, we reveal the phase relationships between the two main output tones and the output intermodulation products. Measurements on IM3 including amplitude and phase are given. Secondly, we proposed a new mathematical relationship on injected and output intermodulation products. Hence, we are the first to identify these interactions in the injection method and give solutions. With this improvement, the IM3 products have been further reduced when the power amplifier is driven harder. In our research, a 60 dB reduction on IM3 is achieved.

b. This new digital injection technique was firstly applied to 16 QAM wideband signals. Because our novel injection technique can effectively control each sub-frequency and consider interactions, it results a 30 dB reduction on spectral regrowth, which is better than the published works. Further, we can manage to reduce one sideband of spectral growth, leaving the other sideband. This can demonstrate its capabilities of dealing with memory effects.

c. We have been the first authors to analyze injection with regard to EVM measurements. We determined that injection does not improve the EVM. So we are the first to combine LUT and injection for wideband signal predistortion. This new L+I linearization can handle nonlinearities and memory effects, hence giving both better EVM (0.7% rms) and ACPR improvements (40dB) than any single technique.

6.3 Suggestions for future work

- The work can be implemented into a FPGA board or DSP board. When using FPGA as a PD, the delay caused by the circuit or the processing can be compensated by adding digital buffer inside the board. Choosing a suitable clock signal is a key work. So far, we have implemented the LUT algorithm into FPGA broad. However, the injection part which will include the convolution integrations is under construction.

- The experiment for injection in thesis is to correct a repeat signal, which is known before the correction. While the signal is unknown in a practical way, the FPGA board can apply pipeline to calculate the injection before sending the signal. To make it simple, we can have three different phase injections (instead of 10 in Chapter 4) to identify the circle (e.g. in Figure 4-8). For example, we can inject the components with identical amplitude but phases of 0^o, 120^o and 240^o. The FPGA board can have three blocks to perform the injection in parallel. We assume the first block is to injection 0^o phase component, the second block is to injection 120^o phase component and the third block is to inject the 240^o phase component. At the same time, the FPGA can have a fourth block to perform the calculation for the correct injection. We can chop the signal which is going to be sent into parts with the same time length. It can be marked with ①, ②, ③, ④ and so on. The performance of the FPGA is listed in Table 6-1.

FPGA (block 1)	①	②	③	④	⑤	……
FPGA (block 2)	①	②	③	④	⑤	……
FPGA (block 3)	①	②	③	④	⑤	……
FPGA (block 4)		①	②	③	④	

Timing	T1	T2	T3	T4	T5	……

Table 6-1 FPGA pipeline

The first line in Table 6-1 represents how block 1 inside the FPGA working in different time period. For example, in the time period T1, it performs phase 0^o injection to signal ①; in the time period T2, it performs phase 0^o injection to signal ②, and so on. The second line in Table 6-1 represents how block 2 which is 120^o phase injection, working in different time period. It is similar to block 1. The third line in Table 6-1 represents how block 3 which is 240^o phase injection, working in different time period. It is similar to block 1 as well. The fourth line in Table 6-1 represents block 4 which is to calculate the correct injection, working in different time period. In T1, because the circle of signal ① is not completed, so it does not carry any performance. In T2, when the circle of signal ① is identified, block 4 will calculate its center and radius and find out the correct inject component for signal ①. In T3, block 4 will calculate the injection for signal ②, and so on. So for any piece of the signal, it will take only two time period to find out the correct injection, which means the delay for this injection is two time period. This PGA parallel working system will shorten the injection measuring time hence to mitigate the time delay issue, and make the injection more realistic.

- The power consumption of the FPGA board plays an important roll for the predistorter, because the original aim of predistortion is to improve the PA's linearity while maintaining its power efficiency. So far, the power consumption of the FPGA board can be more than 1200 mW. This power level indicates that predistorter using FPGA is not ideal for handsets, but it can be implemented into base station.

- The L+I predistortion has the potential to be controlled using artificial intelligence techniques. The advantage is that the coefficients of injection and

LUT and can be calculated automatically rather than manual measurement and calculation.

6.4 Conclusions

In this thesis, we have summarized different published power amplifier models and their inverse models for predistortion. However, memory effects which affect these digital predistortion motivated our further research on digital predistortion.

We have proposed our LUT plus injection predistortion. It has several advantages as follows. Firstly, the injection results reported here are superior to those in previously published works. Secondly it can deal with nonlinearities and memory effects when compared with any single techniques. As a result, it gives much better EVM and ACPR reduction, even when the operated power amplifier or cascaded power amplifier system is driven harder resulting in bigger nonlinearities and memory effects.

This new linearization technique can be further developed by using neural networks to incorporate artificial intelligence capabilities and greater adaptivity. This technique can be applied to using FPGA or DSP boards in the future to maximize its application.

References

[1] K. Y. Chan and A. Bateman, "Analytical and Measured Performance of the Combined Analog Locked Loop Universal Modulator (Callum)," *Iee Proceedings-Communications*, vol. 142, issue 5, pp. 297-306, Oct, 1995.

[2] P. B. Kenington, *High-linearity RF Amplifier Design*. 685 Canton Street, Norwood, MA Artech House, 2000.

[3] H. Jardon and H. Vazquez, "A novel representation of AM-PM conversion," *Emc - a Global Concern: Ieee 1995 International Symposium on Electromagnetic Compatibility, Symposium Record*, issue 401-405, 1995.

[4] R. Blum and M. C. Jeruchim, "Modeling nonlinear amplifiers for communication simulation," *Communications, 1989. ICC 89, BOSTONICC/89. Conference record. World Prosperity Through Communications, IEEE International Conference*, vol. 3, issue 1468-1472, June, 1989.

[5] N. B. Carvalho and J. C. Pedro, "Multi-tone intermodulation distortion performance of 3rd order microwave circuits," *1999 Ieee Mtt-S International Microwave Symposium Digest, Vols 1-4*, issue 763-766, 1999.

[6] A. A. M. Saleh, "Frequency-Independent and Frequency-Dependent Non-Linear Models of Twt Amplifiers," *IEEE Transactions on Communications*, vol. 29, issue 11, pp. 1715-1720, 1981.

[7] J. H. K. Vuolevi, T. Rahkonen, and J. P. A. Manninen, "Measurement technique for characterizing memory effects in RF power amplifiers," *IEEE Transactions on Microwave Theory and Techniques*, vol. 49, issue 8, pp. 1383-1389, Aug, 2001.

[8] M. Xiao and P. Gardner, "Characterisation, analysis and injection of two-tone third-order intermodulation products in an amplifier," *IET Microwaves, Antennas & Propagation*, vol. 3, issue 3, pp. 443-455, 2009.

[9] W. Woo, M. D. Miller, and J. S. Kenney, "A hybrid digital/RF envelope predistortion linearization system for power amplifiers," *IEEE Transactions on Microwave Theory and Techniques*, vol. 53, issue 1, pp. 229-237, Jan, 2005.

[10] A. Richards, K. A. Morris, and J. P. McGeehan, "Removing the effects of baseband impedance on distortion in FET amplifiers," *IET Proceedings-Microwaves Antennas and Propagation*, vol. 153, issue 5, pp. 401-406, Oct, 2006.

[11] M. T. Abuelmaatti, "Frequency-Dependent Nonlinear Quadrature Model for Twt Amplifiers," *IEEE Transactions on Communications*, vol. 32, issue 8, pp. 982-986, 1984.

[12] C. J. Clark, G. Chrisikos, M. S. Muha, A. A. Moulthrop, and C. P. Silva,

"Time-domain envelope measurement technique with application to wideband power amplifier modeling," *IEEE Transactions on Microwave Theory and Techniques*, vol. 46, issue 12, pp. 2531-2540, Dec, 1998.

[13] C. Eun and E. J. Powers, "A new Volterra predistorter based on the indirect learning architecture," *IEEE Transactions on Signal Processing*, vol. 45, issue 1, pp. 223-227, Jan, 1997.

[14] R. Raich, H. Qian, and G. T. Zhou, "Orthogonal polynomials for power amplifier modeling and predistorter design," *IEEE Transactions on Vehicular Technology*, vol. 53, issue 5, pp. 1468-1479, Sep, 2004.

[15] H. C. Ku and J. S. Kenney, "Behavioral modeling of nonlinear RF power amplifiers considering memory effects," *IEEE Transactions on Microwave Theory and Techniques*, vol. 51, issue 12, pp. 2495-2504, Dec, 2003.

[16] D. R. Morgan, Z. X. Ma, J. Kim, M. G. Zierdt, and J. Pastalan, "A generalized memory polynomial model for digital predistortion of RF power amplifiers," *IEEE Transactions on Signal Processing*, vol. 54, issue 10, pp. 3852-3860, Oct, 2006.

[17] L. Ding, G. T. Zhou, D. R. Morgan, Z. X. Ma, J. S. Kenney, J. Kim, and C. R. Giardina, "A robust digital baseband predistorter constructed using memory polynomials," *IEEE Transactions on Communications*, vol. 52, issue 1, pp. 159-165, Jan, 2004.

[18] H. C. Ku, M. D. McKinley, and J. S. Kenney, "Quantifying memory effects in RF power amplifiers," *IEEE Transactions on Microwave Theory and Techniques*, vol. 50, issue 12, pp. 2843-2849, Dec, 2002.

[19] A. Ahmed, E. Srinidhi, and G. Kompa, "Efficient PA Modeling Using Neural Network and Measurement Setup for Memory Effect Characterization in the Power Device," *Microwave Symposium Digest, 2005 IEEE MTT-S International*, issue 473-476, June, 2005.

[20] J. Namiki, "An Automatically Controlled Predistorter for Multilevel Quadrature Amplitude-Modulation," *IEEE Transactions on Communications*, vol. 31, issue 5, pp. 707-712, 1983.

[21] W. Woo and J. S. Kenney, "A new envelope predistortion linearization architecture for handset power amplifiers," *Radio and Wireless Conference, 2004 IEEE*, issue 175-178, 19-22 Sept, 2004.

[22] S. Kusunoki, K. Yamamoto, T. Hatsugai, H. Nagaoka, K. Tagami, N. Tominaga, K. Osawa, K. Tanabe, S. Sakurai, and T. Iida, "Power-amplifier module with digital adaptive predistortion for cellular phones," *IEEE Transactions on Microwave Theory and Techniques*, vol. 50, issue 12, pp. 2979-2986, Dec, 2002.

[23] W. Woo and J. S. Kenney, "A predistortion linearization system for high power amplifiers with low frequency envelope memory effects," *2005 IEEE MTT-S Int. Microwave Symp. Dig.*, issue 4, June, 2005.

[24] S. P. Stapleton and F. C. Costescu, "An Adaptive Predistorter for a Power-Amplifier Based on Adjacent Channel Emissions," *IEEE Transactions on Vehicular Technology*, vol. 41, issue 1, pp. 49-56, Feb, 1992.

[25] S. P. Stapleton, G. S. Kandola, and J. K. Cavers, "Simulation and Analysis of an Adaptive Predistorter Utilizing a Complex Spectral Convolution," *IEEE Transactions on Vehicular Technology*, vol. 41, issue 4, pp. 387-394, Nov, 1992.

[26] L. Ding, R. Raich, and G. T. Zhou, "A Hammerstein predistortion linearization design based on the indirect learning architecture," *Acoustics, Speech, and Signal Processing, 2002. Proceedings. (ICASSP '02). IEEE International Conference on*, vol. 3, issue 2689-2692, 13-17 May, 2002.

[27] T. J. Liu, S. Boumaiza, and F. M. Ghannouchi, "Augmented Hammerstein predistorter for linearization of broad-band wireless transmitters," *IEEE Transactions on Microwave Theory and Techniques*, vol. 54, issue 4, pp. 1340-1349, Apr, 2006.

[28] J. Kim and K. Konstantinou, "Digital predistortion of wideband signals based on power amplifier model with memory," *Electronics Letters*, vol. 37, issue 23, pp. 1417-1418, Nov 8, 2001.

[29] R. Sperlich, J. A. Sills, and J. S. Kenney, "Closed-loop digital pre-distortion with memory effects using genetic algorithms," *Microwave Symposium Digest, 2005 IEEE MTT-S International*, issue 4, June, 2005.

[30] D. Psaltis, A. Sideris, and A. A. Yamamura, "A multilayered neural network controller," *IEEE JNL*, vol. 8, issue 2, pp. 17 - 21, April, 1988.

[31] H. Qian and G. T. Zhou, "A neural network predistorter for nonlinear power amplifiers with memory," *Digital Signal Processing Workshop, 2002 and the 2nd Signal Processing Education Workshop. Proceedings of 2002 IEEE 10th*, issue 312-316, 13-16 Oct, 2002.

[32] K. C. Lee and P. Gardner, "Adaptive neuro-fuzzy inference system (ANFIS) digital predistorter for RF power amplifier linearization," *IEEE Transactions on Vehicular Technology*, vol. 55, issue 1, pp. 43-51, Jan, 2006.

[33] H. M. Deng, S. B. He, and J. B. Yu, "An adaptive predistorter using modified neural networks combined with a fuzzy controller for nonlinear power amplifiers," *International Journal of Rf and Microwave Computer-Aided Engineering*, vol. 14, issue 1, pp. 15-20, Jan, 2004.

[34] K. Krishnakumar, "Backpropagation Algorithm for a Generalized Neural Network Structure," *Proceedings: Ieee Southeastcon 92, Vols 1 and 2*, issue 646-649, 1992.

[35] T. Nitta, "An extension of the back-propagation algorithm to complex numbers," *Neural Networks*, vol. 10, issue 8, pp. 1391-1415, Nov, 1997.

[36] "Foundations of Fuzzy Logic," in *Matlab help files*.

[37] J. S. R. Jang and C. T. Sun, "Neuro-Fuzzy Modeling and Control," *Proceedings of the IEEE*, vol. 83, issue 3, pp. 378-406, Mar, 1995.

[38] J. S. R. Jang, "Anfis - Adaptive-Network-Based Fuzzy Inference System," *IEEE Transactions on Systems Man and Cybernetics*, vol. 23, issue 3, pp. 665-685, May-Jun, 1993.

[39] D. Rabijns, W. Van Moer, and G. Vandersteen, "Spectrally pure excitation signals: Only a dream?" *IEEE Transactions on Instrumentation and*

Measurement, vol. 53, issue 5, pp. 1433-1440, Oct, 2004.

[40] K. J. Cho, D. H. Jang, S. H. Kim, J. Y. Kim, J. H. Kim, and S. P. Stapleton, "An analog compensation method for asymmetric IMD characteristics of power amplifier," *IEEE Microwave and Wireless Components Letters*, vol. 14, issue 4, pp. 153-155, Apr, 2004.

[41] C. Crespo-Cadenas, J. Reina-Tosina, and M. J. Madero-Ayora, "Phase characterization of two-tone intermodulation distortion," 2005 IEEE MTT-S Int. Microwave Symp. Dig., Long Beach, CA, pp.1505-1508, June 2005

[42] C. Crespo-Cadenas, J. Reina-Tosina, and M. J. Madero-Ayora, "IM3 and IM5 phase characterization and analysis based on a simplified newton approach," *IEEE Transactions on Microwave Theory and Techniques*, vol. 54, issue 1, pp. 321-328, Jan, 2006.

[43] F. Ali, M. R. Moazzam, and C. Aitchison, "IMD elimination and CPR improvement for an 800 MHz HBT MMIC power amplifier," Radio Frequency Integrated Circuits (RFIC) Symposium, IEEE, Baltimore,MD, pp.69 - 71, June 1998

[44] A. Singh, J. E. Scharer, J. H. Booske, and J. G. Wohlbier, "Second- and third-order signal predistortion for nonlinear distortion suppression in a TWT," *IEEE Transactions on Electron Devices*, vol. 52, issue 5, pp. 709-717, May, 2005.

[45] M.Modeste, D.Budimir, M.R.Moazzam, and C.S.Aitchison, "Analysis and practical performance of a difference frequency technique for improving the multicarrier IMD performance of RF amplifiers," Technologies for Wireless Applications, 1999. Digest. 1999 IEEE MTT-S Symposium, Vancouver,BC,Canada, pp.53 - 56, Feb. 1999

[46] C. S. Leung and K. K. M. Cheng, "A new approach to amplifier linearization by the generalized baseband signal injection method," *IEEE Microwave and Wireless Components Letters*, vol. 12, issue 9, pp. 336-338, Sep, 2002.

[47] C. W. Fan and K. K. M. Cheng, "Theoretical and experimental study of amplifier linearization based on harmonic and baseband signal injection technique," *IEEE Transactions on Microwave Theory and Techniques*, vol. 50, issue 7, pp. 1801-1806, Jul, 2002.

[48] C. S. Aitchison, M. Mbabele, M. R. Moazzam, D. Budimir, and F. Ali, "Improvement of third-order intermodulation product of RF and microwave amplifiers by injection," *IEEE Transactions on Microwave Theory and Techniques*, vol. 49, issue 6, pp. 1148-1154, Jun, 2001.

[49] X. Q. Li, F. Han, T. M. Lok, M. R. Lyu, and G. B. Huang, "Improvements to the conventional layer-by-layer BP algorithm," *Advances in Intelligent Computing, Pt 2, Proceedings*, vol. 3645, issue 189-198, 2005.

[50] M. Wirth, A. Singh, J. Scharer, and J. Booske, "Third-order intermodulation reduction by harmonic injection in a TWT amplifier," *IEEE Transactions on Electron Devices*, vol. 49, issue 6, pp. 1082-1084, Jun, 2002.

[51] N. Mizusawa and S. Kusunoki, "Third- and fifth-order baseband component injection for linearization of the power amplifier in a cellular phone," *IEEE*

Transactions on Microwave Theory and Techniques, vol. 53, issue 11, pp. 3327-3334, Nov, 2005.

[52] K. A. Remley, D. E. Williams, D. M. M. P. Schreurs, and J. Wood, "Simplifying and, interpreting two-tone measurements," *IEEE Transactions on Microwave Theory and Techniques*, vol. 52, issue 11, pp. 2576-2584, Nov, 2004.

[53] A. Richards, K. A. Morris, and J. P. McGeehan, "Cancellation of electrical memory effects in FET power amplifiers," *Microwave Conference, 2005 European*, vol. 2, issue, 4-6 Oct, 2005.

[54] J. S. Kenney and P. Fedorenko, "Identification of RF Power Amplifier Memory Effect Origins using Third-Order Intermodulation Distortion Amplitude and Phase Asymmetry," *Microwave Symposium Digest, 2006. IEEE MTT-S International*, issue 1121 - 1124, 11-16 June, 2006.

[55] A. Walker, M. Steer, and K. G. Gard, "A vector intermodulation analyzer applied to behavioral modeling of nonlinear amplifiers with memory," *IEEE Transactions on Microwave Theory and Techniques*, vol. 54, issue 5, pp. 1991-1999, May, 2006.

[56] J. P. Martins and N. B. Carvalho, "Spectral filtering setup for uncorrelated multi-tone phase and amplitude measurement," *34Th European Microwave Conference, Vols 1-3, Conference Proceedings*, issue 201-204, 2004.

[57] J. P. Martins and N. B. Carvalho, "Multitone phase and.amplitude measurement for nonlinear device characterization," *Ieee Transactions on Microwave Theory and Techniques*, vol. 53, issue 6, pp. 1982-1989, Jun, 2005.

[58] J. P. Martins, N. B. Carvalho, and J. C. Pedro, "Practical multitone amplitude and phase characterization," *2005 Asia-Pacific Microwave Conference Proceedings, Vols 1-5*, issue 3055-3058, 2005.

[59] J. C. Pedro and J. P. Martins, "Amplitude and phase characterization of nonlinear mixing products," *IEEE Transactions on Microwave Theory and Techniques*, vol. 54, issue 8, pp. 3237-3245, Aug, 2006.

[60] S. Y. Lee, Y. S. Lee, and Y. H. Jeong, "A novel phase measurement technique for IM3 components in RF power amplifiers," *IEEE Transactions on Microwave Theory and Techniques*, vol. 54, issue 1, pp. 451-457, Jan, 2006.

[61] D. Budimir, N. Males-Ilic, B. Milovanovic, and M. Tomic, "Linearization of multichannel amplifiers with the injection of second harmonics into the amplifier and predistortion circuit," *6th International Conference on Telecommunications in Modern Satellite, Cable and Broadcasting Service, 2003.*, vol. 1, issue 214-217, 1-3 Oct, 2003.

[62] J. Yi, Y. Yang, M. Park, W. Kang, and B. Kim, "Analog predistortion linearizer for high-power RF amplifiers," *IEEE Transactions on Microwave Theory and Techniques*, vol. 48, issue 12, pp. 2709-2713, Dec, 2000.

[63] M. Thian, M. Xiao, and P. Gardner, "Digital Baseband Predistortion Based Linearized Broadband Inverse Class-E Power Amplifier," *IEEE Transactions on Microwave Theory and Techniques*, vol. 57, issue 2, pp. 323 - 328, Feb, 2009.

APPENDIX A

The information of power amplifiers ZHL-4240 can be found in the website:

http://www.minicircuits.com/pdfs/ZHL-4240.pdf

APPENDIX B

The information of I/Q Modulation Generator R&S® AMIQ can be found in the website: http://www2.rohde-schwarz.com/product/AMIQ.html

Appendix C

The information of Signal Generator Family R&S SMIQ can be found in the website:

http://www2.rohde-schwarz.com/product/smiq.html

Appendix D

The program below is written in C++ Builder, for the purpose of connecting PC with modulator (AMIQ). The AMIQ has a 14-bit DAC output, which means the normalized voltage can vary from 0 to 1, with the interval of 2^{-14}. As a result, the ratio between the maximum power to the minimum power is 2^{14*2}, which is nearly 84 dBc. All the programs in the appendix are created by the author.

```
#include <vcl.h>
#include <stdio.h>
#include <math.h>
#pragma hdrstop

#include "P_port.h"
//---------------------------------------------------------------------------
#pragma package(smart_init)
#pragma link "MSCommLib_OCX"
#pragma resource "*.dfm"
TForm1 *Form1;
//---------------------------------------------------------------------------
__fastcall TForm1::TForm1(TComponent* Owner)
        : TForm(Owner)
{
}
//---------------------------------------------------------------------------

void __fastcall TForm1::FormCreate(TObject *Sender)
//define the user interface at the beginning of program
{
        auto_i=0;
        auto_j=0;
        auto_k=0;
        if (MSComm->PortOpen==true)
                MSComm->PortOpen=false;
        Button_Con->Enabled=true;
        Button_DisCon->Enabled=false;
        Shape->Shape=stCircle;
        Shape->Brush->Color=clRed;
```

```
        All_InVisible();
        Connection->TabVisible=false;
        ComboBox_Fre->Text="MHz";
        ComboBox_Amp->Text="I:";
        ComboBox_RamQuery->Text="File Name";
        Edit_C2->Visible=false;
        Edit_C3->Visible=false;
        Edit_C4->Visible=false;
        Label_C2->Visible=false;
        Label_C3->Visible=false;
        Label_C4->Visible=false;
        Label_CF2->Visible=false;
        Label_CF3->Visible=false;
        Label_CF4->Visible=false;
        Edit_CF2->Visible=false;
        Edit_CF3->Visible=false;
        Edit_CF4->Visible=false;
        ComboBox_CF2->Visible=false;
        ComboBox_CF3->Visible=false;
        ComboBox_CF4->Visible=false;
        Label_IData->Visible=false;
        Label_QData->Visible=false;
        Edit_IData->Visible=false;
        Edit_QData->Visible=false;
        Edit_DataFile->Visible=true;
        RadioGroup_IQ->ItemIndex=0;
        ProgressBar_SG->Position=0;
}
//---------------------------------------------------------------------------

void __fastcall TForm1::Button_ConClick(TObject *Sender)
//botton for connection
{
        if(MSComm->PortOpen!=true&&ComboBox->Text!="Connection
Config")
        {
                //define port
                if (ComboBox->Text=="Com1")
                        MSComm->CommPort=1;
                else
                        MSComm->CommPort=2;
                //set protocol
                MSComm->Settings="9600,n,8,1";
                MSComm->InputMode=0;
```

```
                MSComm->Handshaking=2;
                MSComm->SThreshold=1;
                MSComm->RThreshold=1;
                MSComm->PortOpen=true;
                //program interface config
                Button_Con->Enabled=false;
                Button_DisCon->Enabled=true;
                Shape->Brush->Color=clGreen;
                All_Visible();
        }
        else if (ComboBox->Text=="Connection Config")
                Application->MessageBox("Port not selected.","Error
Message",MB_OK);
}
//---------------------------------------------------------------------------

void __fastcall TForm1::Button_DisConClick(TObject *Sender)
//click for disconnect
{
        //disconnection
        MSComm->PortOpen=false;
        //program interface config
        Button_Con->Enabled=true;
        Button_DisCon->Enabled=false;
        Shape->Brush->Color=clRed;
        All_InVisible();
}
//---------------------------------------------------------------------------

void __fastcall TForm1::Button_SendClick(TObject *Sender)
//botton for send command
{
        if (!MSComm->PortOpen)
                Application->MessageBox("Port not open.","Error
Message",MB_OK);
        else
                Transmit();
}
//---------------------------------------------------------------------------

void __fastcall TForm1::Transmit()
//function for transmit text in "connection page"
{
        if (!MSComm->PortOpen)
```

```
                Application->MessageBox("Port not open.","Error
Message",MB_OK);
        else
        {
                MSComm->Output=StringToOleStr(Edit->Text+"\n");
                Edit->Text="T: "+Edit->Text;
                Memo1->Lines->Add(Edit->Text);
                Edit->Text="";
        }
}
//---------------------------------------------

void __fastcall TForm1::All_Visible()
//all pages visible
{
        Property->TabVisible=true;
        Signal_Gen->TabVisible=true;
}
//---------------------------------------------

void __fastcall TForm1::All_InVisible()
//all pages invisible
{
        Property->TabVisible=false;
        Signal_Gen->TabVisible=false;
}
//---------------------------------------------

void __fastcall TForm1::EditKeyPress(TObject *Sender, char &Key)
//if "enter" then transmit--in "connection page"
{
        if (Key==13)
                Transmit();
}
//---------------------------------------------------------------------------

void __fastcall TForm1::MSCommComm(TObject *Sender)
//if received any char in serial port
{
        AnsiString str;
        OleVariant s;
        if(MSComm->CommEvent==comEvReceive)
        {
                //if buffer got data
```

```
                while (MSComm->InBufferCount)
                {
                        //receive data
                        s=MSComm->Input;
                        //change to AnsiString data
                        str=str+s.AsType(varString);
                        for (int i=0;i<90999999;i++);
                }
                if (PageControl->ActivePageIndex==0)
                // if the buff receive Rthreshold number of data
                        //display data into memo
                        Memo1->Lines->Add("R: "+str);
                else if (PageControl->ActivePageIndex==1)
                        Memo2->Lines->Add(str);
        }
}
//---------------------------------------------------------------------------
```

Appendix A

C++builder graphic user interface program for connecting PC with modulator AMIQ (designed by the author)

```
void __fastcall TForm1::ClearClick(TObject *Sender)
//pop up menu for memo in "connection page"
{
        if (PageControl->ActivePageIndex==0)
                Memo1->Text="";
        else if (PageControl->ActivePageIndex==1)
                Memo2->Text="";
}
//---------------------------------------------------------------------------

void __fastcall TForm1::Button_RSTClick(TObject *Sender)
//command of reset
{
        MSComm->Output=StringToOleStr("*RST\n");
}
//---------------------------------------------------------------------------

void __fastcall TForm1::Button_idnClick(TObject *Sender)
//command of identification
{
        MSComm->Output=StringToOleStr("*IDN?\n");
```

```
}
//---------------------------------------------------------------------------

void __fastcall TForm1::Botton_SineClick(TObject *Sender)
//command of sending sine wave
{
        MSComm->Output=StringToOleStr("MMEM:LOAD
RAM,'SINE.WV'\nARM\nTRIG\noutput:i fix\noutput:q fix\n");
}
//---------------------------------------------------------------------------

void __fastcall TForm1::Edit_ampKeyPress(TObject *Sender, char &Key)
//command of changing amplitude
{
        if (Key==13)
        {
                if (ComboBox_Amp->Text=="I:")
                        MSComm->Output=StringToOleStr("OUTP:I:AMPL
"+Edit_amp->Text+"v\nOUTP:I var\n");
                else if (ComboBox_Amp->Text=="Q:")
                        MSComm->Output=StringToOleStr("OUTP:Q:AMPL
"+Edit_amp->Text+"v\nOUTP:Q var\n");
        }
}
//---------------------------------------------------------------------------

void __fastcall TForm1::Edit_clocKeyPress(TObject *Sender, char &Key)
//command of changing clock
{
        if (Key==13)
        {
                MSComm->Output=StringToOleStr("CLOC
"+Edit_cloc->Text+ComboBox_Fre->Text+"\n");
        }
}
//---------------------------------------------------------------------------

void __fastcall TForm1::Button_clocClick(TObject *Sender)
//command of asking clock
{
        MSComm->Output=StringToOleStr("SOUR:CLOCK?\n");
}
//---------------------------------------------------------------------------
```

```
void __fastcall TForm1::Button_AmpClick(TObject *Sender)
//command of asking amplitude
{

MSComm->Output=StringToOleStr("OUTP:"+ComboBox_Amp->Text+"AMPL?\n")
;
}
//---------------------------------------------------------------------------

void __fastcall TForm1::Button_RamQueryClick(TObject *Sender)
//command of asking tag
{
        if (ComboBox_RamQuery->Text=="File Name")
                MSComm->Output=StringToOleStr("MEM:NAME?\n");
        else if (ComboBox_RamQuery->Text=="All Tag")
                MSComm->Output=StringToOleStr("MEM:DATA?\n");
        else
                MSComm->Output=StringToOleStr("MEM:DATA?
RAM,'"+ComboBox_RamQuery->Text+"'\n");
}
//---------------------------------------------------------------------------

void __fastcall TForm1::Button_DualClick(TObject *Sender)
//command of sending dultone waveform
{
        MSComm->Output=StringToOleStr("MMEM:LOAD
RAM,'dualtone.WV'\nARM\nTRIG\noutput:i fix\noutput:q fix\n");
}
//---------------------------------------------------------------------------

void __fastcall TForm1::Button_FilClick(TObject *Sender)
//command of sending filter
{

MSComm->Output=StringToOleStr("OUTP:"+ComboBox_FIL_Ch->Text+"filt
"+ComboBox_FIL->Text+"\n");
}
//---------------------------------------------------------------------------

void __fastcall TForm1::Button_filterClick(TObject *Sender)
//command of asking filter
{

MSComm->Output=StringToOleStr("OUTP:"+ComboBox_FIL_Ch->Text+"filt?\n");
```

```
}
//---------------------------------------------------------------------------

void __fastcall TForm1::Button_mineClick(TObject *Sender)
//command of sending self generate waveform
{
        Sig_Gen();
}

//---------------------------------------------------------------------------
void __fastcall    TForm1::Sig_Gen()
{
        ProgressBar_SG->Position=0;
        unsigned short Data[60000];
        float data_float;
        int i,num;
        AnsiString num1,num2;
        FILE *fp,*fp1,*fp2;
        OleVariant Txbuff;
        if (RadioGroup_IQ->ItemIndex==0)
        //reading combine data
        {
                fp=fopen(Edit_DataFile->Text.c_str(),"rt");
                num=0;
                //reading data
                while (1)
                {
                        if (fscanf(fp,"%f",&data_float)==EOF)
                                break;
                        Data[num]=(unsigned
short)(32768.0+(data_float*32000.0)+0.5);
                        Data[num]&=0xFFFC;
                        num++;
                }
                num--;
                fclose(fp);
        }
        else
        //reading IQ signal respectivly
        {
                fp1=fopen(Edit_IData->Text.c_str(),"rt");
                fp2=fopen(Edit_QData->Text.c_str(),"rt");
                num=0;
                //reading data
```

```
                    while (1)
                    {
                            if (fscanf(fp1,"%f",&data_float)==EOF)
                                    break;
                            Data[num]=(unsigned
short)(32768.0+(data_float*32000.0)+0.5);
                            Data[num]&=0xFFFC;
                            num++;
                            if (fscanf(fp2,"%f",&data_float)==EOF)
                                    break;
                            Data[num]=(unsigned
short)(32768.0+(data_float*32000.0)+0.5);
                            Data[num]&=0xFFFC;
                            num++;
                    }
                    num--;
                    fclose(fp1);
                    fclose(fp2);
            }
            ProgressBar_SG->Position=2;
            if (num%2==0)
                    num--;
            //send file info
            num2=AnsiString((num+1)*2+3);
            num1=AnsiString(23+num2.Length()+(num+1)*2+6);
            MSComm->Output=StringToOleStr("*RST\n");
            MSComm->Output=StringToOleStr("mmem:data                    'mycur.wv',
#"+AnsiString(num1.Length())+num1+"{TYPE:   WV,   0}{WAVEFORM-"+num2+":
0,#");
            MSComm->PortOpen=false;
            MSComm->InputMode=1;
            MSComm->PortOpen=true;
            ProgressBar_SG->Position=5;
            //send bitstream
            for (i=0;i<=num;i++)
            {
                    Txbuff=VarArrayCreate(OPENARRAY(int,(0,1)),varByte);
                    Txbuff.PutElement((unsigned char)Data[i],0);
                    Txbuff.PutElement((unsigned char)(Data[i]/256),1);
                    MSComm->Output=Txbuff;
                    ProgressBar_SG->Position=5+(int)(i*94/num);
            }
            MSComm->PortOpen=false;
            MSComm->InputMode=0;
```

```
        MSComm->PortOpen=true;
        MSComm->Output=StringToOleStr("}\n");
        //load waveform
        ProgressBar_SG->Position=100;
        MSComm->Output=StringToOleStr("MMEM:LOAD
RAM,'mycur.WV'\nARM\nTRIG\noutput:i fix\noutput:q fix\n");
}
//---------------------------------------------------------------------------

void __fastcall TForm1::ComboBox_Num_BChange(TObject *Sender)
//command of changing number of carrier
{
        if (ComboBox_Num_B->ItemIndex==0)
        {
                Edit_C2->Visible=false;
                Edit_C3->Visible=false;
                Edit_C4->Visible=false;
                Label_C2->Visible=false;
                Label_C3->Visible=false;
                Label_C4->Visible=false;
                Label_CF2->Visible=false;
                Label_CF3->Visible=false;
                Label_CF4->Visible=false;
                Edit_CF2->Visible=false;
                Edit_CF3->Visible=false;
                Edit_CF4->Visible=false;
                ComboBox_CF2->Visible=false;
                ComboBox_CF3->Visible=false;
                ComboBox_CF4->Visible=false;
        }
        else if (ComboBox_Num_B->ItemIndex==1)
        {
                Edit_C2->Visible=true;
                Edit_C3->Visible=false;
                Edit_C4->Visible=false;
                Label_C2->Visible=true;
                Label_C3->Visible=false;
                Label_C4->Visible=false;
                Label_CF2->Visible=true;
                Label_CF3->Visible=false;
                Label_CF4->Visible=false;
                Edit_CF2->Visible=true;
                Edit_CF3->Visible=false;
                Edit_CF4->Visible=false;
```

```
                ComboBox_CF2->Visible=true;
                ComboBox_CF3->Visible=false;
                ComboBox_CF4->Visible=false;
        }
        else if (ComboBox_Num_B->ItemIndex==2)
        {
                Edit_C2->Visible=true;
                Edit_C3->Visible=true;
                Edit_C4->Visible=false;
                Label_C2->Visible=true;
                Label_C3->Visible=true;
                Label_C4->Visible=false;
                Label_CF2->Visible=true;
                Label_CF3->Visible=true;
                Label_CF4->Visible=false;
                Edit_CF2->Visible=true;
                Edit_CF3->Visible=true;
                Edit_CF4->Visible=false;
                ComboBox_CF2->Visible=true;
                ComboBox_CF3->Visible=true;
                ComboBox_CF4->Visible=false;
        }
        else if (ComboBox_Num_B->ItemIndex==3)
        {
                Edit_C2->Visible=true;
                Edit_C3->Visible=true;
                Edit_C4->Visible=true;
                Label_C2->Visible=true;
                Label_C3->Visible=true;
                Label_C4->Visible=true;
                Label_CF2->Visible=true;
                Label_CF3->Visible=true;
                Label_CF4->Visible=true;
                Edit_CF2->Visible=true;
                Edit_CF3->Visible=true;
                Edit_CF4->Visible=true;
                ComboBox_CF2->Visible=true;
                ComboBox_CF3->Visible=true;
                ComboBox_CF4->Visible=true;
        }
}
//---------------------------------------------------------------------------
```

```
void __fastcall TForm1::RadioGroup_IQClick(TObject *Sender)
{
//changing data source of self generation
        if (RadioGroup_IQ->ItemIndex==0)
        {
                Label_IData->Visible=false;
                Label_QData->Visible=false;
                Edit_IData->Visible=false;
                Edit_QData->Visible=false;
                Edit_DataFile->Visible=true;
        }
        else
        {
                Label_IData->Visible=true;
                Label_QData->Visible=true;
                Edit_IData->Visible=true;
                Edit_QData->Visible=true;
                Edit_DataFile->Visible=false;
        }
}
//---------------------------------------------------------------------------

void __fastcall TForm1::Button_BALQueryClick(TObject *Sender)
//Balance query
{
        MSComm->Output=StringToOleStr("outp:type?\n");
}
//---------------------------------------------------------------------------

void __fastcall TForm1::Button_Bal_SendClick(TObject *Sender)
//Balance define
{
        if (ComboBox_BAL->ItemIndex==0)
                MSComm->Output=StringToOleStr("outp:type bal\n");
        else
                MSComm->Output=StringToOleStr("outp:type UNB\n");

}
//---------------------------------------------------------------------------

void __fastcall TForm1::Button_BAL_AMPClick(TObject *Sender)
//Balance amplitude query
{
```

```
        if (ComboBox_BAL_IQ->ItemIndex==0)
                MSComm->Output=StringToOleStr("outp:i:ampl:bal?\n");
        else
                MSComm->Output=StringToOleStr("outp:q:ampl:bal?\n");
}
//---------------------------------------------------------------------------

void __fastcall TForm1::Edit_BALKeyPress(TObject *Sender, char &Key)
//balance amplitude define
{
        if (Key==13)
        {
                if (ComboBox_BAL_IQ->ItemIndex==0)
                        MSComm->Output=StringToOleStr("outp:i
var\noutp:i:ampl:bal "+Edit_BAL->Text+"V\n");
                else
                        MSComm->Output=StringToOleStr("outp:q
var\noutp:q:ampl:bal "+Edit_BAL->Text+"V\n");
        }
}
//---------------------------------------------------------------------------

void __fastcall TForm1::Edit_passwordKeyPress(TObject *Sender, char &Key)
//identification
{
        if (Key==13&&Edit_password->Text=="AABBCC")
        {
                Connection->TabVisible=true;
                Edit_password->Text="";
                Password->TabVisible=false;
        }
}
//---------------------------------------------------------------------------


void __fastcall TForm1::BitBtn_AutoClick(TObject *Sender)
{
        RadioGroup_IQ->ItemIndex=1;
        Label_IData->Visible=true;
        Label_QData->Visible=true;
        Edit_IData->Visible=true;
        Edit_QData->Visible=true;
        Edit_DataFile->Visible=false;
        Edit_IData->Text="I"+AnsiString(auto_j)+AnsiString(auto_k)+".txt";
```

```
		Edit_QData->Text="Q"+AnsiString(auto_j)+AnsiString(auto_k)+".txt";
		auto_k++;
		if (auto_k==10)
		{
			auto_k=0;
			auto_j++;
			if (auto_j==10)
			{
				auto_j=0;
				auto_i++;
			}
		}
		Sig_Gen();
		MSComm->Output=StringToOleStr("CLOC 100mhz\noutp:type bal\n");
}
//---------------------------------------------------------------------------

void __fastcall TForm1::Button_SetIJKClick(TObject *Sender)
{
		auto_i=ComboBox_I->ItemIndex;
		auto_j=ComboBox_J->ItemIndex;
		auto_k=ComboBox_K->ItemIndex;
}
//---------------------------------------------------------------------------
```

APPENDIX E

The program below is written in Matlab. All the programs in appendix E are for injection in a two-tone test for Chapter 3. The first program is used to generate a two-tone test signal with the calculated injection of IM3L & IM3U. The second one is to measure the phase and amplitude of the IM3L & IM3U. The third one is to identify the centre and radius of the circle for calculating R_{lower}, $R_{upper\text{-}lower}$ in equation 3.33 in Chapter 3. The fourth one is to identify the centre and radio of the circles for calculating R_{upper}, $R_{lower\text{-}upper}$ in equation 3.33 in Chapter 3. The fifth one is to calculate the correction for injected IM3L & IM3U.

----------1----------

```
% Define Tone spacing (TS) MHz and sample rate=100MHz (in AMIQ)
TS=10;

% Frequency component
W1=TS/2;
W2=-TS/2;
Lower=W2-TS;
Upper=W1+TS;

% Interval
i=0:1:200-1;

% IMD
exp_L=0;%0.02*exp(2j*pi*0.2);
exp_U=0;%0.02*exp(2j*pi*0.1);
IMD_i=cos(2*pi*Lower*i/100)*exp_L+cos(2*pi*Upper*i/100)*exp_U;
IMD_q=sin(2*pi*Lower*i/100)*exp_L+sin(2*pi*Upper*i/100)*exp_U;
IMD=IMD_i+1j*IMD_q;

% Carrier
Carrier_i=2*cos(2*pi*W1*i/100);
Carrier_q=0;
Carrier=Carrier_i+1j*Carrier_q;

Input=(Carrier+IMD)/3;
```

```
Input=Input/max(Input);

%write file
tti=['I00.txt'];
ttq=['Q00.txt'];
ftti = fopen(tti, 'wt');
fttq = fopen(ttq, 'wt');
fprintf(ftti,'%18.17f\n',real(Input));
fprintf(fttq,'%18.17f\n',imag(Input));
fclose(ftti);
fclose(fttq);

-----------------------------------------2-----------------------------------------

for i=0:9
    y(i+1)=load([num2str(i),'.mat']);
    %frequency component
    TS=10;
    Com(i+1,1)=y(i+1).Y(2050-TS*60-1);
    Com(i+1,2)=y(i+1).Y(2050-TS*20-1);
    Com(i+1,3)=y(i+1).Y(2050+TS*20-1);
    Com(i+1,4)=y(i+1).Y(2050+TS*60-1);
    %lower/upper frequency phase
    Lower_fre(i+1)=exp(1i*angle(Com(i+1,2)*Com(i+1,2)*conj(Com(i+1,3))));
    Upper_fre(i+1)=exp(1i*angle(Com(i+1,3)*Com(i+1,3)*conj(Com(i+1,2))));

    %ratio
    Lower_R(i+1)=Com(i+1,1)/Lower_fre(i+1);
    Upper_R(i+1)=Com(i+1,4)/Upper_fre(i+1);
end

-----------------------------------------3-----------------------------------------

%tone spacing
TS=10;
for i=0:9
    y(i+1)=load([num2str(i),'.mat']);
    %frequency component
    Com(i+1,1)=y(i+1).Y(2050-TS*60-1);
    Com(i+1,2)=y(i+1).Y(2050-TS*20-1);
    Com(i+1,3)=y(i+1).Y(2050+TS*20-1);
    Com(i+1,4)=y(i+1).Y(2050+TS*60-1);
    %lower/upper frequency phase
    Lower_fre(i+1)=Com(i+1,2)*Com(i+1,2)/Com(i+1,3);
```

```
    Upper_fre(i+1)=Com(i+1,3)*Com(i+1,3)/Com(i+1,2);
    %ratio
    Lower_R(i+1)=Com(i+1,1)/(Lower_fre(i+1)/abs(Lower_fre(i+1)));
    Upper_R(i+1)=Com(i+1,4)/(Upper_fre(i+1)/abs(Upper_fre(i+1)));
End

%finding circle
%left 3rd order
x=0;
Num_Cir=0;
for i=1:8
    for j=i+1:9
        for k=j+1:10
            a=2*(real(Lower_R(j))-real(Lower_R(i)));
            b=2*(imag(Lower_R(j))-imag(Lower_R(i)));

c=(real(Lower_R(j)))^2+(imag(Lower_R(j)))^2-(real(Lower_R(i)))^2-(imag(Lower_
R(i)))^2;
            d=2*(real(Lower_R(k))-real(Lower_R(j)));
            e=2*(imag(Lower_R(k))-imag(Lower_R(j)));

f=(real(Lower_R(k)))^2+(imag(Lower_R(k)))^2-(real(Lower_R(j)))^2-(imag(Lower_
R(j)))^2;
            Num_Cir=Num_Cir+1;
            x(Num_Cir)=(b*f-e*c)/(b*d-e*a)+1i*(d*c-a*f)/(b*d-e*a);
        end
    end
end

%refind center
meanx=mean(x);
covx=cov(x)^0.5;
i=1;
j=0;
xx=0;
while (i<=Num_Cir)
    if abs(x(i)-meanx)<covx;
        j=j+1;
        xx(j)=x(i);
    end
    i=i+1;
end
Center_left=mean(xx);
Gain_need_left=abs(Center_left)/mean(abs(Lower_R(:)-Center_left));
```

```
i=1;
while
(angle((-Center_left)/(Lower_R(i)-Center_left))<0)||(angle((-Center_left)/(Lower_R(
mod(i,10)+1)-Center_left))>0)
      i=i+1;
end
a=angle((-Center_left)/(Lower_R(i)-Center_left));
b=angle((Lower_R(mod(i,10)+1)-Center_left)/(Lower_R(i)-Center_left));
Phase_need_left=(i-1+a/b)/10;
subplot(1,2,1);
plot(Lower_R);
hold on;
plot(Lower_R(1),'o');
plot([0 Center_left]);
plot(Center_left,'*');
grid on

%right 3rd order
x=0;
Num_Cir=0;
for i=1:8
      for j=i+1:9
            for k=j+1:10
                  a=2*(real(Upper_R(j))-real(Upper_R(i)));
                  b=2*(imag(Upper_R(j))-imag(Upper_R(i)));

c=(real(Upper_R(j)))^2+(imag(Upper_R(j)))^2-(real(Upper_R(i)))^2-(imag(Upper_R
(i)))^2;
                  d=2*(real(Upper_R(k))-real(Upper_R(j)));
                  e=2*(imag(Upper_R(k))-imag(Upper_R(j)));

f=(real(Upper_R(k)))^2+(imag(Upper_R(k)))^2-(real(Upper_R(j)))^2-(imag(Upper_
R(j)))^2;
                  Num_Cir=Num_Cir+1;
                  x(Num_Cir)=(b*f-e*c)/(b*d-e*a)+1i*(d*c-a*f)/(b*d-e*a);
            end
      end
end

%refind center
meanx=mean(x);
covx=cov(x)^0.5;
i=1;
j=0;
```

```
xx=0;
while (i<=Num_Cir)
      if abs(x(i)-meanx)<covx;
            j=j+1;
            xx(j)=x(i);
      end
      i=i+1;
end
Center_right=mean(xx);
subplot(1,2,2);
plot(Upper_R);
hold on;
plot(Upper_R(1),'o');
plot(Center_right,'*');
plot([0 Center_right]);
grid on;

A1=Center_left;
B1=Lower_R(1)-Center_left;
C2=Upper_R(1)-Center_right;

-----------------------------------------4-----------------------------------------

%tone spacing
TS=10;
for i=0:9
      y(i+1)=load([num2str(i),'.mat']);
      %frequency component
      Com(i+1,1)=y(i+1).Y(2050-TS*60-1);
      Com(i+1,2)=y(i+1).Y(2050-TS*20-1);
      Com(i+1,3)=y(i+1).Y(2050+TS*20-1);
      Com(i+1,4)=y(i+1).Y(2050+TS*60-1);
      %lower/upper frequency phase
      Lower_fre(i+1)=Com(i+1,2)*Com(i+1,2)/Com(i+1,3);
      Upper_fre(i+1)=Com(i+1,3)*Com(i+1,3)/Com(i+1,2);
      %ratio
      Lower_R(i+1)=Com(i+1,1)/(Lower_fre(i+1)/abs(Lower_fre(i+1)));
      Upper_R(i+1)=Com(i+1,4)/(Upper_fre(i+1)/abs(Upper_fre(i+1)));
End

%finding circle
%left 3rd order
x=0;
Num_Cir=0;
```

```
for i=1:8
    for j=i+1:9
        for k=j+1:10
            a=2*(real(Lower_R(j))-real(Lower_R(i)));
            b=2*(imag(Lower_R(j))-imag(Lower_R(i)));

c=(real(Lower_R(j)))^2+(imag(Lower_R(j)))^2-(real(Lower_R(i)))^2-(imag(Lower_
R(i)))^2;
            d=2*(real(Lower_R(k))-real(Lower_R(j)));
            e=2*(imag(Lower_R(k))-imag(Lower_R(j)));

f=(real(Lower_R(k)))^2+(imag(Lower_R(k)))^2-(real(Lower_R(j)))^2-(imag(Lower_
R(j)))^2;
            Num_Cir=Num_Cir+1;
            x(Num_Cir)=(b*f-e*c)/(b*d-e*a)+1i*(d*c-a*f)/(b*d-e*a);
        end
    end
end

%refind center
meanx=mean(x);
covx=cov(x)^0.5;
i=1;
j=0;
xx=0;
while (i<=Num_Cir)
    if abs(x(i)-meanx)<covx;
        j=j+1;
        xx(j)=x(i);
    end
    i=i+1;
end
Center_left=mean(xx);
subplot(1,2,1);
plot(Lower_R);
hold on;
plot(Lower_R(1),'o');
plot(Center_left,'*');
plot([0 Center_left]);
grid on

%right 3rd order
x=0;
Num_Cir=0;
```

```
for i=1:8
    for j=i+1:9
        for k=j+1:10
            a=2*(real(Upper_R(j))-real(Upper_R(i)));
            b=2*(imag(Upper_R(j))-imag(Upper_R(i)));

c=(real(Upper_R(j)))^2+(imag(Upper_R(j)))^2-(real(Upper_R(i)))^2-(imag(Upper_R
(i)))^2;
            d=2*(real(Upper_R(k))-real(Upper_R(j)));
            e=2*(imag(Upper_R(k))-imag(Upper_R(j)));

f=(real(Upper_R(k)))^2+(imag(Upper_R(k)))^2-(real(Upper_R(j)))^2-(imag(Upper_
R(j)))^2;
            Num_Cir=Num_Cir+1;
            x(Num_Cir)=(b*f-e*c)/(b*d-e*a)+1i*(d*c-a*f)/(b*d-e*a);
        end
    end
end

%refind center
meanx=mean(x);
covx=cov(x)^0.5;
i=1;
j=0;
xx=0;
while (i<=Num_Cir)
    if abs(x(i)-meanx)<covx;
        j=j+1;
        xx(j)=x(i);
    end
    i=i+1;
end
Center_right=mean(xx);
Gain_need_right=abs(Center_right)/mean(abs(Upper_R(:)-Center_right));
i=1;
while
(angle((-Center_right)/(Upper_R(i)-Center_right))<0)||(angle((-Center_right)/(Upper_
R(mod(i,10)+1)-Center_right))>0)
    i=i+1;
end
a=angle((-Center_right)/(Upper_R(i)-Center_right));
b=angle((Upper_R(mod(i,10)+1)-Center_right)/(Upper_R(i)-Center_right));
Phase_need_right=(i-1+a/b)/10;
subplot(1,2,2);
```

```
plot(Upper_R);
hold on;
plot(Upper_R(1),'o');
plot(Center_right,'*');
plot([0 Center_right]);
grid on;
A2=Center_right;
B2=Upper_R(1)-Center_right;
C1=Lower_R(1)-Center_left;

-----------------------------------------5-----------------------------------------

Coe=[conj(B1),conj(C1);C2,B2];
RE=[conj(-A1);-A2];
KPhi=inv(Coe)*RE;
KPhi(1)=conj(KPhi(1));
KPhi
```

APPENDIX F

The program below is written in Matlab. All the programs in appendix F are for injection in a 16 QAM signal for Chapter 4. The first program is used to generate a 16 QAM signal with the injection. The second one is to measure the phase and amplitude of the spectral regrowth and calculate the injection for spectral regrowth.

----------1----------

```
Code=[0 1 2 3 randint(1,46,[0,15])];
Points_Symbol=10;
Roll_off=0.2;
Group_Delay=100;
Code_length=length(Code);
for i=1:Code_length
    if (Code(i)==0)
        Code_I(i)=3;Code_Q(i)=3;
    elseif (Code(i)==1)
        Code_I(i)=1;Code_Q(i)=3;
    elseif (Code(i)==2)
        Code_I(i)=-1;Code_Q(i)=3;
    elseif (Code(i)==3)
        Code_I(i)=-3;Code_Q(i)=3;
    elseif (Code(i)==4)
        Code_I(i)=3;Code_Q(i)=1;
    elseif (Code(i)==5)
        Code_I(i)=1;Code_Q(i)=1;
    elseif (Code(i)==6)
        Code_I(i)=-1;Code_Q(i)=1;
    elseif (Code(i)==7)
        Code_I(i)=-3;Code_Q(i)=1;
    elseif (Code(i)==8)
        Code_I(i)=3;Code_Q(i)=-1;
    elseif (Code(i)==9)
        Code_I(i)=1;Code_Q(i)=-1;
    elseif (Code(i)==10)
        Code_I(i)=-1;Code_Q(i)=-1;
    elseif (Code(i)==11)
        Code_I(i)=-3;Code_Q(i)=-1;
    elseif (Code(i)==12)
        Code_I(i)=3;Code_Q(i)=-3;
    elseif (Code(i)==13)
        Code_I(i)=1;Code_Q(i)=-3;
```

```
        elseif (Code(i)==14)
            Code_I(i)=-1;Code_Q(i)=-3;
        elseif (Code(i)==15)
            Code_I(i)=-3;Code_Q(i)=-3;
        end
end
Input_Mod=rcosflt([complex(Code_I,Code_Q),complex(Code_I,Code_Q),complex(C
ode_I,Code_Q)],1,Points_Symbol,'fir',Roll_off,Group_Delay);
Input_Mod=Input_Mod(Points_Symbol*Code_length+Group_Delay*Points_Symbol:
Points_Symbol*Code_length*2+Group_Delay*Points_Symbol-1)*0.6/max(abs(Input
_Mod));

for j=0:9
%Open file
tti=['I0' num2str(j) '.txt'];
ttq=['Q0' num2str(j) '.txt'];


%cubic injection
Inject=Input_Mod.*Input_Mod.*conj(Input_Mod);
Inject_fft=fft(Inject);
for i=1:500
        if abs(Inject_fft(i))<0.1
            Inject_fft(i)=0.1*Inject_fft(i)/abs(Inject_fft(i));
        end
end
%sideband elimination
Inject_fft(91:410)=0;
%inband elimination
Inject_fft(1:30)=0;
Inject_fft(471:500)=0;

%brick wall
Inject_fft_w=0.2*ones(500,1);
%sideband elimination
Inject_fft_w(91:410)=0;
%inband elimination
%Inject_fft_w(1:30)=0;
Inject_fft_w(1:90)=0;
Inject_fft_w(471:500)=0;

%Inject_fft_w=0*ones(500,1);
%Inject_fft_w(40)=0.2;
```

```
Inject_Amp=0.1;
Inject_fft=Inject_fft_w*exp(2i*pi*(j/10))*Inject_Amp;%+Inject_fft_w.*Filter1.';%+0
.5*Inject_fft.*Filter2.'+Inject_fft_w.*Filter3.';
Inject=ifft(Inject_fft);

ftti = fopen(tti, 'wt');
fttq = fopen(ttq, 'wt');
fprintf(ftti,'%18.17f\n',real(Input_Mod+Inject));
fprintf(fttq,'%18.17f\n',imag(Input_Mod+Inject));
fclose(ftti);
fclose(fttq);
end
plot(Input_Mod);
axis([-1,1,-1,1]);
xlabel([dec2hex(Code)';dec2bin(Code,4)']);

-------------------------------------------2-------------------------------------------

Symbol_length=50;
Points_Symbol=10;
for File_Index=0:9
    load([num2str(File_Index),'.mat']);
    Covariance=xcov(abs(Input_Mod),abs(Y(1:500)));
    [M,Time_delay]=max(Covariance);
    j=File_Index+1;

Out(j,:)=Y(Symbol_length*Points_Symbol*2-Time_delay:Symbol_length*Points_Sy
mbol*3-Time_delay-1);
    In=Input_Mod.';
    Length=length(In);
    In_fft=fft(In)/Length;
    Out_fft=fft(Out(j,:))/Length;
    if (File_Index==0)
        Gain=mean(abs(Out_fft(10:20)./In_fft(10:20)));
    end
    %Cubic_ref=(In).*(In).*conj(In);
    %Cubic_ref_fft=fft(Cubic_ref)/Length;
    %Cir(j,:)=(Out_fft-Gain*In_fft)./Cubic_ref;
    Cir(j,:)=fft(Out(j,:)-Gain*In)/Length;
end
%finding left circle
for fre=1:500;
    Cov(fre)=0;
    if ((fre>=31&&fre<=190)||(fre>=311&&fre<=470))
```

```
            Pos=Cir(:,fre);
            Num_Cir=0;
            for i=1:8
                  for j=i+1:9
                        for k=j+1:10
                              a=2*(real(Pos(j))-real(Pos(i)));
                              b=2*(imag(Pos(j))-imag(Pos(i)));

c=(real(Pos(j)))^2+(imag(Pos(j)))^2-(real(Pos(i)))^2-(imag(Pos(i)))^2;
                              d=2*(real(Pos(k))-real(Pos(j)));
                              e=2*(imag(Pos(k))-imag(Pos(j)));

f=(real(Pos(k)))^2+(imag(Pos(k)))^2-(real(Pos(j)))^2-(imag(Pos(j)))^2;
                              Num_Cir=Num_Cir+1;
                              x(Num_Cir)=(b*f-e*c)/(b*d-e*a)+1i*(d*c-a*f)/(b*d-e*a);
                        end
                  end
            end
            Center=mean(Pos);
            Cov(fre)=cov(x)^0.5/mean(abs(Pos(:)-mean(x)));
            Gain_need=abs(Center)/mean(abs(Pos(:)-Center));
            i=1;
            while
(angle((-Center)/(Pos(i)-Center))<0)||(angle((-Center)/(Pos(mod(i,10)+1)-Center))>0)
                  i=i+1;
            end
            a=angle((-Center)/(Pos(i)-Center));
            b=angle((Pos(mod(i,10)+1)-Center)/(Pos(i)-Center));
            Phase_need=(i-1+a/b)/10;

            if (Gain_need>2)
                  Filter(fre)=Gain_need*exp(2i*pi*Phase_need);
            else
                  Filter(fre)=Gain_need*exp(2i*pi*Phase_need);
            end
            %if (Cov(fre)>4)
            %       Filter(fre)=Filter(fre)/Cov(fre);
            %end
      else
            Filter(fre)=0;
      end
end
```

APPENDIX G

The program below is written in Matlab. All the programs in appendix G are for L+I in a 16 QAM signal for Chapter 5. The first program is used to generate input signal for LUT measurement. The second one is to measure the input-output relation for LUT. The third one is to generate L+I input signal. The fourth one is to calculate the injection.

----------1----------

```
double Int;
Int=2/(2^11);
LUT_Input=-0.6:Int:0.6;
LUT_Input_=0.6-Int:-Int:-0.6+Int;
LUT_Input=[LUT_Input LUT_Input_];


%write file
tti=['I00.txt'];
ttq=['Q00.txt'];
ftti = fopen(tti, 'wt');
fttq = fopen(ttq, 'wt');
fprintf(ftti,'%18.17f\n',LUT_Input);
fprintf(fttq,'%18.17f\n',0*LUT_Input);
fclose(ftti);
fclose(fttq);
```

----------2----------

```
LUT_Out=Y(1:length(LUT_Input)+1);
for i=1:length(LUT_Out)
      if real(LUT_Out(i))<0
            LUT_Out(i)=-LUT_Out(i);
      end
end
LUT_Out=sort(LUT_Out);
Pre_Ang=angle(mean(LUT_Out(1:1000)));
LUT_Out=LUT_Out/max(abs(LUT_Out))/exp(1i*Pre_Ang);
LUT_In=linspace(0,1,length(LUT_Out))';

Ang=angle(LUT_Out);
for j=1:5000
      Ang1(1)=(Ang(1)*2+Ang(2))/3;
```

```
        if abs(Ang1(1))>abs(Pre_Ang)/100
            Ang1(1)=Ang1(1)/100;
        end
        for i=2:length(Ang)-1;
            Ang1(i)=(Ang(i-1)+Ang(i)+Ang(i+1))/3;
            if i<700&&abs(Ang1(i))>abs(Pre_Ang)/100
                Ang1(i)=Ang1(i)/100;
            end
        end
        Ang1(length(Ang))=(Ang(length(Ang))*2+Ang(length(Ang)-1))/3;
        Ang=Ang1;
end
Ang=Ang-Ang(1);
subplot(1,2,1);
plot(abs(LUT_In),abs(LUT_Out));
hold on;
plot(abs(LUT_Out),abs(LUT_In),'r');
title('AM/AM')
subplot(1,2,2);
plot(abs(LUT_In),Ang);
hold on;
plot(abs(LUT_Out),-Ang,'r');
title('AM/PM')

for i=1:length(LUT_Out)
        LUT_In(i)=LUT_In(i)/(exp(1i*Ang(i)));
        LUT_Out(i)=abs(LUT_Out(i));
end

-----------------------------------------3-----------------------------------------

for j=0:9
%Open file
tti=['I0' num2str(j) '.txt'];
ttq=['Q0' num2str(j) '.txt'];

%cubic injection
Inject=Input_Mod.*Input_Mod.*conj(Input_Mod);
Inject_fft=fft(Inject);
for i=1:500
        if abs(Inject_fft(i))<0.1
            Inject_fft(i)=0.1*Inject_fft(i)/abs(Inject_fft(i));
        end
end
```

```
%sideband elimination
Inject_fft(91:410)=0;
%inband elimination
Inject_fft(1:30)=0;
Inject_fft(471:500)=0;

%brick wall
Inject_fft_w=0.15*ones(500,1);

%sideband elimination

%Inject_fft_w(111:390)=0;

Inject_fft_w(191:310)=0;

%inband elimination
Inject_fft_w(1:30)=0;
Inject_fft_w(471:500)=0;

Inject_Amp=0;
Inject_fft=Inject_fft_w*exp(2i*pi*(j/10))*Inject_Amp+Inject_fft_w.*Filter1.';%+Inje
ct_fft_w.*Filter2.';%+Inject_fft.*Filter.'*0.3;
Inject=ifft(Inject_fft);

Input_Mod_temp=Input_Mod;
Input_Mod=Input_Mod+Inject;

for i=1:length(Input_Mod)
      j=1;
      while ((LUT_Out(j)<abs(Input_Mod(i)/0.6))&&(j<length(LUT_Out)));
            j=j+1;
      end
      % in the range for LUT
      if (j<=length(LUT_Out))
            Mod=(abs(Input_Mod(i)/0.6)-LUT_Out(j-1))/(LUT_Out(j)-LUT_Out(j-1));

Input_LUT(i,1)=(LUT_In(j-1)+Mod*(LUT_In(j)-LUT_In(j-1)))*0.6*exp(1i*angle(In
put_Mod(i)));
      else
      % out of range for injection

slope=(mean(LUT_In(round(0.9*length(LUT_In)):length(LUT_In)))-LUT_In(length(
LUT_In)))/(mean(LUT_Out(round(0.9*length(LUT_Out)):length(LUT_Out)))-1);
```

```
            Input_LUT(i,1)=(abs(Input_Mod(i)/0.6)-1)*slope*0.6+Input_Mod;
            if Input_LUT(i,1)>1
                Input_LUT(i,1)=1;
            end
        end
end

Input_Mod=Input_Mod_temp;

ftti = fopen(tti, 'wt');
fttq = fopen(ttq, 'wt');
fprintf(ftti,'%18.17f\n',real(Input_LUT));
fprintf(fttq,'%18.17f\n',imag(Input_LUT));
fclose(ftti);
fclose(fttq);
end
plot(Input_LUT);
axis([-1,1,-1,1]);
xlabel([dec2hex(Code)';dec2bin(Code,4)']);

-----------------------------------------4----------------------------------------

Symbol_length=50;
Points_Symbol=10;
for File_Index=0:9
        load([num2str(File_Index),'.mat']);
        Covariance=xcov(abs(Input_Mod),abs(Y(1:500)));
        [M,Time_delay]=max(Covariance);
        j=File_Index+1;
Out(j,:)=Y(Symbol_length*Points_Symbol*2-Time_delay:Symbol_length*Points_Sy
mbol*3-Time_delay-1);
        In=Input_Mod.';
        Length=length(In);
        In_fft=fft(In)/Length;
        Out_fft=fft(Out(j,:))/Length;
        if (File_Index==0)
            Gain=mean(abs(Out_fft(10:20)./In_fft(10:20)));
        end
        %Cubic_ref=(In).*(In).*conj(In);
        %Cubic_ref_fft=fft(Cubic_ref)/Length;
        %Cir(j,:)=(Out_fft-Gain*In_fft)./Cubic_ref;
        Cir(j,:)=fft(Out(j,:)-Gain*In)/Length;
end
%finding left circle
```

```
for fre=1:500;
    Cov(fre)=0;
    if ((fre>=31&&fre<=190)||(fre>=311&&fre<=470))
        Pos=Cir(:,fre);
        Num_Cir=0;
        for i=1:8
            for j=i+1:9
                for k=j+1:10
                    a=2*(real(Pos(j))-real(Pos(i)));
                    b=2*(imag(Pos(j))-imag(Pos(i)));
c=(real(Pos(j)))^2+(imag(Pos(j)))^2-(real(Pos(i)))^2-(imag(Pos(i)))^2;
                    d=2*(real(Pos(k))-real(Pos(j)));
                    e=2*(imag(Pos(k))-imag(Pos(j)));
f=(real(Pos(k)))^2+(imag(Pos(k)))^2-(real(Pos(j)))^2-(imag(Pos(j)))^2;
                    Num_Cir=Num_Cir+1;
                    x(Num_Cir)=(b*f-e*c)/(b*d-e*a)+1i*(d*c-a*f)/(b*d-e*a);
                end
            end
        end
        Center=mean(Pos);
        Cov(fre)=cov(x)^0.5/mean(abs(Pos(:)-mean(x)));
        Gain_need=abs(Center)/mean(abs(Pos(:)-Center));
        i=1;
        while
(angle((-Center)/(Pos(i)-Center))<0)||(angle((-Center)/(Pos(mod(i,10)+1)-Center))>0)
            i=i+1;
        end
        a=angle((-Center)/(Pos(i)-Center));
        b=angle((Pos(mod(i,10)+1)-Center)/(Pos(i)-Center));
        Phase_need=(i-1+a/b)/10;

        if (Gain_need>2)
            Filter(fre)=Gain_need*exp(2i*pi*Phase_need);
        else
            Filter(fre)=Gain_need*exp(2i*pi*Phase_need);
        end
        %if (Cov(fre)>4)
        %       Filter(fre)=Filter(fre)/Cov(fre);
        %end
    else
        Filter(fre)=0;
    end
end
```

Publish Papers

- M. Xiao and P. Gardner, "Digital Baseband Injection Techniques to Reduce Spectral Regrowth in Power Amplifier," *IEEE MTT-S Int. Microwave Symp. Dig.*, Atlanta, Georgia, June 2008

- M. Xiao and P. Gardner, "Characterisation, analysis and injection of two-tone third-order intermodulation products in an amplifier," *IET Microwaves, Antennas & Propagation*, vol. 3, issue 3, pp. 443-455, 2009.

- M. Thian, M. Xiao, and P. Gardner, "Digital Baseband Predistortion Based Linearized Broadband Inverse Class-E Power Amplifier," *IEEE Transactions on Microwave Theory and Techniques*, vol. 57, issue 2, pp. 323 - 328, Feb, 2009.